University of Zurich[UZH]

Department of Geography

Reconstruction of Holocene landscape evolution using mires situated in the Göschenen valley

GEO 511 Master's Thesis

Author
Alessandra Musso
10–758–431

Supervised by
Prof. Dr. Markus Egli
Prof. Dr. Max Maisch
MSc. Max Boxleitner

Faculty representative
Prof. Dr. Markus Egli

30.11.2016
Department of Geography, University of Zurich

Summary

The present work comprised a primarily pedological examination of two mires and an adjoining slope in order to reconstruct the environmental conditions and their changes during the Holocene. It was conducted in the valley on Göschenen, in the Central Swiss Alps.
A secondary task was to calculate statistical model using Partial Least Squares in order to predict elemental contents based solely on mid–IR spectra.

The valley of Göschenen experienced erosion by the converged ice masses of Damma and Chelen glaciers during the last glacial. After their retreats, they left behind an array or geomorphologic features that can be used to reconstruct the various stages of their retreats. Even with the possibility of absolute age determination of such features, the amount of information that can be gained from them is limited.

One source of past environmental information that had not been tapped so far in Göschenen valley had been the soils and the mires. Soils are open and dynamic systems that are strongly connected to environmental conditions such as precipitation or temperature. Mires are valuable environmental archives as they act as a sink for organic matter and preserve an array of environmental information.

The aim of this study was to use these environmental archives in order to expand the existing knowledge on how the environment of the Göschenen valley landscape had changed after the glacial termination and the retreat of the glacier.

We sampled in two locations, Börtli and Brätschenflue, where we sampled mires, and the soil of an adjoining slope as well.

We used an broad variety of tools. We for example covered basic physical and chemical parameters such as bulk density, water content, pH, and grain size distributions to comprehend the basic properties of both soil and peat.

The backbone of our analyses was the total elemental composition (determined using XRF). It enabled us to detect deposits of detritus in the mires, and to recognize shifts in chemical weathering.

Mid-IR spectral analysis with DRIFT provided information on the presence or absence of secondary minerals which accompany the weathering of primary minerals.

Age determination was conducted using radiocarbon dating. It provided absolute ages for the peat and enabled us to reconstruct a timeline and compare our findings with previous studies.

We were also given the opportunity to do a palynological analysis in cooperation with the University of Wroclaw, Poland. It was a valuable addition, as it gave us information on the vegetation composition and dynamics, which is also strongly dependent on the environment.

The mires at Börtli and Brätschenflue had peat dating back as far as the beginning of the Atlantic, roughly 9200 years ago. It meant that the information we could extract would cover mostly the mid– to late–Holocene.

Our findings enabled us to reconstruct a timeline of enhanced weathering and erosion during the Holocene. We detected deposits in the mire that could be connected to strong erosion processes happening on the slope. It supported the hypothesis that phases of regressive soil formation preferentially occurred during cold shifts.
The palynological results strongly supported the pedological results, and in fact added a lot of depth to this study.
Radiocarbon dating was an invaluable tool in correlating the results to previous palynological studies from this area.

There is still room for improvement of the information gained from the mires. There are parameters such as peat humification, eolian deposits or the increasing human influence that could have added further useful insights. We could detect them but not analyze them any more closely with the data and the resolution at hand.
The temporal resolution posed a challenge at times. Future studies of this kind should focus on ensuring a high temporal resolution in order to make more robust interpretations of the data.
A different sampling strategy and a closer examination of the soils might also help better understand the pedogenesis and the erosive processes on the slope. Mass balances would help quantifying rates of soil production or soil erosion on the slope.

The secondary task where we used DRIFT spectra to statistically predict elemental contents in the peat, was concluded successfully. We could accurately predict contents of e.g. silicon or aluminium in the peat with Partial Least Squares models. The only drawback was the small size of our database. It could, however, be extended using data from other peats, and the models better validated.

TABLE OF CONTENTS

Figures and tables

1. Introduction

1.1. Objectives

The aim of this study was to fill in the blanks on how the environment of the Göschenen valley landscape had evolved during the Holocene. There already is geomorphologic data available on when approximately there had been glacial retreats, but while they cover the late–glacial well, they do not provide much information about Holocene climate shifts. Palynological data was also available and offered information about vegetation composition and dynamics which are strongly connected to shifts in the environment, though not entirely. The one environmental archive that had not been examined yet were the mires. We therefore sampled peat in mires and tried to reconstruct Holocene environmental conditions such as weathering and erosion.

1.2. Background

Global climate has changed dramatically during the past billions years. The continents used to be in different positions over time, and temperatures, and atmospheric CO_2 levels were also much higher than today several hundred million years ago. Today's configuration with two glaciated poles is therefore a unique one that didn't occur until 2.7 Million years (Ma) ago after the closure of the Panama strait. While the south pole had already been glaciated for almost 35Ma, the northern high latitudes lacked the humidity to build up ice sheets (Zachos et al., 2001).
Before the closure, there was a direct connection between the Atlantic and the Pacific water masses which balanced out their salinity. With the closure of the Panama strait, however, there began a build–up in salinity in the Atlantic coupled with a decrease in the Pacific. The motor of which is evaporation of water in the Atlantic which is transported westward by the trade winds into the Pacific where it is precipitated again (Haug et al., 2001).

This process allowed the onset of today's Great Conveyor Belt which transports warm water masses (and thus humidity) from the lower latitudes into the higher latitudes of the Northern Hemisphere (Broecker, 1991). The build–up of Northern Hemisphere ice sheets and the strengthening of the conveyor belt was needed for the global climate to be able to dip into ice ages.

The current 100'000 years (100ka) period of glacial (ice ages) and interglacial cycles only began 800ka ago (*fig.1–1*; Lisiecki and Raymo, 2005). The last ice age began 110–120ka ago and reached a last maximum extension (called the Last Glacial Maximum, LGM) around 23ka ago (depending on the geographic location). The stepwise termination began around 18ka ago and came to an abrupt end 11.7ka ago, after the Northern Hemisphere cooling of the Younger Dryas. The subsequent (global) warming marked the end of the Pleistocene and beginning of the current Holocene interglacial (Denton et al. 2010; Clark et al. 2012, Shakun et al. 2012).

With the gradual retreat of the alpine glaciers after the LGM, the vegetation was able to spread higher and higher into mountain valleys and repopulate the eroded and barren landscape carved out by the glaciers. The valleys of the Alps have been inhabited for millennia. Especially the Eastern Alps were used early on (as early as 5000 BC) as sources for ores (Presslinger and Eibner, 2003). Trade routes using mountain passes were established and became the basis of a profitable economy and considerable strategic value (Walser, 1998). Mountaineering became very popular in the 19th century which not only sparked the still–big alpine tourism, but an interest in the glaciers and geomorphologic features as well. A lot of the glaciological, geomorphologic and palynological research has been conducted in the Rhaetian and Central Alps (e.g. Burga, 1989, 1993, 1998; Maisch, 1982).

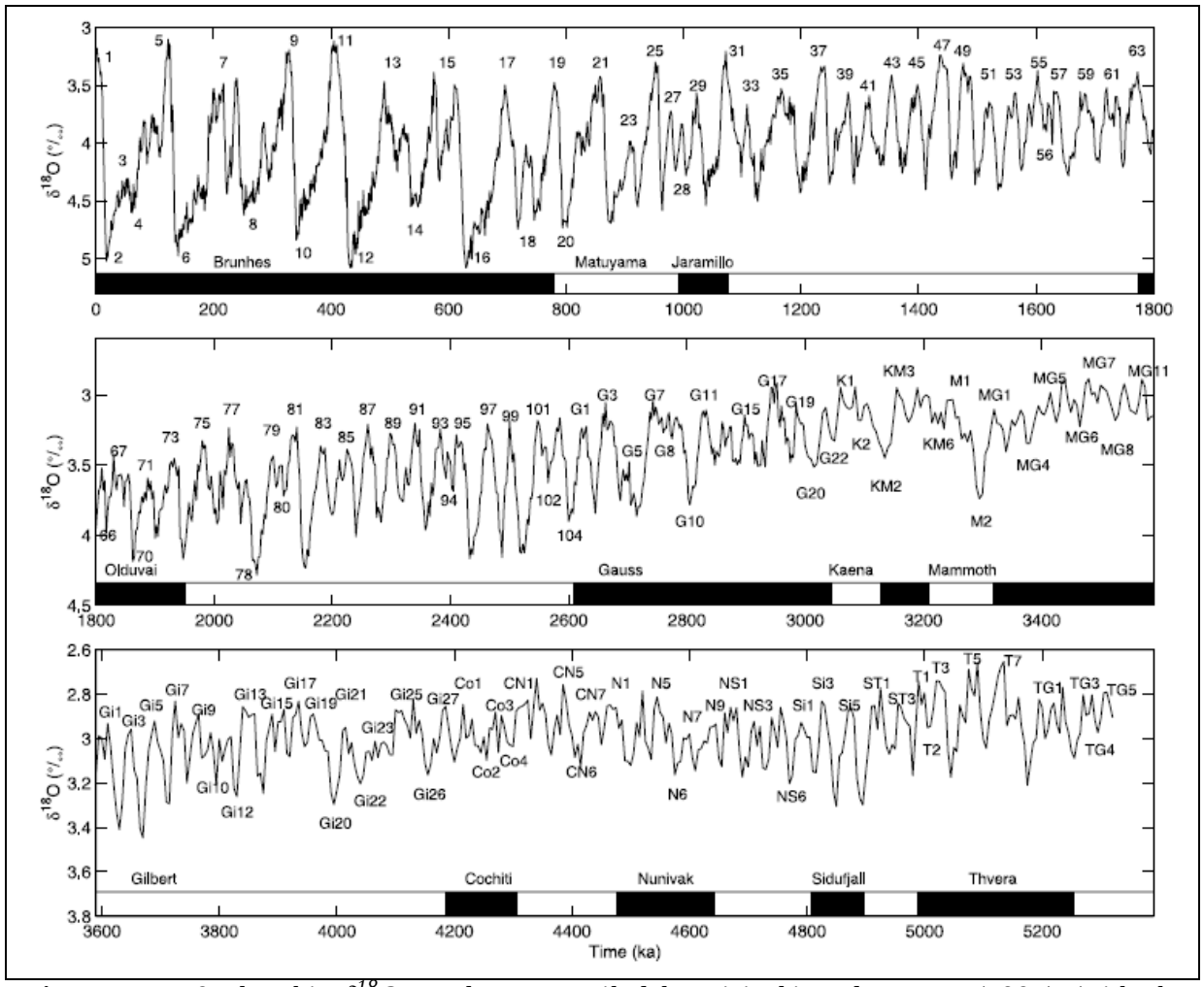

Fig. 1–1: *LR04 benthic $\delta^{18}O$ stack as compiled by Lisiecki and Raymo (2005) (with the paleomagnetic record). Benthic $\delta^{18}O$ is used as a proxy for global ice volume and temperature. A decrease in $\delta^{18}O$ means an increase in temperature and decrease ice volume.*

While pollen analysis can be combined with radiocarbon dating to link the data to a temporal axis, it is challenging to do with geomorphologic data alone. A link between colder/warmer climate, glacial advances/retreats and the corresponding features in the terrain (i.e. moraines) an be made, but it lacked precision. The timing of e.g. a glacial retreat cannot be pinned down

with absolute age. Ivy–Ochs (1996) developed a method using in–situ produced isotopes ^{10}Be, ^{26}Al and ^{36}Cl. These isotopes are radioactive and are produced by cosmic radiation and accumulate in e.g. rock surfaces. That makes them suitable to measure the amount of time a rock surface has been exposed to the surface (hence the name: Surface Exposure Dating). The actual calculation of the exposure age is complicated as many factors need to be included, such erosion rates, atmospheric and topographic shielding, latitude and exposition.

1.3. Study location

This study has been conducted in the Göschenen valley, located in the central Swiss Alps. It is an addition to a larger project in which PhD student Max Boxleitner from the Institute of Geography (University of Zurich) conducted a series of Surface Exposure Datings on moraines in several valleys in the central Swiss Alps, one of which was Göschenen valley. There are a number of moraines scattered in the valley that recorded the positions and approximate sizes of the once converged Damma and Chelen glaciers which had flown through. The glacier had left behind a relatively wide and flat terrain which used to be inhabited and is called "Göschener Alp" (*fig. 1–2*). While the absolute age determination of moraines would shed more light on the timing of several glacier retreats, the present study was to focus on the information than could be retrieved from mires regarding the Holocene climate and landscape evolution.

Fig. 1–2: *Göschener Alp shortly before the construction of the dam (Kraftwerk Göschenen AG)*

The Göschener Alp settlement was inhabited by farmers and was abandoned to make space for a barrier lake for electrical power production. The dam was completed in 1960 and is still

in operation today and the former landscape of meadows is now dominated by the lake and its dam (Kaufmann, 1998).

There have been a number of palynological studies conducted on the former grounds of the Göschener Alp by Zoller (e.g. 1960, 1966) shortly before the dam was built. There is mention of several short and more or less severe climatic shifts to cooler and wetter climate during the Holocene that were registered by pollen archives in other parts of the Swiss Alps as well (e.g. Magny and Richoz, 1998). These climatic shifts have an impact on the vegetation and on soil development as they present more difficult living conditions for plants and animals, and are associated with enhanced soil erosion. We examined two mires which are situated on the orographic left of the Göschenen valley (see *fig.1–3* and *1–4*). One location, Börtli was suitable to examine both the mire and the soil from the adjacent slope and see how they are linked erosion–wise. From the other location, Brätschenflue, just above the lake, we analyzed two peat cores and measured an array of organic and inorganic parameters.

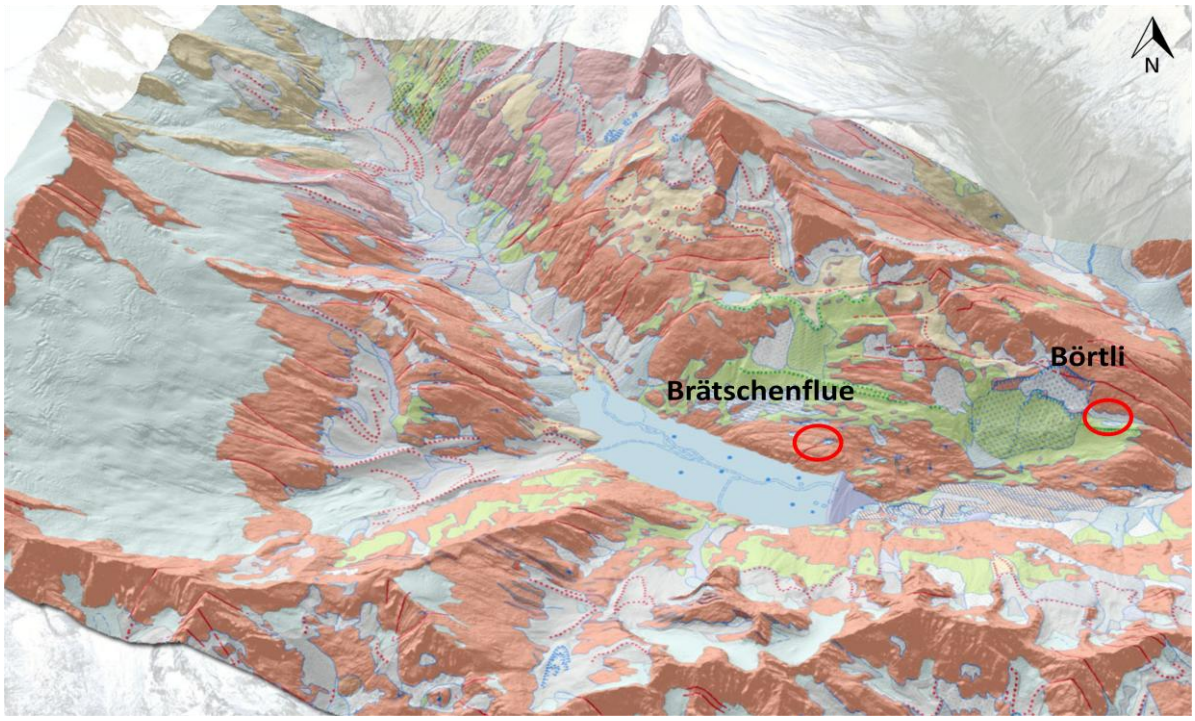

Fig. 1–3: *3D surface model of the Göschenen valley. In the west, the remnants of the Damma glacier. Leading east, the Göschenen valley with the lake (where the former settlement "Göschener Alp" was located) and the two sites Brätschenflue and Börtli on the orographic left. (created by Max Maisch, 2015)*

Fig. 1–4: *View from Brätschenflue towards today's Damma glacier in the south–west. (A.Musso, 2015)*

1.4. Mires as environmental archives

Mires are water logged soils with a peat layer of at least 30cm thickness. More peat (i.e. organic matter) is produced than decomposed so that a net accumulation occurs. The reduced decomposition is due to the inhibition of microbial activity. The water displaces the air from the pores, and with no oxygen available, the microbial fauna cannot decompose the dead plant matter, causing it to accumulate (Blume et al., 2010).

The surface rises with each life cycle of plants, building up a stratigraphy with the oldest matter at the bottom and the newest at the surface. This and the fact that the water (and everything dissolved in it) doesn't experience much vertical or horizontal movement, makes them valuable environmental archives that preserve an array of organic and inorganic information over long periods of time.

Often, mire formation starts in (anoxic) ponds or lakes inside a topographic depression. The organic matter accumulates over a long enough period to fill basin and the pond or lake disappears. Such mires are called fens (ger.: Niedermoore). (*fig. 1–5*). They are characterized by higher nutrient contents and a pH 4–7.5, depending on the chemistry of the groundwater they are connected to.
Ombrotrophic mires or (raised) bog are typically dome–shaped and are not dependent from the groundwater. Their water supply fully depends on precipitation. Meteoric water is slightly acidic and contains almost no nutrients, so that ombrothophic mires are also acidic (pH <3–4) and very poor in nutrients. (Succow and Joosten, 2001, Blume et al., 2010)

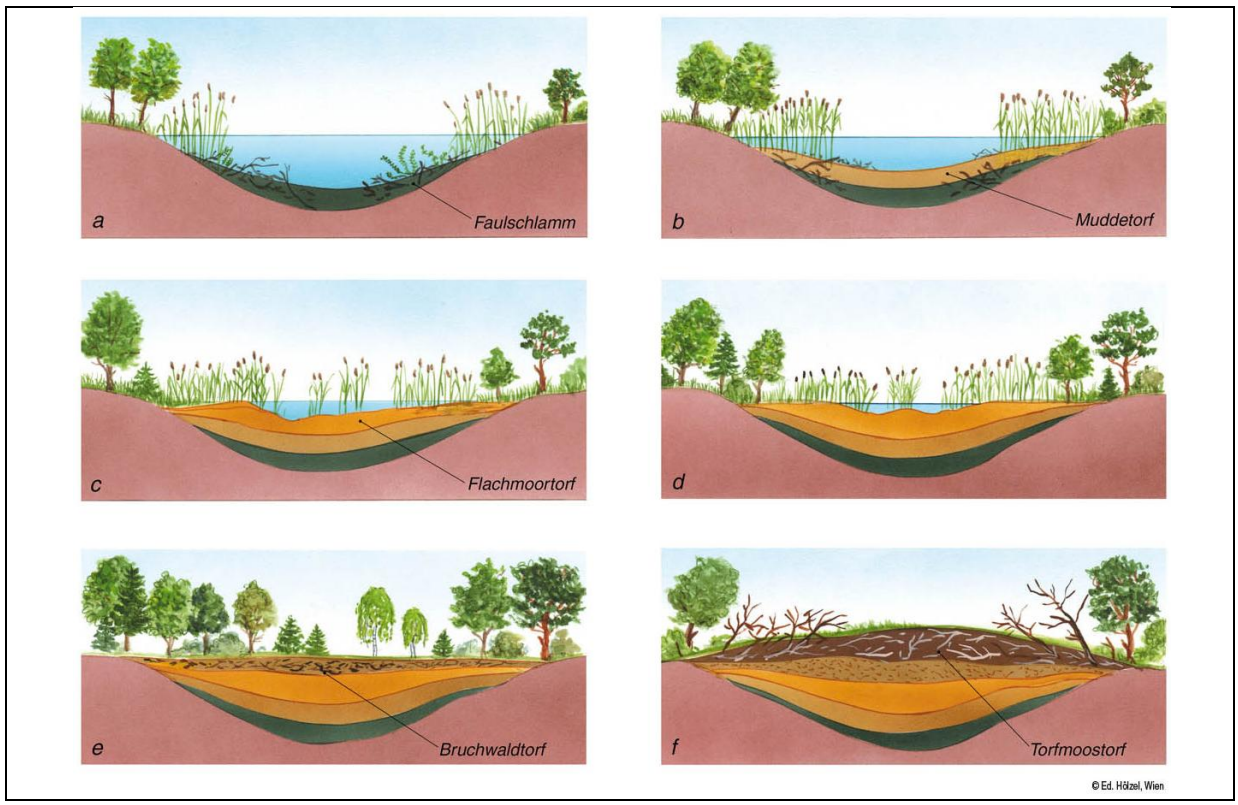

Fig. 1–5: *a–f: Exemplary steps of a mire formation in a pond. (Cholewa, 2010)*

The advantage of mires as Holocene environmental archives is their accessibility and the lower costs in effort and money drill cores in compared to ice sheets or the ocean floor.

Information about the past development of the mire can gained through different parameters. The following were examined in this study: palynology (pollen analysis to reconstruct past vegetation cover in the area), bulk density (compaction of the peat, accumulation rates), pH, C/N ratio (nutrient and carbon cycling) (Blackford, 2000, Chambers and Charman, 2004).

We also did an elemental analysis using X–ray fluorescence (XRF) which we used to compare the contents of elements abundant in rocks and soils. Sudden inputs of mineral matter are unusual for an environment that is dominated by organic matter. Mineral matter gets for example blown in as dust or is washed from adjoining slopes during heavy rain events.

The elemental composition of the peat also provides information about the weathering, which in turn allows (qualitative) conclusions about the environmental conditions such as temperature or precipitation.

The presence of secondary minerals (detected with mid–IR using DRIFT) can provide some additional information on weathering paths as well.

Finally, radiocarbon dating (using accelerated mass spectrometry AMS) was applied to obtain absolute ages and to construct a age–depth profile. That allowed us to pin the above gained information to a temporal axis and to compare it with climate data. Such different organic and inorganic parameters from both soil and mire have successfully been combined before by Böhlert et al. (2011) and Jäger et al. (2015) to make conclusions about the landscape history, soil formation, and weathering paths in a location near Lucerne in central Switzerland.

1.5. Soil formation and weathering as indicators of past environmental conditions

Dokuchaev (1883) and Jenny (1941) set the basis of the concept of soil formation and concluded that soil formation is a function of five independent factors: ‘time’, ‘climate’, ‘topography’, ‘organisms’, and ‘parent material’.

There are two directions soil formation or pedogenesis can take: progressive and regressive. Progressive soil formation is characterized by a deepening an differention (horizonation) of the soil profile, physical and chemical weathering, and mineral transformation. It means that the primary minerals from the parent rock or sediment are dissolved and altered and their elements leached with rain water.
Regressive soil formation is accompanied by the shallowing and simplification of the profile. A removal of surface material or the deposition of unweathered materials lead to a

rejuvenation of the soil surface (Johnson and Watson–Stegner, 1987, Egli and Poulenard, 2016).

Elemental contents of the mires may offer hints about eolian inputs or deposition of detritus from outside the mires. Strong precipitation events are likely to be recorded in the mire as layers of fine or coarse sand which has been washed down from the slope. These events are more likely to occur during colder and wetter climatic periods, the same way as droughts are more likely to happen during warmer and dryer climatic periods (Meehl et al., 2000). Therefore, if a rainstorm was strong enough to wash sand from the slope into the mire, it is more likely that it occurred during a period of cooler and wetter climate (see also Jäger et al., 2015).

There are also elements that accumulate in environmental archives predominantly via atmospheric input (i.e. washing out by rain). Elements such as for example lead, mercury or nitrogen come into atmospheric circulation through human activity such as mining, industrial emissions or farming. These “alien” elements can therefore be of use as proxies of human activity (Shotyk et al., 1998; Madsen, 1981, Buijsman et al., 1987. Though we did observe increasing contents of heavy metals towards the surface of the peat, it was of no immediate interest of this study. It was, however, a useful qualitative indicator for how much human disturbance the mires have been objected to.

Weathering indices, originally developed by geologists, have proved useful tools in soil science (Reiche, 1943, Fedo et al., 1995, Price and Velbel, 2003). These indices are based on a simple principle: They use ratios of more mobile elements to less mobile elements. Chemical weathering and leaching typically occurs through meteoric water (precipitation) that dissolves minerals and salts of the parent rock minerals. They are constantly dissolved over time and the elements are either washed out (leached) or they are fixed again by forming secondary minerals such as clays.
There are elements which are more easily soluble than others and that are subsequently more prone to leaching. These are referred to as “mobile” elements, while those elements with low solubility are called “immobile”, though strictly speaking, there are no insoluble elements – or oxides, as elements mostly occur in soils as oxides or hydroxides (Kabata–Pendias, 2011 ; Price and Velbel, 2003).

1.6. Palynology as a tool for assessing existing plant species and their abundance in the past

Pollen are spread by plants and are preserved in lake sediments, mires, and in loess as well, as there they are protected from degradation unlike in the open environment. Pollen analysis has been a valuable tool in paleoclimatology for more than a century. It uses mostly cores from lake sediments and mires. Palynological studies were actually the majority of the research that has been conducted in mires or peatlands for a long time and are is still very prominent (Chambers and Charman, 2004).
Pollen analysis gives insight to the amount of pollen in the air during a given time period, the plant species and their relative abundance. Shifts in arboreal and shrub or grass pollen contents for example often indicate a shift in temperature and precipitation and can thus be used to reconstruct past environmental conditions. The appearance, dominance or absence of a combination of species with a certain ecological niche also gives clues as to what kind of environmental conditions probably had prevailed during a time period (Burga and Perret, 1998)
There are several climatic shifts during the Holocene (11.7ka to present) that not only occurred in the Swiss Alps, but were registered in environmental archives throughout Europe (Zoller, 1960, Burga, 1979, Haas et al., 1998). This thesis focuses on the following climatic shifts (ages given in (uncalibrated 14C) years before present (present=1950 AD) (Röthlisberger et al., 1966, Burga, 1979, Haas et al., 1998; fig. 1–6):

Göschenen cold phases I and II (*ger.: Göschener Kaltphasen*, 2830–2270 yrs BP and 1600–1200 yrs BP)

Löbben oscillation (*Löbben Schwankung*, 3500–3100 yrs BP)

Piora oscillations *(Piora Kaltphasen*, 5200–4200 yrs BP, corresponds to the 4.2ka event)

Misox oscillation (*Misoxer Schwankung*, 7500–6000 yrs BP, corresponds to the 8.2ka event)

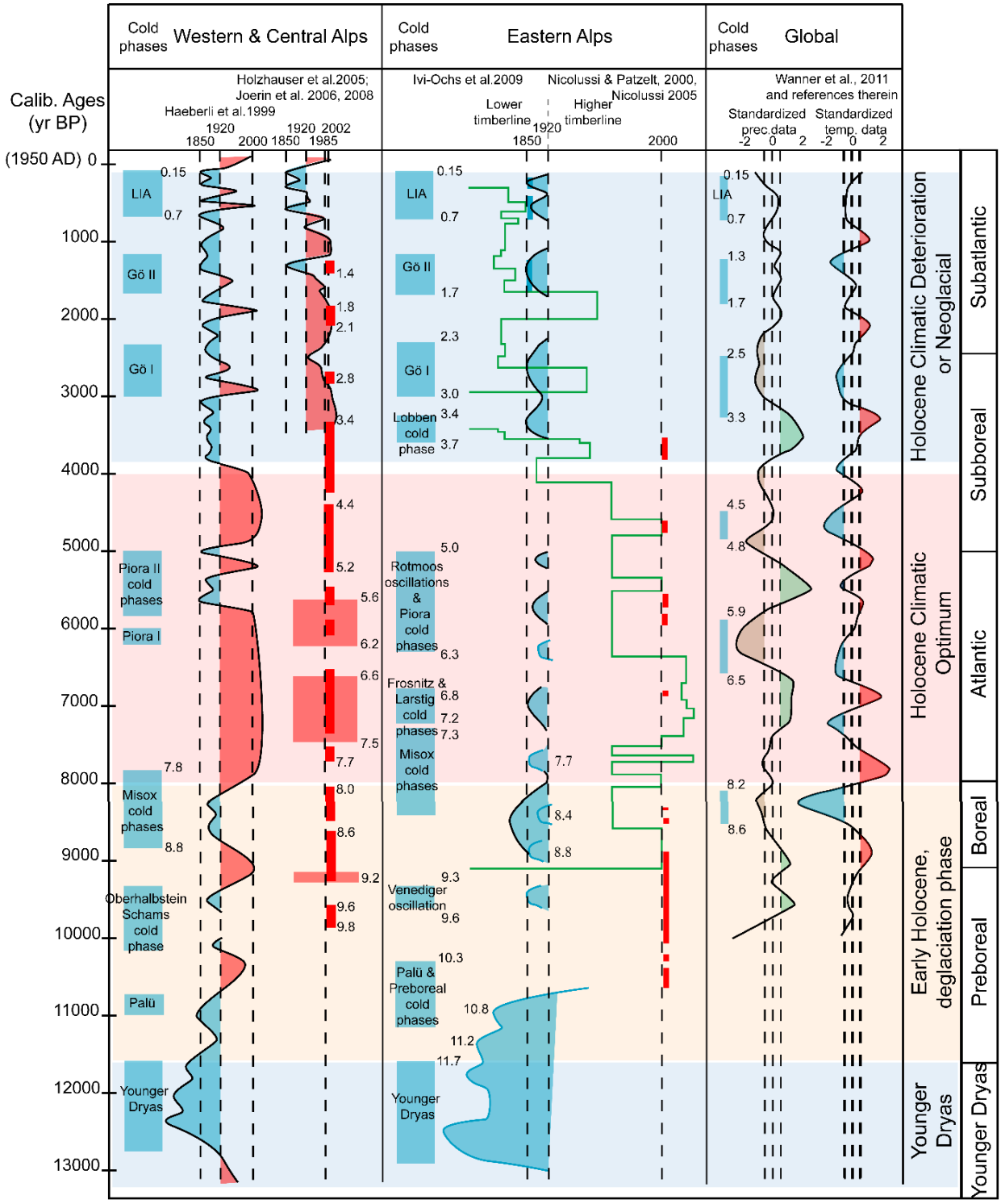

Fig. 1–6: *Cold and warm phases during the Holocene in the Western, Central and Eastern Alps, and on a global scale. Timescale is given in cal. yrs. BP. (Savi et al., 2014, Appendix)*

1.7. Radiocarbon dating for age determination of organic matter

Age determination of the peat samples was done by radiocarbon dating, as the mires were expected to have formed during the early Holocene (starting 11.7ka ago). Radiocarbon (^{14}C) is a radioactive isotope that is produced in the upper atmosphere by cosmic radiation.

Stable ^{14}N isotopes lose one proton in the process and become a ^{14}C which is radioactive. These carbon isotopes are incorporated into CO_2 molecules and enter the carbon cycle via plants that incorporate it through photosynthesis. They exchange their carbon constantly as long as they live by building up new cells with fresh CO_2 from the atmosphere.
After an organism's death, the carbon exchange ceases and the ^{14}C content decreases due to its radioactive decay (half–life approx. 5730 yrs) *(fig.1–7)*. By measuring the ratio between (the most abundant carbon isotope) ^{12}C and the remaining ^{14}C it is possible to calculate the age (American Chemical Society).

There are fluctuations in the amount of cosmic radiation that reaches the earth's atmosphere so that radiocarbon production is not constant over time. A calibration is therefore necessary to obtain the correct radiocarbon age. This can be done using calibration curves that were developed using dendrochronology and are updated regularly.

Radiocarbon dating can be used for age determination back up to 50ka (Reimer et al., 2013). Because of uncertainties in the measurement of ^{14}C and the following calibration (due to so called "plateaus" in the calibration curve), calibrated radiocarbon ages are given as age ranges, which can be span several decades to several hundred years.

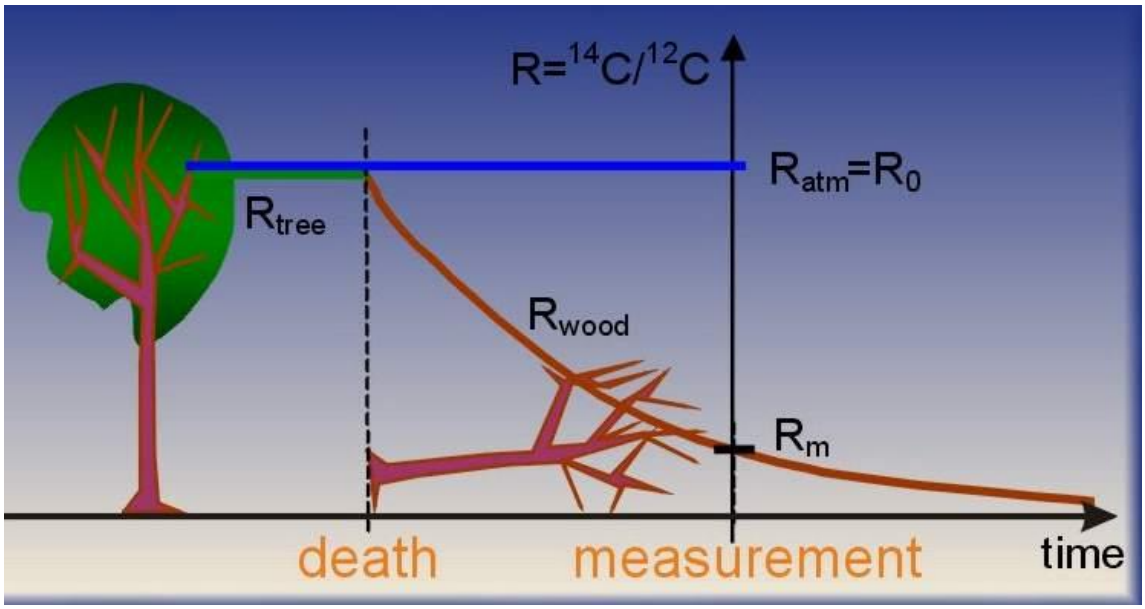

Fig. 1–7: *Simplified comic of how the ^{14}C content in organic matter as a function of time. ^{14}C:^{12}C is the same as the atmosphere's as long as the organism lives and exchanges carbon. After death, no more carbon exchange with the atmosphere occurs and the present ^{14}C decays and diminishes according to its half–life.*
(EHU, http://www.ehu.eus/biomoleculas/isotopos/jpg/?C=M;O=A)

1.8. Research Questions and Hypotheses

Based on our goal to better understand the dynamics of soil formation and the environmental conditions during the Holocene, we formulated the following research questions and hypotheses that guided our research.

Can phases favoring or inhibiting soil formation be recognized in the mires?
H: *Phases of progressive or regressive soil formation can be identified in the Göschenen mires.*

Is there a (geochemical) connection between the mires and soils on the nearby slopes?
H: *The mire acts as a catchment for leached elements from the slope.*

Can regressive soil formation phases be connected to climatic cold shifts?
H: *Phases of regressive soil formation can be connected to cold shifts.*

Can we predict elemental contents based on infrared spectroscopy (DRIFT) by making a statistical model?
H: *Infrared spectroscopy can be used to predict the contents of single elements in the peat with statistical models.*

2. Methods

2.1. Sites

This study took place in the valley of Göschenen (Göscheneralptal) and was conducted at two locations, ca. 2km apart, both at the orographic left of the Damma glacier that passed through during the last ice age.

2.1.1. Börtli site

Börtli site is situated at 1800m.a.s.l. (46°39′27.253″N 8°31′14.602″E) and lies in between a slope (slope 45°, exposition 160°) and the outside of a moraine (*fig. 2–1*).

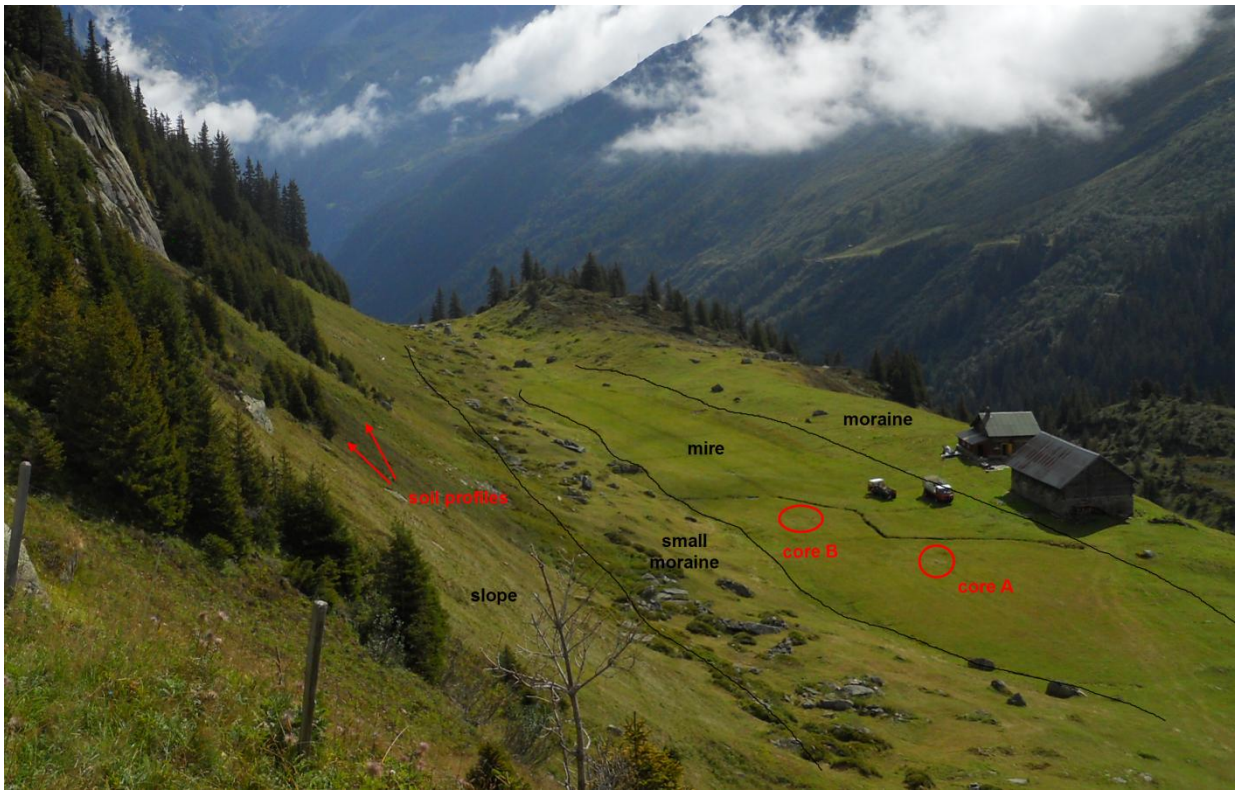

Fig. 2–1: *Börtli mire from above. In the centre of the picture, the mire with both cores and the network of small drainage ditches. (A. Musso, 2015)*

2.1.1.1. Soil profiles

The soil samples were obtained from two soil pits dug into the slope above the Börtli mire. The pits were approximately 30m apart and had difference in elevation of 10–20m. They were chosen for to cover the spatial variability of the slope: the upper profile (Profile 1) was located underneath a group of small coniferous trees; the lower profile (Profile 2) was open grass. Digging was difficult due to the combination of steep and slippery slope and large rocks in the soil. We only reached a depth of 70–80cm. In addition to the samples, two density cores were taken per horizon.

2.1.1.2. Peat cores

To obtain the peat cores, two different drills were used. At Börtli we used the motorized Humax drill whenever possible. The peat became too waterlogged at some depth and the cores could not be retrieved anymore. The Macaulay ("Russian peat drill") was therefore used instead. The terrain at Brätschenflue was not suitable for the heavy equipment of the Humax.

The cores segment lengths were 25cm for the Humax and 50cm for the Macaulay drill. The Humax drill has a telescopic system of tubes of decreasing diameters (8cm, 5cm and 3.5cm) being consecutively drilled into the ground. The Macaulay peat drill produced half–cores with a diameter of 5cm.

The samples were stored and transported in plastic shells (Humax) or in acrylic glass half tubes wrapped in aluminium foil (Macaulay). Top and bottom of each piece were marked and labeled with the corresponding depth.

Börtli proofed difficult to drill due to a thick layer of wood approximately 2m below surface and rocks further below. We drilled in two spots, ca. 30m apart (Börtli A and Börtli B), inside an 2m radius at each spot (see *fig. 2–1).*
Using the various partial cores from each spots we assembled two cores extending from top to bottom, reaching a depth of 300cm (Börtli A) and 285cm (Börtli B), respectively.

2.1.2. Brätschenflue site

Brätschenflue (BF) landscape was an different from Börtli. Many small ponds and bogs were scatted over an area of roughly 30ha lying in small-scale depressions in the bedrock (*fig. 2–2*). There were no slopes directly connected to the sampled mires, which is why we only sampled peat.

We sampled two such small mires and so obtained two cores (BF A and BF B). In contrary to Börtli, these mires were separated from each other and are probably subjected to slightly different hydrological conditions (on a micro-scale) and also show the spatial variability of these environmental archives at this location.
The cores of BF A and BF B reached a depth of 300cm and 220cm respectively.

Fig.2–2: *Mire of core Brätschenflue A. The position of the people in the picture marks the edge of the pond which lies to the left. The core was taken in the dark–brown mound in the lower centre of the image. (A. Musso, 2015)*

2.2. Sample preparation and measurements

The sample preparation was conducted according to the lab procedures of Egli et al. (2015).

2.2.1. Preliminary preparation before measurements

The soil samples were dried for 48h at 70°C.

The peat cores (*fig.2–3*) were kept wrapped in aluminium foil and stored at <5°C until further use to inhibit microbial activity and to prevent algae growth. The cores were cut at 10cm intervals and were dried at 70°C for at least 48h.

Further preparation involved sieving to 2mm to separate the skeleton from the fine earth fraction, and milling of the latter for further analysis.

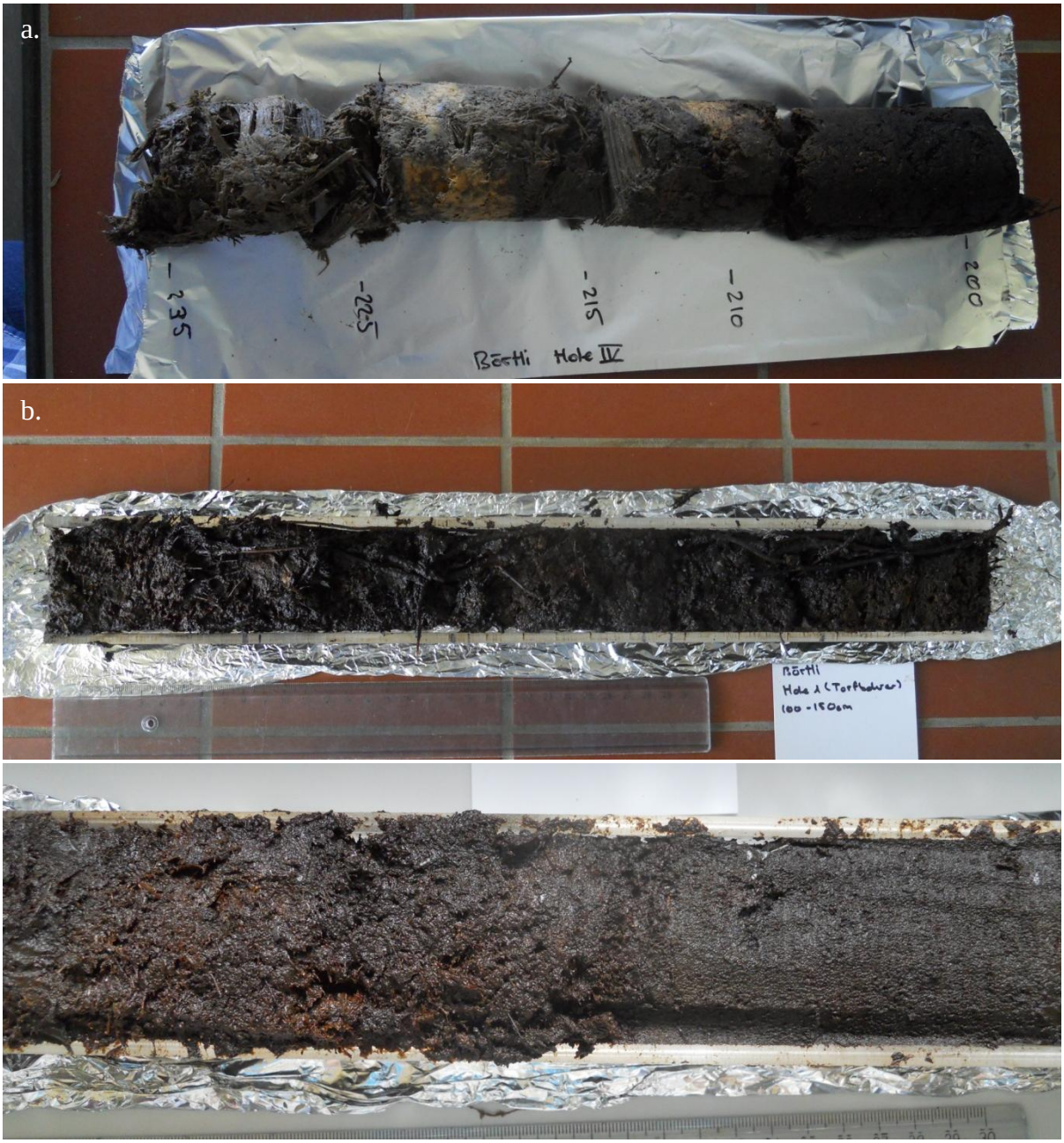

Fig. 2–3: *Peat cores from Börtli A and Brätschenflue A.* ***a.*** *Layer of massive wood from below 200cm in Börtli A.* ***b.*** *Heterogeneous peat at 100–150cm with either roots or twigs in Börtli A.* ***c.*** *Abrupt change of peat decomposition state at 260cm in BF A. (A. Musso, 2015)*

The original 10cm depth resolution had to be adjusted as there was often not enough fine material to work with. Samples were therefore pooled when necessary to create 20cm.

2.2.2. Grain size

The grain size distribution was measured for the soil profiles only. The fine earth fraction (<2mm) was treated with 3% H_2O_2 and was wet sieved to 32µm (*fig.2–4*). The <32µm fraction was further measured with X-rays (Sedigraph 5100) to obtain the distribution down to 1µm. The data from the wet sieving was later merged with the X–ray measured data.

Fig. 2–4: *One soil sample split into different grain size fractions. (A. Musso)*

2.2.3. pH

Soil and peat pH were measured in 0.01M $CaCl_2$ solution. The ratio of grams of sample to milliliters of solution was 1:10g/ml for soil and 1:12.5g/ml for the peat samples. The latter ratio was chosen for practical reasons because of the large absorption capacity of the organic matter.

The samples with the $CaCl_2$ solution were stirred for 25min and left to settle for another 25min prior to measurement.

2.2.4. Loss on Ignition

The Loss on Ignition procedure was a modified version of the procedure Heiri et al (2001) proposed. The milled samples and the ceramic crucibles (that were to hold the samples during combustion) were oven–dried at 60°C for 12h to remove all moisture. The samples were stored in a desiccator to protect them from humidity.

Approximately 2g of sample (if available) were weighed into the crucibles.

Experience from other LOI experiments in this laboratory had shown that samples very rich in carbon were prone to combust violently and parts would go airborne. To counter this, we introduced a slower, step–wise temperature ramp that should allow the burning to happen in a more controlled, less violent manner.
At first, the oven (with the samples) was heated to 105°C for 15min to remove any water (as a safety measure as there should not be any water left after the previous drying).
In a second step, temperature was increased to 350°C and kept stable for 1h. It is the temperature where most of the burning occurs.
Finally, the temperature was increased to 550°C and held for 5.5h.
The samples were removed while the oven was still at >100°C and stored in an desiccator to cool down before weighing.
We observed no more sample fragment that had gone airborne, proving this step–wise temperature ramp a reliable, time–saving procedure for very carbon–rich samples like peat. Replicate measurements showed that the reproducibility of the results was excellent.

2.2.5. Radiocarbon dating

Radiocarbon dating was conducted on five samples from Börtli and seven from Brätschenflue. The samples chosen stemmed from pieces of wood or fiber of the >2mm fraction of the cores. We abstained from dating bulk peat because of the heterogeneity of the peat and the unclear origins of the components.
The samples were prepared in the radiocarbon laboratory of the Department of Geography, UZH, under the guidance of radiocarbon lab technician Ivan Woodhatch. AMS measurement was conducted in the Laboratory for Ion Beam Physics, ETH Zürich.
Samples were pretreated with acid–alkaline–acid baths to remove contaminants: first, the removal the carbonates (acid, HCl), then of the humic acids (alkaline, NaOH), and to prevent any modern CO_2 absorption, again treatment with acid (HCl).
After drying the samples at 110°C overnight, subsamples were placed into quartz ampoules together with CuO and a strand of silver wool. They were evacuated and sealed (*fig. 2–5a.).*
The ampoules were heated in a muffle oven to 900°C for 2h to burn the sample and produce CO_2. The cooled ampoules (*fig. 2–5b*.) were inserted into the "crack machine", broken open and the CO_2 moved into the reactor chamber, where 6–7mg of iron oxide powder had been placed earlier onto a copper crucible. It functiones as a catalyst in the chemical reaction where CO_2 is cracked and graphite produced.
The CO_2 gas was mixed with an appropriate amount of H_2 gas and heated to 600°C in order to catalytically reduce the CO_2 to graphite. The graphite would adsorb onto the iron powder and could be removed and filled into vials *(fig. 2–5 c.*).
The graphite samples were measured by accelerated mass spectroscopy (AMS) at the Institute for Ion Beam Physics (Federal Institute of Technology Zürich, ETH) on the 8th February 2016. Two samples were measured in May 2016.
The 14C ages were calibrated with Oxcal (online Version 4.2.) using the IntCal13 calibration curve (OxCal 4.2.; Reimer et al. 2013).

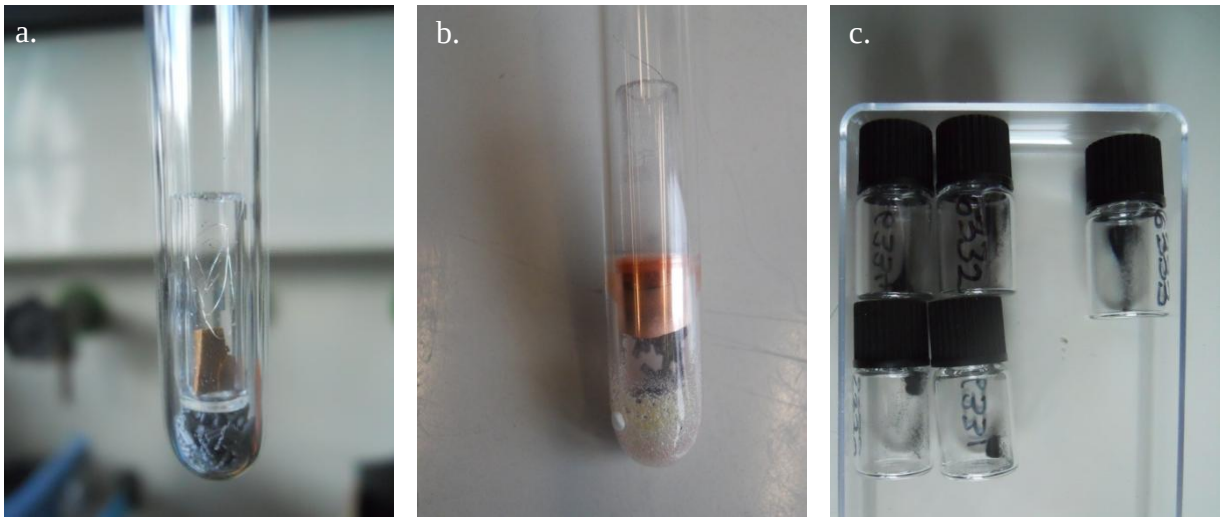

Fig. 2–5: a. *Ampoule with sample and silver wire on top and Cu oxide at the bottom.* ***b.*** *Ampoule after burning, now filled with CO_2, ready for cracking.* ***c.*** *Graphite samples waiting to be shipped to ETH for AMS measurement. (A.Musso, 2016)*

2.2.6. Geochemistry (XRF)

The dried, sieved and milled sampled were measured with energy–dispersive X–ray fractionation to gain the concentrations of most of the elements between Na and U.
The milling was first done in a planetary mill. The milling degree was unsatisfactory and we repeated the milling step using a horizontal mill with tungsten carbide vessels and balls.

2.2.6.1. Elemental Composition

The XRF data were composed of the new measurements (samples that were measured again after being milled a second time) and old measurements (first measurements and samples which had no or not enough material left for re–milling and re–measuring). The new measurements were assumed to be in order (we crosschecked with the data of Egli et al. 2001).
In a first step, only the main elements that made up the sample were picked: Na, Mg, Al, Si, P,S, K, Ca, Ti, Mn, Fe. (The other elements were so small in abundance that they could be ignored.) The sum of these elements gave the inorganic matter.
We calculated the factors from first measurement to second measurement where possible and applied these factors to the samples that had only one measurement.
We took the resulting percentages of the inorganic matter and used them to calculate the oxide contents as this is the form in which these elements mostly occur in the soil. We now worked with percentages of Na_2O, MgO, Al_2O_3, SO_3, SiO_2, P_2O_5, K_2O, CaO, TiO_2, MnO, Fe_2O_3. We also normalized their sums to 100%.
For the following “fine tuning” we did not care about the contents anymore but about the proportion between the elements to each other. XRF is a fine method to determine the contents of heavier elements but it has its limits when it comes to the lighter elements. Na for example was quite off (compared to Si) in some samples and needed to be adjusted.

Generally, the samples taken at Börtli needed much more fine tuning than the soils or the peat from Brätschenflue. This adjustment didn't have a strong influence on the end result for the individual element contents as they were so small compared to the LOI.
After the fine tuning step, the oxide percentages were recombined with the LOI, adding the inorganic matter with the organic matter content so that the overall sum of the contents was 100%. Now the numbers were ready for use.

2.2.6.2. Ratio to the Upper Crust Standard and the Central Aaregranite

To compare the contents of the most abundant elements, the ratio to a standard can be calculated. Often, the Upper Crust Standard by Taylor and McLennan (1985) is used. If a value was missing, it was filled in from the data of Ronov and Yaroshevsky (1969) (data obtained from Yanagi, 2011).
A ratio >1 indicates a gain, and a ratio <1 indicates a depletion relative to the standard. The Central Aaregranite, the parent rock of the region, has been chemically analyzed by geologist Urs Schaltegger (1989) in the Grimsel region, less than 20km southeast of the Göschenen valley.

2.2.6.3. Weathering indices

There are several kinds of indices used in geology and in soil science. They serve different purposes, one of them being a measurement for weathering or erosion. The weathering indices used for this thesis were obtained from different authors and show different ideas of how one can capture a soil's weathering history (see *tab. 2–I, fig. 2–6*).

Tab. 2–I: These indices need to be calculated with molar ratios, not weight percentages. Otherwise the ratios will be biased because of the different elemental weights.

Name	**Formula**	**Original Source**
WIP: Weathering Index of Parker	$\left[\left(\frac{2Na}{0.35}\right)+\left(\frac{Mg}{0.9}\right)+\left(\frac{2K}{0.25}\right)+\left(\frac{CaO}{0.7}\right)\right]*100$	Parker, 1970 Harnois, 1988
CIA: Chemical Index of Alteration	$\left[\frac{Al_2O_3}{Al_2O_3+CaO+Na_2O+K_2O}\right]*100$	Nesbitt and Young, 1984
CIW: Chemical Index of Weathering	$\left[\frac{Al_2O_3}{Al_2O_3+CaO+Na_2O}\right]*100$	Harnois, 1988
MWPI: modified Weathering Potential Index	$\left[\frac{Na_2O+K_2O+CaO+MgO}{Na_2O+K_2O+CaO+MgO+SiO_2+Al_2O_3+Fe_2O_3}\right]*100$	Vogel, 1975 (modified after Reiche, 1943)
B Index	$\left[\frac{CaO+K_2O+Na_2O}{Al_2O_3+CaO+K_2O+Na_2O}\right]*100$	Kronberg & Nesbitt, 1981
(K+Ca)/Ti	$\frac{K+Ca}{Ti}$	Harrington and Whitney, 1987

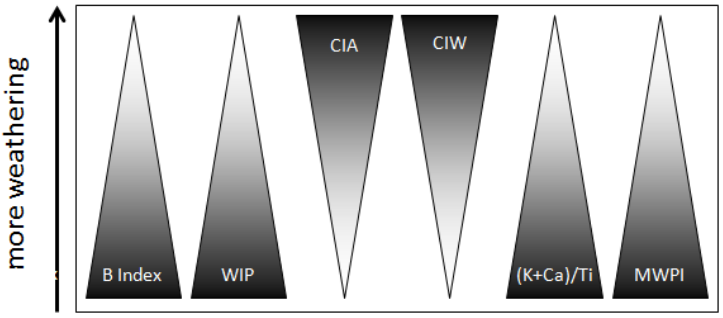

Fig. 2–6: *Relationship between a variety of weathering indices and the amount of weathering. For example B Index is large when little weathering occurred and becomes smaller with more weathering.*

None of these indices is perfect on its own. It's by combining them that one may reconstruct the "big picture".

The WIP values have been corrected for LOI, as this index works not only with the ratios among the elements, but introduces another number. We had to correct the elemental composition for LOI, as the high organic content would strongly dilute the inorganic content and skew the WIP.

2.2.7. C and N content (CHN)

Less than 2mg peat and 3–5mg soil were filled into tin capsules to be measured in a combustion analyzer. The amount of sample weighed was adapted to the roughly estimated carbon content. Too much carbon would oversaturate the sensors.

The samples were measured at the Department of Evolutionary Biology and Environmental Studies (University of Zurich) by René Husi. The standard used was EDTA, which is suitable for these kinds of (high carbon content) samples. It has a carbon content of approx. 41%.

2.2.8. Mineral composition (DRIFT)

Diffuse Reflectance IR Fourier Transformation is a handy tool to gain insight on the organic and inorganic components of soil samples. Looking at key peaks for different soil minerals we can see mineral weathering in our two profiles (Egli et al., 2015).
The CHN measurement showed the peat to have very high C contents (up to 56%). To avoid saturation of the measured absorption with DRIFT, we used KBr to dilute the samples, as KBr is "invisible" to infrared light. We used a ratio of sample: KBr of 1:9 (for both soil and peat).

The resulting spectra were normalized, cut at wavenumber 400 (to avoid the noise below 400) and corrected for baseline. The spectra were examined by eye and determined whether or not

absorption peaks were occurring at certain key wave lengths. The checklist used with the wavelengths in question for different minerals was kindly provided by M. Egli.

2.2.9. Palynological analysis

The palynological analysis was conducted by Dr. Malgorzata Malkiewicz at the Laboratory of Paleobotany, Department of Stratigraphical Geology at the University of Wroclaw.
For the interpretations we were supported by Prof. Dr. Jaroslaw Waroszewski, from the Institute of Soil Science and Environmental Protection at the University of Wroclaw.

One peat core from each site was chosen and prepared according to standard procedures (Moore et al., 1991; Tinner et al., 2005; Malkiewicz et al., 2016).

The preparation included several separate steps: (1) treatment with 10% HCl, 10% KOH, 40% HF, 10% HCl, (2) acetolysis, (3) mounting in glycerol and (4) staining with Fuchsine.

At least 1000 pollen grains per sample were identified and counted, using an optical microscope (Axiostar, Zeiss) with a magnification 400x.
The identified taxa could be subdivided into 3 groups: trees (both coniferous and deciduous) and shrubs, herbaceous plants, and cryptogams.

The data was plotted using POLPAL for Windows (Nalepka and Walanus, 2003).

3. Results

3.1. Soil: Börtli

3.1.1. Soil profiles

The horizons in profile 1 were identified in the field as Ah (0–5cm), AE (5–15cm), Bs (15–60cm), BC (60–unknown). The C horizon could not be reached due to difficulties with the terrain. The horizons of Profile 2 were Ah (0–5cm), AE (5–18cm), BsI (18–60cm), BsII (60–unknown). The C horizon was not reached in this profile either. The excavations were impeded because of the large quantity of large rocks of different shapes scattered in the soil (see *fig. 3–1*).

In both profiles, the AE horizon was only faintly distinguishable from the Ah horizon, mainly due to its more grayish hue.

Fig. 3–1: *Profile 2 with large granitic rocks (white) protruding. (A. Musso, 2015)*

3.1.2. Bulk density, water content, pH and grain size distribution

Dry bulk density in the two soil profiles was between 0.5–0.7g/cm^3 in the top horizon and increased with depth to ca. 1.20–1.30g/cm^3 in the bottom horizon (*fig. 3–2)*. The two profiles show minor differences in the top 15cm but have the same bulk density further below.
Water content in profile 1 was high at the surface and it decreased rapidly through the topmost 10cm and stabilized at around 20% with depth. The water content in profile 2 decreased with depth as well, but more moderately. The main difference in the two profiles lies in the AE horizon.
pH varied from 3.6 to 4.5. It was in both profiles highest in the AH, and in the BC and BSII horizon respectively, and lowest in the AE horizon.

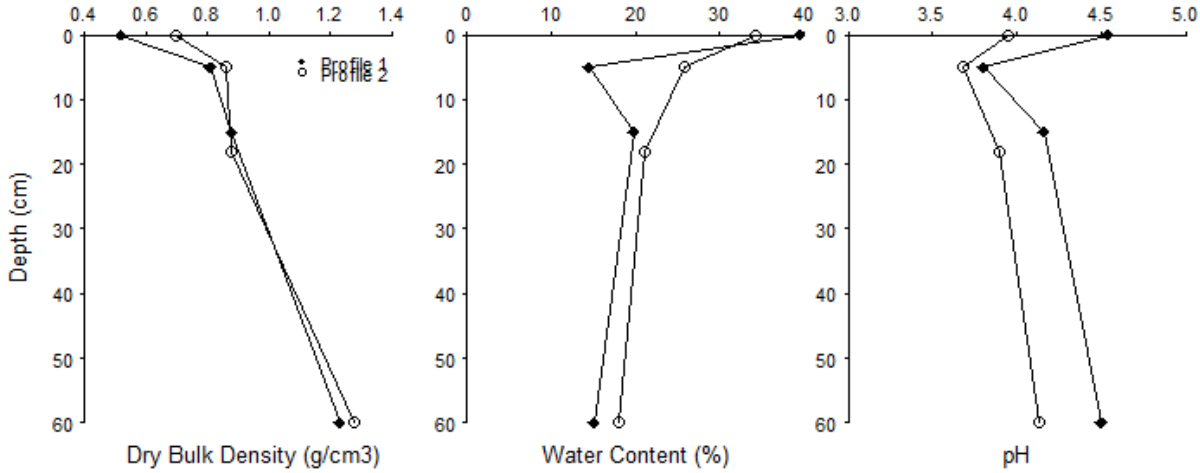

*Fig. **3–2**: Left to right: Dry bulk density (in g/cm^3), water content (%) and pH ($CaCl_2$).*

The grain size distribution (*fig. 3–3)* showed a smooth succession from one horizon to the next in Profile 1 but less so in Profile 2. The slope's top horizons had the smallest sand (7.1–9.0%) and largest clay contents (18.1–25.0%), while the bottom horizons contained by far the most sand (62.7–71.3%) and little clay (4.1–4.2%).

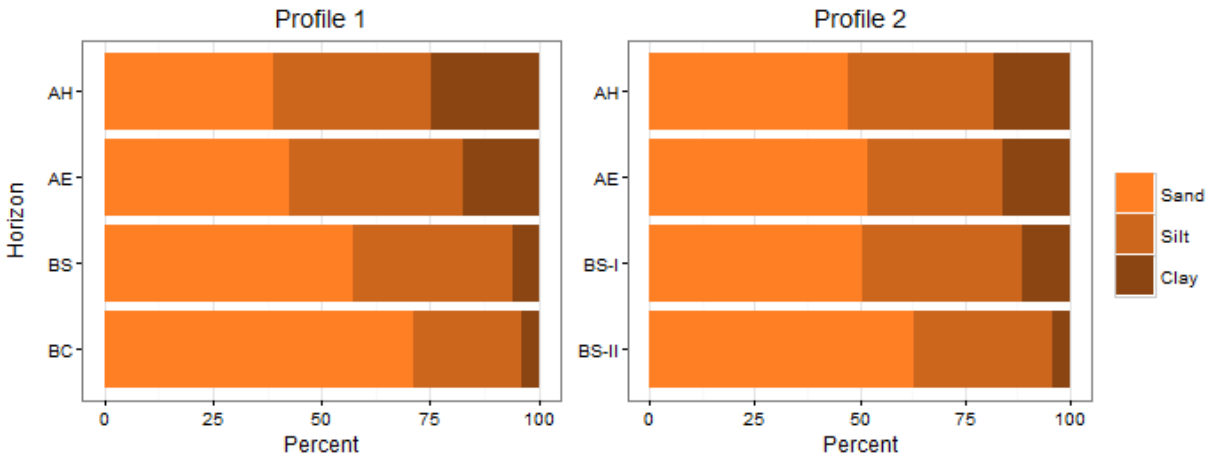

***Fig. 3–3:** Grain size distribution: Sand (250–63 µm), Silt (63–2 µm) and Clay (<2 µm) contents given in cumulative percentages for each horizon.*

3.1.3. Carbon, Nitrogen and Loss on Ignition

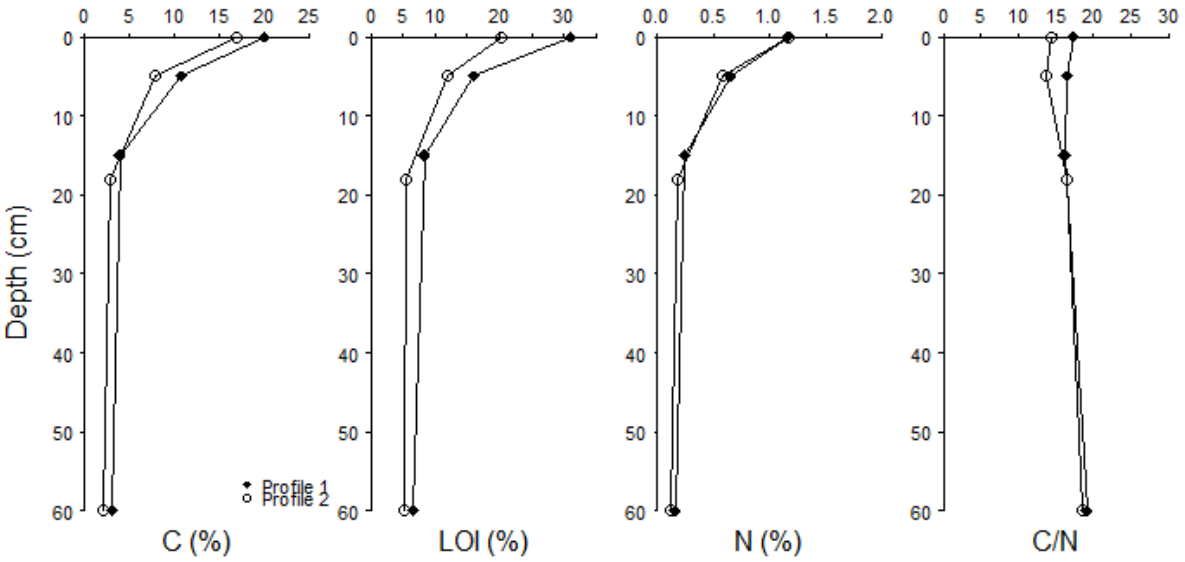

Fig. 3–4: *Carbon (%), Loss on Ignition (%), Nitrogen (%) and C/N ratio of both soil profiles as a function of depth.*

Carbon content (*fig. 3–4)* decreases with depth in both profiles: the maximum carbon content of 20% occurs in the Ah horizon and stabilizes at a minimum of 3–5% at the bottom. Loss on Ignition and nitrogen content also show highest values at the top which decrease and stabilize with depth. The C/N ratio shows only little variation, except for a slight difference between the profiles in the Ah and AE horizons.

3.1.4. Elemental Composition and Weathering

The SiO_2 is smallest in the Ah horizons (45% in Profile 1, 56% in Profile 2) and rapidly increases to a maximum of 59% and 66% respectively in the BS and BsI horizons (*fig. 3–5)*. The difference between the profiles decreases with further depth and the SiO_2 content stabilizes between 57–61%. The SiO_2 content of this slope's soil fit well with the data from Egli et al. (2001) which were also taken in the geological formation of the Aare Massiv.
TiO_2 and ZrO_2 show similar trends. TiO_2 in Profile 1 is consistently higher than in Profile 2. ZrO_2 is more abundant in Profile 2 below the top 10cm, but both profiles have the same ZrO_2 content in their Ah and AE horizons.
The Al_2O_3/TiO_2 shows a general trend of relative decrease in Al_2O_3 with depth. The differences between the profiles are most pronounced close to the surface and they almost vanish in the bottom horizon. Generally, Profile 2 has more Al_2O_3 relative to TiO_2 than Profile 1.

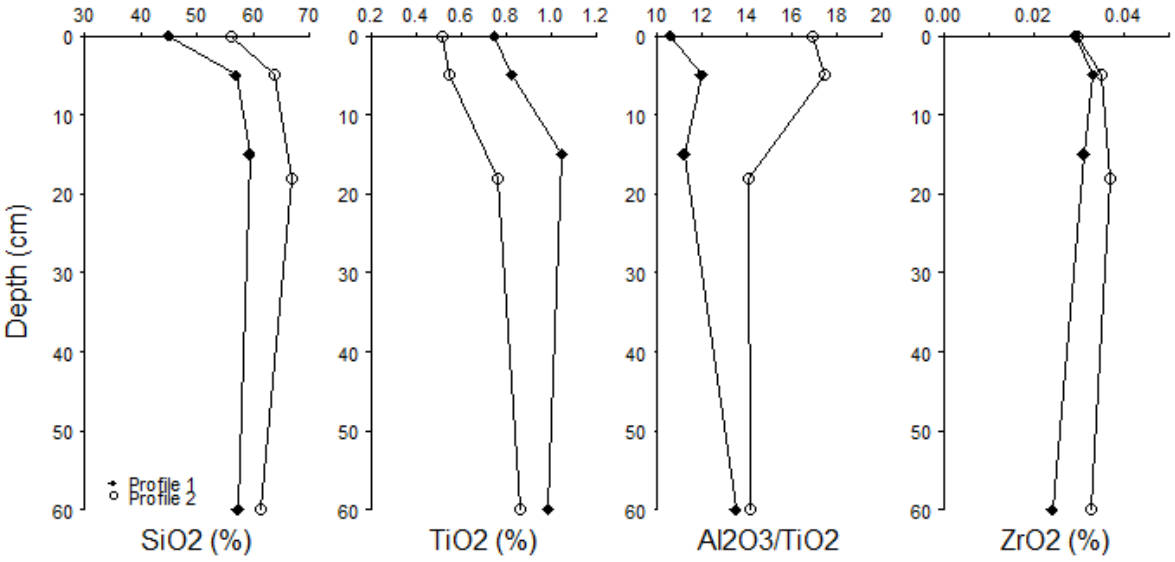

Fig. 3–5: *Silicon–, titanium– and zirconium–oxides (mass–%). Al_2O_3 was normalized to TiO_2 to see the relative accumulation or depletion of Aluminium independent from the inorganic matter content.*

A comparison of the major elements with the Upper Continental Crust and the soils' parent rock, the Central Aare–granite, is plotted in *fig. 3–6*. The elements measured in the soils that had the largest differences to the UCC are mostly plant essential elements phosphorous (slightly elevated in the A horizons), calcium (0.24–0.3), iron (2.3–3.1), and also titanium (1.7–2–0). In comparison to the Central Aare–granite, the magnesium (3.4–4.8), phosphorous (2.6–3.7), titanium (3.2–3.8) and iron (2.3–3.1). There are some differences between the upper two horizons of the profiles (Ah–AE) and the lower two horizons (Bs–BC). In summary, the soils have similar or slightly lower contents to both the UCC, except for calcium, titanium and iron. The comparison with the Central Aare–granite brought out the accumulation of plant essential elements such as magnesium, phosphorous, calcium, iron, and titanium as well.

The peat had a high variability from sample to sample and no clear depth trend but the average of the two cores show an identical profile. The contents of the peat were much lower than either standard, with exception of P which was the only element more abundant in the peat than in the standards. The differences to the either standard were limited to plant essential elements such as magnesium, phosphorous, calcium and iron. The large accumulation of plant essential elements brought in by plants overprints the elemental contents of the mineral matter even stronger than in the soils.

Weathering indices (*fig. 3–7)* indicated that the soil material was more altered with increasing depth when using the (K+Ca)/Ti ratio, B Index, WIP, CIA and CIW. There are consistent differences in the degree of weathering between the two profiles. Profile 1 is more weathered than Profile 2. The differences between the profiles increase slightly with depth.

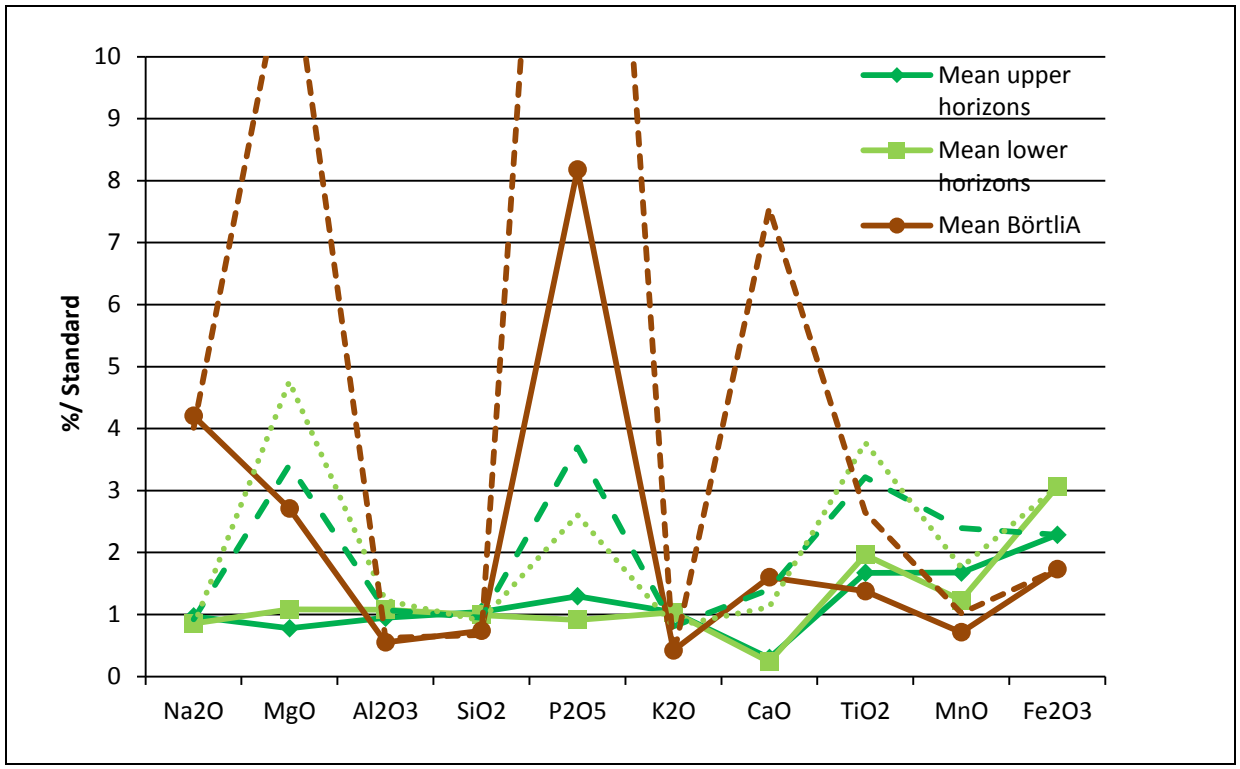

Fig.3–6: *Continuous lines: Ratio of measured elemental content to the Upper Crust Standard by Taylor and McLennan (1985) and Ronov and Yaroshevsky (1969). Dashed lines: Ratio to the parent rock, Aare–granite (Schaltegger, 1989). Y–axis: The scale was shortened to improve readability. X–axis: The most abundant elements (as oxides). The sum of elements was corrected for LOI.*

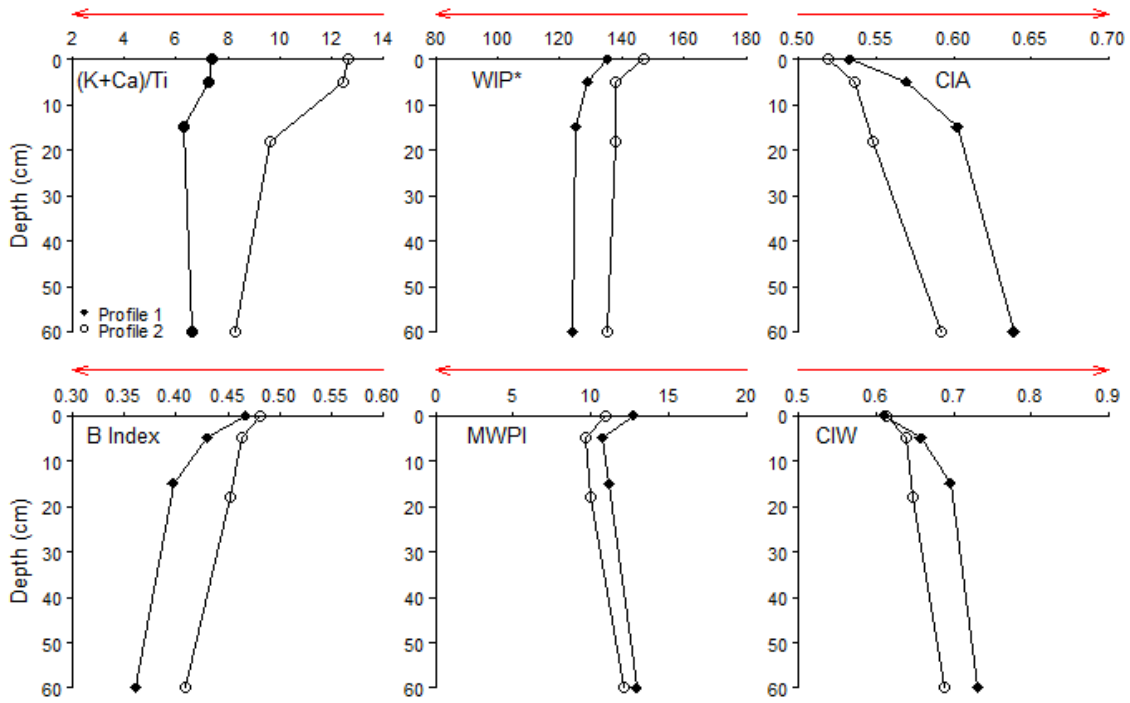

Fig. 3–7: Weathering Indices*. Top row: (K+Ca)/Ti ratio, Weathering Index of Parker, Chemical Index of Alteration. Bottom row: B Index, Modified Weathering Potential Index, Chemical Index of Weathering. The arrows on top of the x–axes indicate towards more weathering. *WIP was corrected for LOI.*

3.1.5. Minerals (DRIFT)

The list in *tab. 3–I* is the end–result of a qualitative evaluation on the likelihood of the presence of the most important minerals.
The absorption curves of each sample were analyzed by eye and the presence or absence of characteristic absorption peaks which each mineral produces were noted in a list.
In a second step, the list was evaluated qualitatively to assess the likelihood of the presence of a mineral in each sample (*tab. 3–I* ; procedure: Egli et al. 2015).

Quartz and Muscovite are the most prominent minerals in these two soil profiles, reflecting the mineral content of the granitic parent rock of the soil. Kaolinite, Gibbsite and Imogolite are secondary minerals that are formed during the chemical weathering of primary minerals such as feldspar, mica, or quartz.
Kaolinite is a layered silicate mineral ($Al_2Si_2O_5(OH)_4$) that is a good indicator for chemical weathering.
Gibbsite is the most abundant of the Al–Hydroxides ($Al(OH)_3$) that is also formed secondarily from weathered feldspars, mica and clay minerals. It's omnipresence in all horizons of both profiles also reflects the granitic parent rock (Blume et al., 2010).

Tab. 3–I: *Qualitative evaluation of the likelihood of the presence of a mineral based on the presence of tell–tale absorption peaks in the MIR–spectrum using DRIFT (procedure by Egli et al. 2015).* ***Samples 1–4: profile 1, samples 13–16: profile 2.*** *x: presence of mineral very likely, (x): presence of mineral is questionable. no sign: most likely absence of mineral.*

Sample	**1**	**2**	**3**	**4**	**13**	**14**	**15**	**16**
Horizon	Ah	AE	Bs	BC	Ah	AE	BsI	BsII
Kaolinite		x	x		x	x	x	
Gibbsite	(x)	(x)	x	x	(x)	x	x	(x)
Imogolite	x		x	x	(x)			(x)
Quartz	(x)	x	x	x	x	x	x	x
Muscovite	x	x	x	x	(x)	(x)	x	x

3.2. Peat: Börtli

3.2.1. Bulk Density, Water Content and pH

Bulk density (*fig. 3–8*) decreased linearly from 0.2 to 0.1g/cm^3 for the first 50–100cm. Börtli A core shows little variation and only one peak at 200cm depth, which speaks for the homogeinity of the peat in this mire. Börtli B core has several abrupt rises in bulk density which were also registered in the water content. Maximum values occur at the peat base. In general, there was a slight decrease trend from top to bottom.
Water content, reflecting the pore space in the peat column shows a high variations and differences between the cores, though some common trends recognizable. The range of this ratio of water to peat weight lies between 2–14. Both cores show an increasing water content for the first 50cm. The highest water content was reached in Core A at 165cm with a ratio of over 90%. Both cores show a parallel increase and then decrease bewteen 200cm and the base. Some indentations or in the curve coincide with those of the bulk density (e.g. 80–90cm, 120–200cm in Core B)
The pH ranges from 3.3 to 3.5. They are highest at the surface, sink to below 3.5 between 50–90cm and rise again with depth to values around 3.8. Again, core B shows a bit more variation than core A.

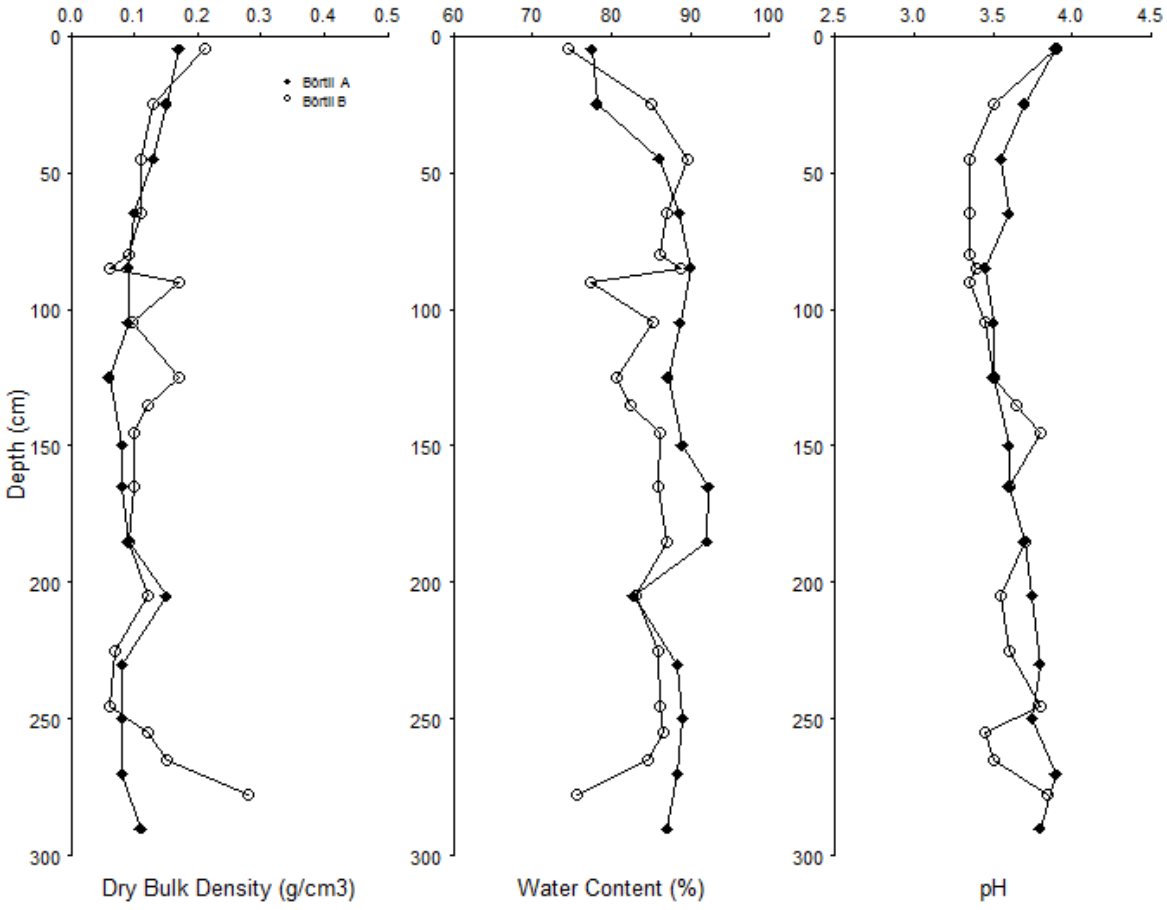

***Fig. 3–8**: Left to right: Dry bulk density (in g/cm^3), water content(%) and pH ($CaCl_2$). Black diamonds:Börtli A; circles: Börtli B.*

3.2.2. Carbon, Loss on Ignition, Nitrogen and Phosporous

The total carbon contents (*fig. 3–9*) lie mostly between 50–55% and can be assumed to represent the organic carbon, as no carbonates would be expected under such acidic conditions. The lowest carbon contents occurred at the top and bottom, and at depths where layers of detritus were found.
Core B showed depths with lower contents where sand layers of several millimeters thickness were found (125cm, 135cm, 205cm and 277cm). This detritus is visible in the LOI profile and in the nutrient ratios (C/N, C/P, N/P) as well. C/N ratios lie between 20 and 50 with an outlier at the peat surface (C/N=10). They showed no clear depth–trend, except for the top 70cm where a slight rise with depth can be recognized.

Both C/P and N/P show a large variability throughout the profile. C/P values generally lie between 90–3600 with an outlier at around 5850. Peaks of P depletion were found at depths of 125–165cm (C/P=2500–3000), 205cm (C/P=3600) and 250cm (C/P=3200) in Börtli A, and at 80cm (C/P=5800) and 165–185cm (C/P=3900) in Börtli B. The C/N values are mostly below the C/N=40 threshold (*fig. 3–9*, red line).
A C/N ratio larger than 40 indicates that microbial decomposition is limited by nitrogen. The Börtli peat lies mostly below this threshold, except for few isolated peaks (most prominently: 205cm in Börtli A core). The same threshold for phosphorous lies at C/P=1000. Only the top 65cm in Börtli A and the top 25cm in Börtli B core are below this threshold; the rest of the profiles are highly depleted in phosphorous.

N/P values lie between 8–120 and the curve has the same shape as the C/P curve. The depths at which the ratio shifted markedly are the same at which the C/P ratio spiked (i.e. where P was strongly depleted relative to carbon). Börtli A showed maxima at 125–165cm (N/P=30–38), 205cm (N/P=52) and 250–270cm (N/P=36).
Börtli B had maxima at 80cm (N/P=128) and 165–185cm (N/P=33–41). The N/P threshold at N/P=15 (*fig. 3–9*, red line) marks the equilibrium point between N and P. A N/P ratio <14 indicates a limitation in nitrogen, a ratio >16 indicates a limitation in phosphorous. It confirms the results from the individual C/N and C/P ratios.

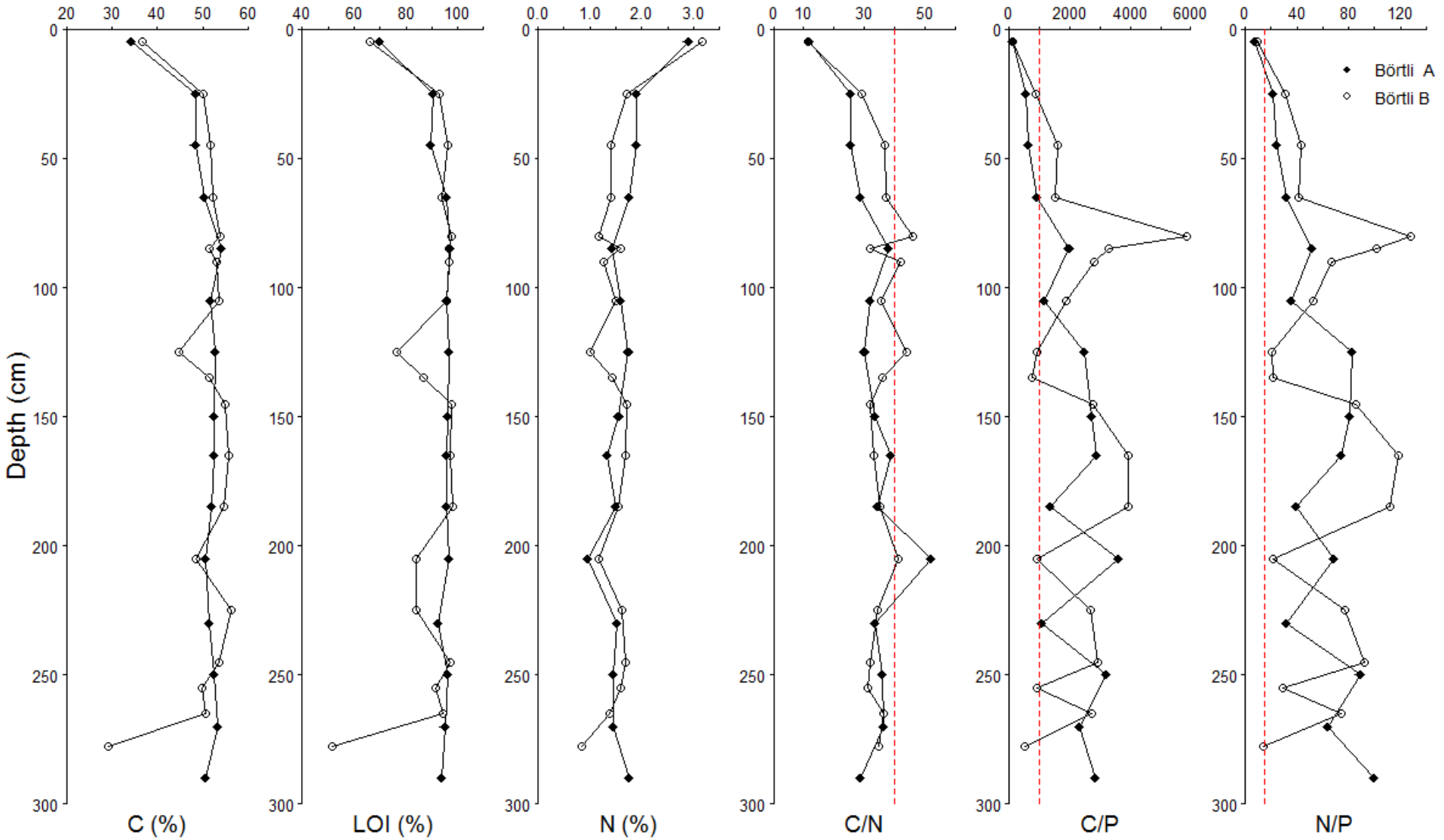

Fig. 3–9: *Carbon (%), Loss on Ignition (%), Nitrogen (%), and the nutrient ratios of C/N, C/P and N/P of both Brätschenflue cores plotted against depth (cm). Red dotted lines: C/N=40, C/P=1000, N/P=15. C/N>40 indicates microbial limitation in N, C/P>1000 in P, N/P<14 in N, and N/P>16 indicates limitation in P (after Wang et al., 2014, Koerselman and Meulman, 1996)*

3.2.3. Elemental Composition and Weathering

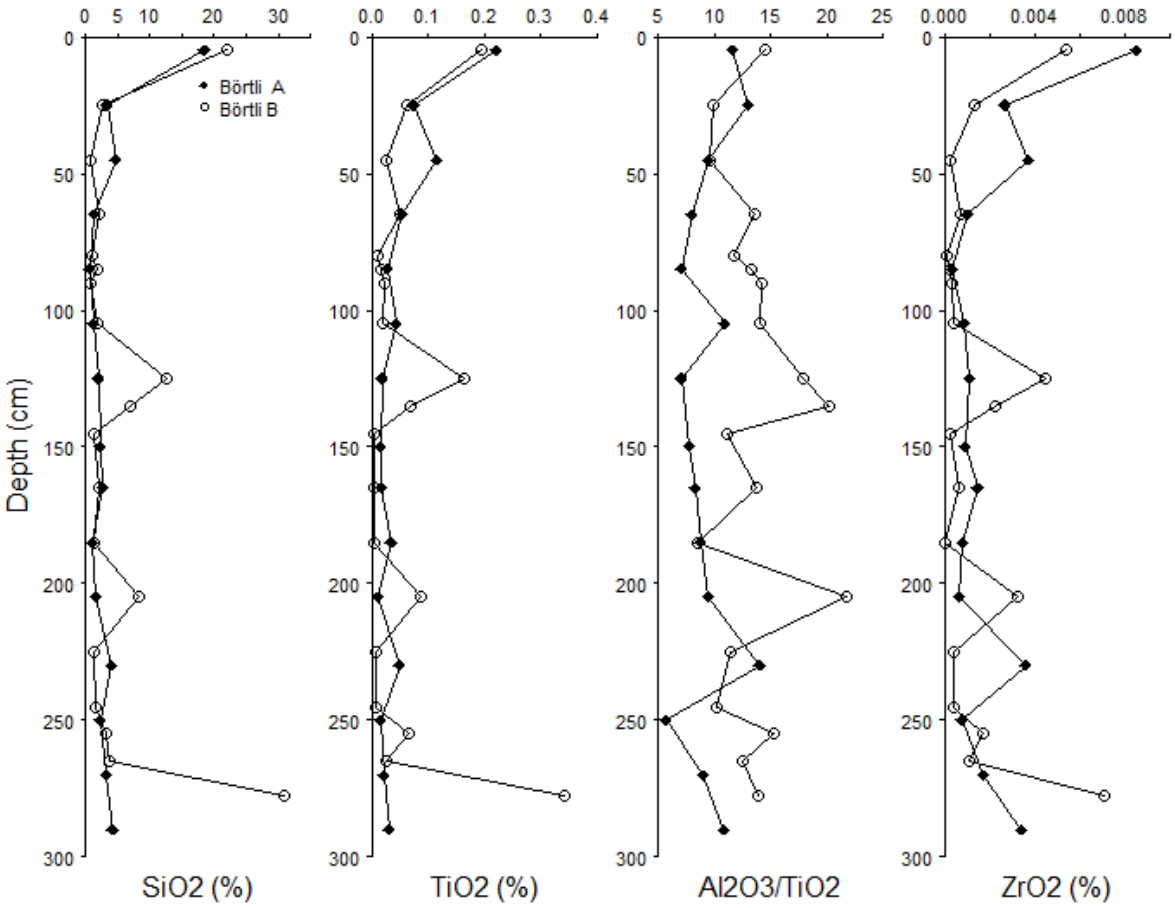

Fig. 3–10: *Silicon–, titanium– and zirconium–oxides (mass–%). Al_2O_3 was normalized to TiO_2 to see the relative accumulation or depletion of aluminium independent from the inorganic matter content.*

The SiO_2 content shows very little variation in the Börtli A core whereas core B has two distinct peaks at 125 to 135 and at 205cm *(fig. 3–10*). These coincide with the four detritus layers found in the peat at 125cm, 135cm, 205cm and 278cm.
TiO_2 contents run parallel to the SiO_2 contents and show the same peaks where the detritus layers occurred. The by far largest amount of titanium was measured at the base of the mire in core B.

Al_2O_3:TiO_2 ratio reveals differences in the depletion of aluminium in core A compared to core B. The maxima occur at the same depths as the detritus layers.
The ZrO_2 curve runs parallel to the TiO_2, showing at which depths larger or smaller amounts of mineral matter was introduced to the peat.

The weathering indices of the peat cores (*fig. 3–11*) show large variations in the profile. There are certain pronounced peaks and depressions that appear in several of the indices. The detritus layers found in Börtli B core at 125cm, 135cm and 205cm and at the base at 278cm

are indicated to be more weathered than the surrounding peat by most indices. Especially the B Index seems very clear, showing large differences between the depths containing detritus layers and the peat above and below. There are, however, no large differences between the cores in terms of degree of weathering, aside from single peaks and depressions that only occur in one of the cores (e.g. at 50cm).

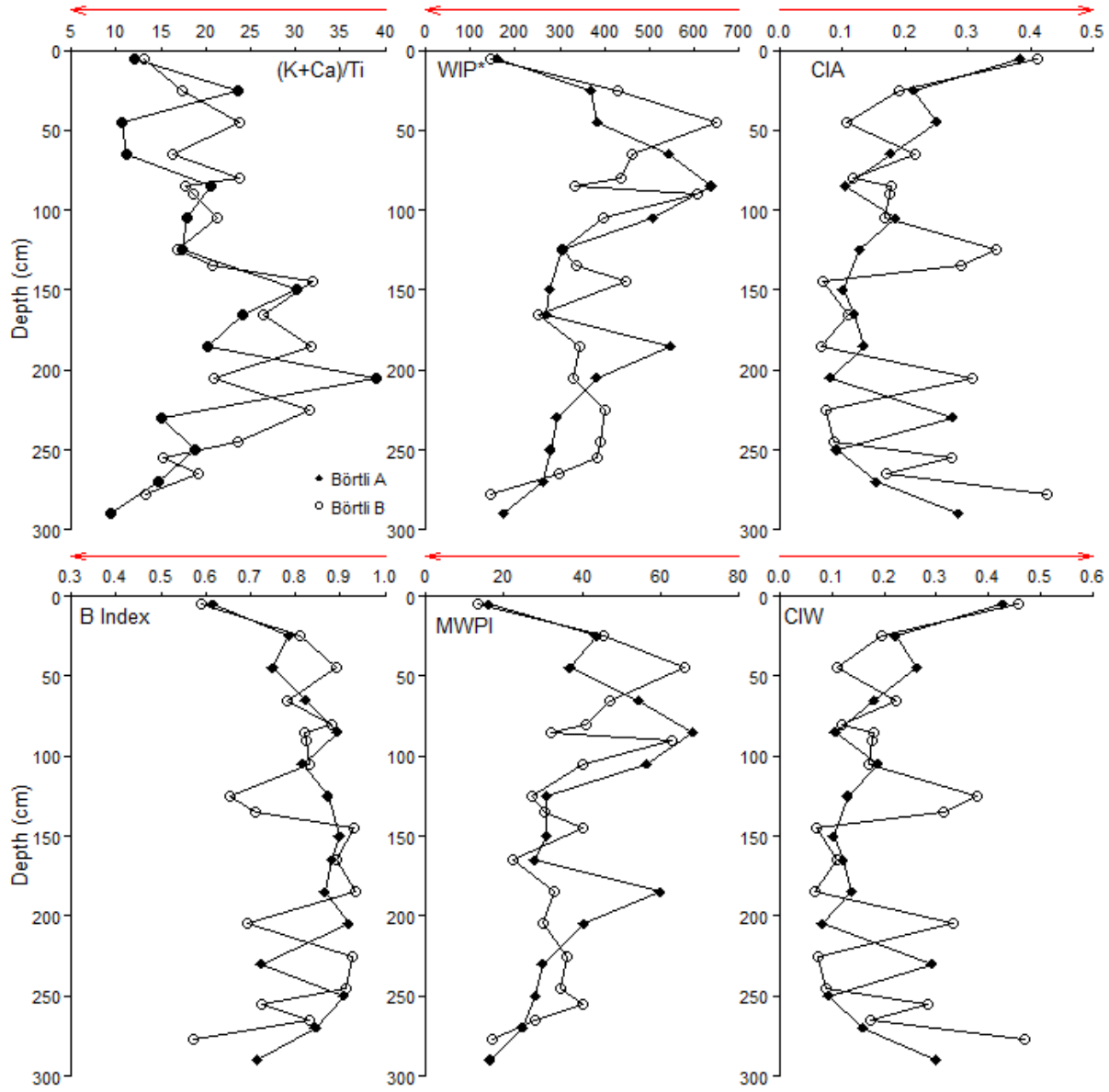

Fig. 3–11: Weathering Indices. *Top row: (K+Ca)/Ti ratio, Weathering Index of Parker, Chemical Index of Alteration. Bottom row: B Index, Modified Weathering Potential Index, Chemical Index of Weathering. The arrows on top of the x–axes indicate towards more weathering. *WIP was corrected for LOI.*

3.2.4. Minerals (DRIFT)

The qualitative assessment on the presence of typical minerals to be expected from weathered granite is compiled in *tab. 3–II*. Börtli A (*tab. 3–II.A*) shows a presence of the secondary mineral Kaolinite and Gibbsite in the top 85cm and 105cm respectively. Quartz is likely to be present given the parent material of the area but the concentrations seem to be too small for it to give a clear absorption signal in the DRIFT.
The same situation exists for muskovite. Börtli B (*tab. 3–II.B*) was several meters closer to the slope and had also picked up some signals from soil erosion. Accordingly, the minerals show a stronger presence.
Kaolinite is also certainly present in the top 85cm and most likely appears again at 205cm and 255cm and might eve span the depths 165–265cm.
Muskovite seems to be present throughout the entire depth of the core, but not very distinctly so.
The depths at which the sand layers had been found (125cm, 135cm, 205cm, and 49cm) show a presence of kaolinite, gibbsite, perhaps quartz and muscovite. The presence of these minerals cannot be wholly confirmed as the large organic matter content (LOI around 90% or higher) made the identification some of the peaks difficult.

Tab. 3–II: A. *Börtli A core.* ***B.*** *Börtli B core. Qualitative evaluation of the likelihood of the presence of a mineral based on the presence of tell–tale absorption peaks in the MIR–spectrum using DRIFT (procedure by Egli et al. 2015). x: presence of mineral very likely, (x): presence of mineral is questionable. no sign: most likely absence of mineral.*

A. Börtli A

Sample	**24**	**26**	**28**	**30**	**32**	**34**	**3674**	**7677**	**5178**	**5380**	**5582**	**8485**	**8687**	**8889**	**9091**
Depth (cm)	5	25	45	65	85	105	125	150	165	185	205	230	250	270	290
Kaolinite	x	x	x	x	x		(x)			(x)		(x)			
Gibbsite	x	x	(x)		x	x	(x)		(x)	(x)	x				
Imogolite			(x)	x	(x)		(x)	(x)	(x)	x	(x)	(x)	x	(x)	
Quartz	x			(x)	(x)	x	(x)	(x)	(x)	(x)	(x)	(x)			(x)
Muskovite	(x)					(x)	(x)	(x)			(x)				(x)

B. Börtli B

Sample	**37**	**39**	**41**	**43**	**45**	**100**	**46**	**112117**	**119**	**120**	**121**	**103**	**105**	**107**	**109**	**47**	**48**	**49**
Depth (cm)	5	25	45	65	80	85	90	105	125	135	145	165	185	205	225	255	265	277.5
Kaolinite	x	x	x	x	x	x		(x)		x		(x)	(x)	x	(x)	x	(x)	
Gibbsite	x		x	(x)	x	(x)	(x)	(x)	x	x	x	x	x	x	x	(x)	x	x
Imogolite	(x)			(x)	(x)	(x)	x		x	x	(x)	x	x	x	x	(x)	(x)	x
Quartz	x	(x)		(x)	x	(x)	x	x	(x)	(x)	(x)	(x)	(x)	(x)	(x)	(x)	(x)	x
Muskovite	(x)	(x)	(x)	(x)	x	(x)	(x)	(x)	(x)	(x)	(x)	(x)	(x)	x	(x)	x	(x)	x

3.2.5. Radiocarbon Ages

The 14C ages were calibrated with the IntCal13 curve (Reimer et al., 2013), using the online calibration tool Oxcal (Oxcal). For the comparison with pollen derived data taken from literature, the uncalibrated radiocarbon ages will be used in the further discussion (*tab. 3–III*).

The ages increase almost linearly down to a depth of 160cm from where on the peat age increases more steeply. Together with the stable bulk density it indicates that peat had accumulated more slowly in the first 1000 years of the bog's existence.
The bottom data point (sample no. 103) shows an age inversion. The real age might lie between 8000 and 8500 yrs BP.

Tab. 3-III: *Radiocarbon results Börtli.*

Sample ID	**UZH– / ETHZ– Numbers**	**Depth (cm)**	**Material**	**$\delta^{13}C$ (‰)**	**Uncalibrated ^{14}C age (yrs BP)**	**Calibrated age range with 95.4% probability (yrs cal. BP)**
115C15AM**40**	UZ–6335 / ETH–66271	30–40	Peat	−25.0 ± 1.0	1745 ± 24	1714–1570
115C15AM**46**	UZ–6336 / ETH–66272	85–95	Wood	−24.9 ± 1.0	3391 ± 25	3695–3576
115C15AM**49**	UZ–6337 / ETH–66273	160–170	Wood	−26.5 ± 1.0	5758 ± 27	6640–6485
115C15AM**59**	UZ–6338 / ETH–66274	235–245	Fiber	−28.2 ± 1.0	8084 ± 30	9121–8815
115C15AM**103**	UZ–6339 / ETH–66275	270–285	Bark/ wood	−25.3 ± 1.0	7112 ± 29	8001–7866

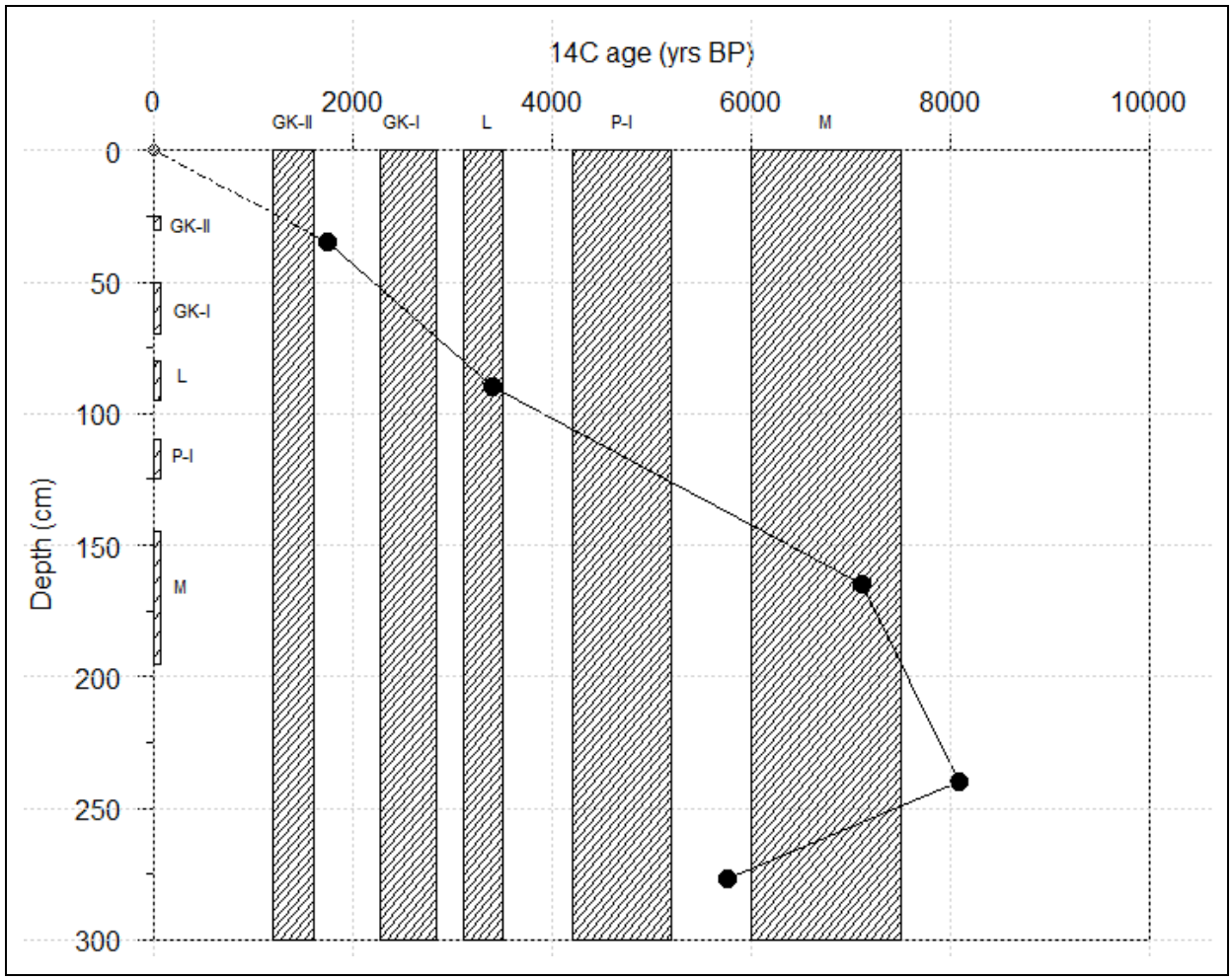

Fig. 3–12: *Uncalibrated radiocarbon ages (black dots). Shaded areas: Climatic shifts (germ. names): GKI and II: Göschener Kaltphase I and II (2830–2270 yrs BP, and 1600–1200 yrs BP), L: Löbben Schwankung (3500–3100 yrs BP); P: Piora Kaltphasen (5200–4200 yrs BP); M: Misoxer Schwankung (7500–6000 yrs BP. (Burga and Perret, 1998). The bars at the y–axis: depth range in the peat to which the climatic shifts correspond. Continuous lines: Assumption of linear peat accumulation and no peat erosion to facilitate interpretation. Dashed line and circle: assumption that at depth zero the age is zero (i.e. "present") as well.*

3.2.6. Pollen

The most dominant tree pollen were Alnus and *Picea abies*, and to a lesser amount *Corylus avellana, Quercus, Ulmus, Abies Alba* and *Fagus sylvatica*. Of the herbs, the most abundant were Cyperaceae (undiff.), Poaceae (undiff.), Apiaceae (undiff.), Ateraceae (undiff) and *Filicales monoletae*.

The AP:NAP ratio was 80–90% and fairly stable, showing only one broad peak in non–arboreal pollen between 170 and 220cm (ca. 7500–8000 yrs BC).

The lower part of the core (230–285cm, 7800 to around 8500 yrs BP) was dominated by Betula (30–48%) and a share of *Picea abies* (ca. 17%). There is a disruption apparent as Betula decreases from 230cm on and Populus, Viburnum, Juniperus, Calluna, Hedera helix and especially Cyperacea (from 4–7 to 30%) increase. There is a reversal shortly after, as Betula experienced a strong increase again, reestablishing dominance.

There was a hiatus noted at a depth of 120–150cm, deprived of pollen. The course of Alnus and of *Picea abies*, and the disproportion of the pollen courses above and below this gap prove that the climatic shift was abrupt. It also proves that the gap must be much larger than 30cm. This speaks for the intensive erosion processes at the Börtli site related to the surrounding relief and the climate oscillations.

After (above) the sedimentological gap, the dominance of Betula diminishes and the Alnus (40%) and *Picea abies* (up to 45%) take over. The appearance of Salix (at 65cm, ca. 2500 yrs BP) suggests more humid climatic conditions, and Fagus and Carpinus indicate a warmer climate. There is also an appearance of typically human–related species, such as Brassicaceae, *Plantago lanceolata*, Calluna and Galium.

(J. Waroszewski, written communication Nov. 2016)

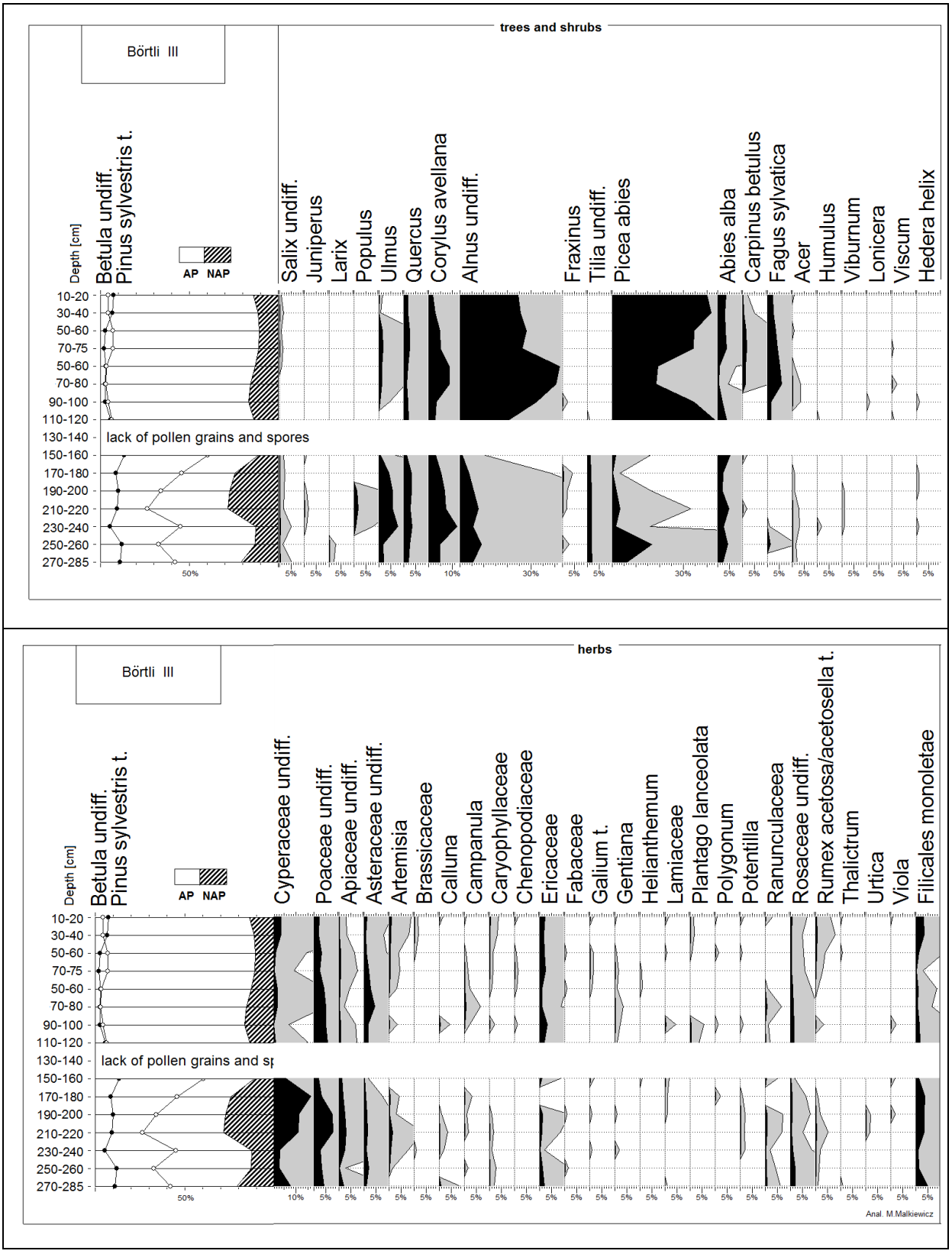

Fig. 3–13: *Pollen diagram for the Börtli mire, divided in half with depth and AP/NAP ratio on the left. Top: Trees and shrubs. Bottom: Herbs. (Analysis: M. Malkiewicz)*

3.3. Peat: Brätschenflue

Unlike at the Börtli site, the two cores at Brätschenflue (BF) were not obtained from the same bog and do not have the same depth, though the aerial distance was only roughly 100m. The maximum depth reached while coring was 300cm (BF A core). BF B core is only 220cm long.
The different depths of the mires mean that the same depths do not have the same age and therefore do not correspond directly to each other. The age difference can be as large as 1000 years.

3.3.1. Bulk Density, water content and pH

Dry bulk density is very low in both cores especially in BF A, rarely reaching above 0.1g/cm^3 *(fig. 3–14)*. Core B is denser at the top (just below 0.2g/cm^3), decreases slightly down to a depth of 70cm and rises again. There is a zone of low density at 150cm which extends down to 200cm. The base itself is as dense as 0.5g/cm^3, mostly due to the detritus.
Water contents show the inverse relationship between water content (or pore space) and the bulk density, showing low contents when the dry bulk density increases and vice versa.
The BF A core's topmost peat has a pH of 3.4 (core B: 3.6). pH and increases to 3.5 until 100cm. After that it increases to 3.7. Highest values are found at the bottom of the mire. From 250cm downwards, the pH increases sharply and reaches a maximum of 4.2 at the base of both cores.

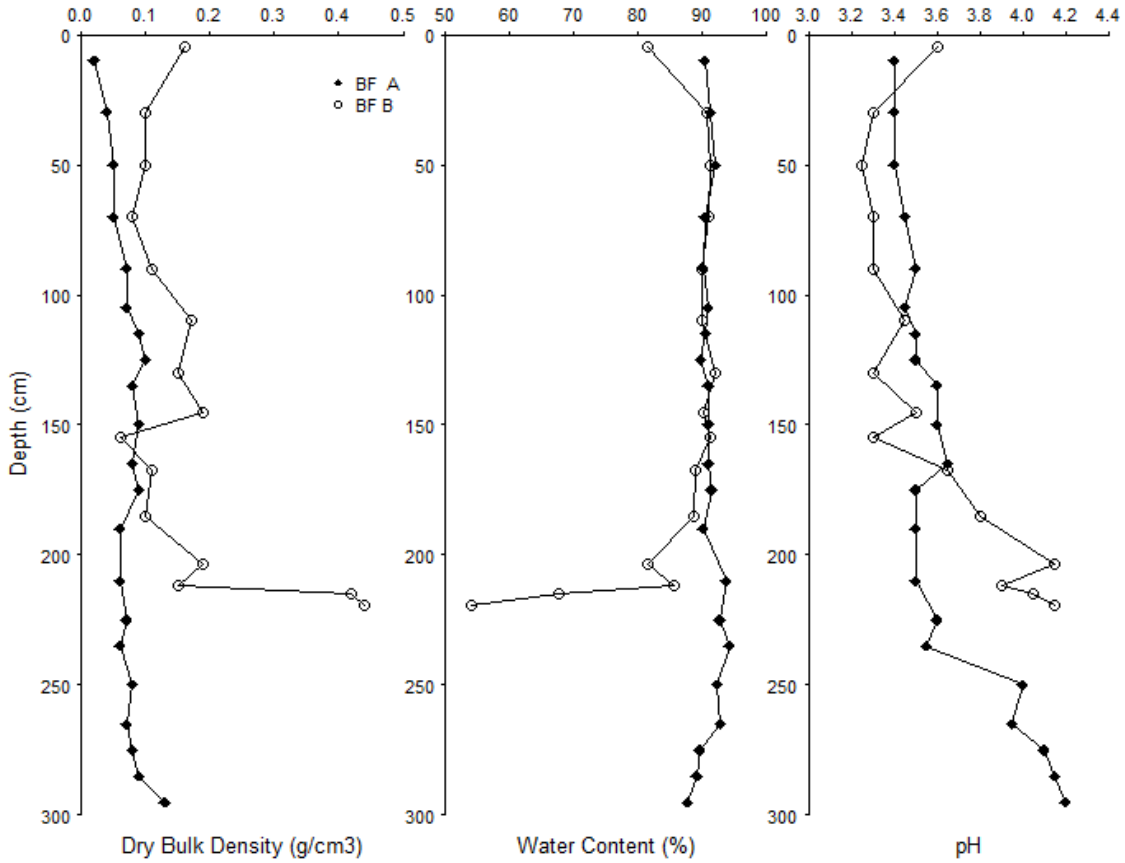

***Fig.3–14**: Dry bulk density (in g/cm^3), water content (%) and pH ($CaCl_2$).*

3.3.2. Carbon, Loss on Ignition, Nitrogen and Phosporous

Carbon contents lie mostly between 45–50% in the upper 150cm and decreased to 30% at the base in the BF A core and 10% in BF B (*fig. 3–15*). Loss on Ignition values correlate strongly with Carbon contents as it can be assumed that there are no carbonates present due to the acidic conditions and the granitic surroundings. Both C and LOI decrease towards the base of the bog as the mineral content increases.

Nitrogen contents of both cores lie roughly between 1–3% (*fig. 3–15*). Core BF A has a very stable content of ca. 2–2.5% N down to a depth of 175cm. There are two minima at 190cm and 235cm (both 0.9%), but the content stabilizes again from 250cm on to the base (300cm) at 2.2–2.5%. The nitrogen in Core BFB decreases constantly below the surface to a minimum of 1.2% and rises again up until a depth of 110cm (1.8%). There is another maximum at 179cm of 3.1% N. Below that the nitrogen content sinks to 1.2% at the core base.

The C/N values mirror the nitrogen contents for both cores (*fig. 3–15),* except in the bottom 50cm of BF B, where it stabilizes at 14–16 because the carbon content of BF B decreases as well as the nitrogen. Core BF A has a C/N ratio between 17 and 22 down to a depth of 175cm. The two maxima at 190cm (C/N=48) and 235cm (C/N=57) mirror the two minima of the nitrogen content. The same connection is recognizable for the maxima in BF B at 50cm (C/N=40) and 125cm (C/N=31). Most values lied below the C/N=40 threshold, indicating that in both BF A and BF B cores, the microbial communities were not limited in nitrogen. Only the afore mentioned peaks of nitrogen depletion were above the threshold.

C/P values show only small oscillations throughout the profile (*fig. 3–15*). BF A has C/P ratio between 890–1400 down to 165cm. There are two large peaks at 190cm (C/P=2566) and at 235cm (C/P=2130). Below that, from 250–295cm the C/P ratio becomes stable again (C/P=236–544). This is similar to the BF B core, except that from 167.5cm on to the base at 219cm the ratio decreases (C/P=140–442 and the minimum at 219cm of C/P=96). The line at C/P=1000 shows that in most of the BF A and BF B profiles microbial decomposition is limited by phosphorous. Only in the bottom 50cm of both cores the phosphorous supply is sufficiently high.

The N/P curve was similar to the C/P but not entirely (*fig. 3–15*). BF A was stable (N/P=46–65) down to 105cm, where a maximum of N/P=70 was measured, followed by a small but distinct minimum at125cm (N/P=47). N/P was stable between 150–225cm (N/P around 55) and decreased to a minimum of N/P=17 at the base at 295cm. BF B showed even fewer oscillations. It was stable down to 145cm, showing a slight increase (N/P= 23 to 56). It was followed by a decrease with oscillations down to the base at 219cm (N/P= 37 to 17). The N/P ratio indicates that almost the entire depth of both BF A and BF B cores is limited in phosphorous. Only the bottom 30cm are close to the equilibrium line at N/P=15.

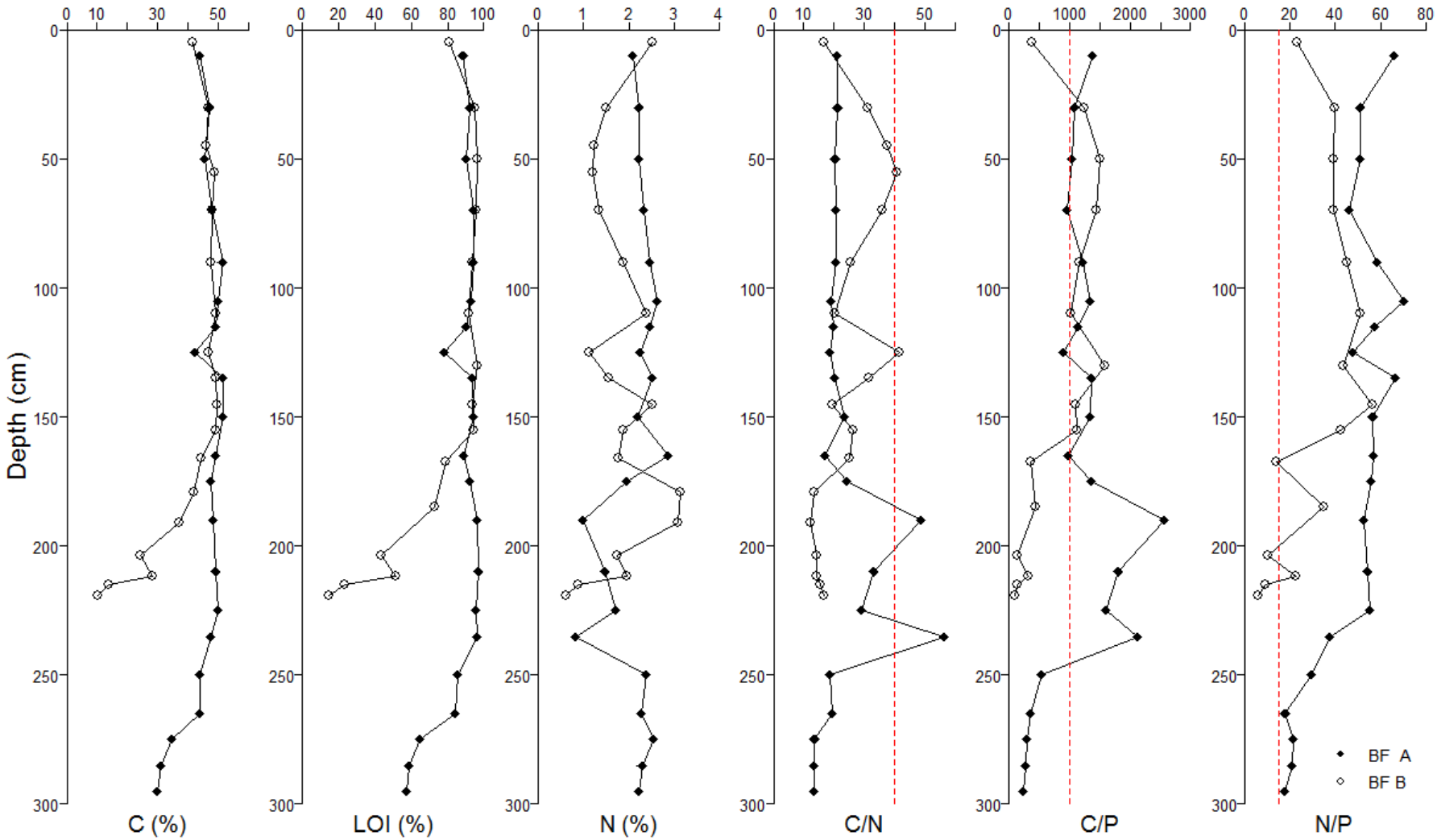

Fig. 3–15: *Carbon (%), Loss on Ignition (%), Nitrogen (%), and the nutrient ratios of C/N, C/P and N/P of both Brätschenflue cores plotted against depth (cm). Red dotted lines: C/N=40, C/P=1000, N/P=15. C/N>40 indicates microbial limitation in N, C/P>1000 in P, N/P<14 in N, and N/P>16 indicates limitation in P (after Wang et al., 2014, Koerselman and Meulman, 1996)*

3.3.3. Elemental Composition and Weathering

Similar to the organic matter content, the silicon content is stable, with one peak at ca 130cm in core A (*fig. 3–16*). It increases towards the base of the peat as the peat becomes increasingly "silty" and "sandy" (rather than fibery). As the mineral contents increase, so do titanium and zirconium.

The Al_2O_3:TiO_2 ratio lies between 5–20. Core A is fairly stable to a depth of 175cm after which is rises considerably, indicating an accumulation of aluminium relative to titanium.

ZrO_2 shows the same peaks at 125cm and 165cm in BF A as SiO_2, TiO_2 and the Al_2O_3:TiO_2 ratio, indicating a small input of mineral matter. It also indicates a mineral input at 165cm in BF B, and perhaps at 200cm as well, though seeing how close to the base the latter is, it is difficult to distinguish between base sediment and washed in sediment.

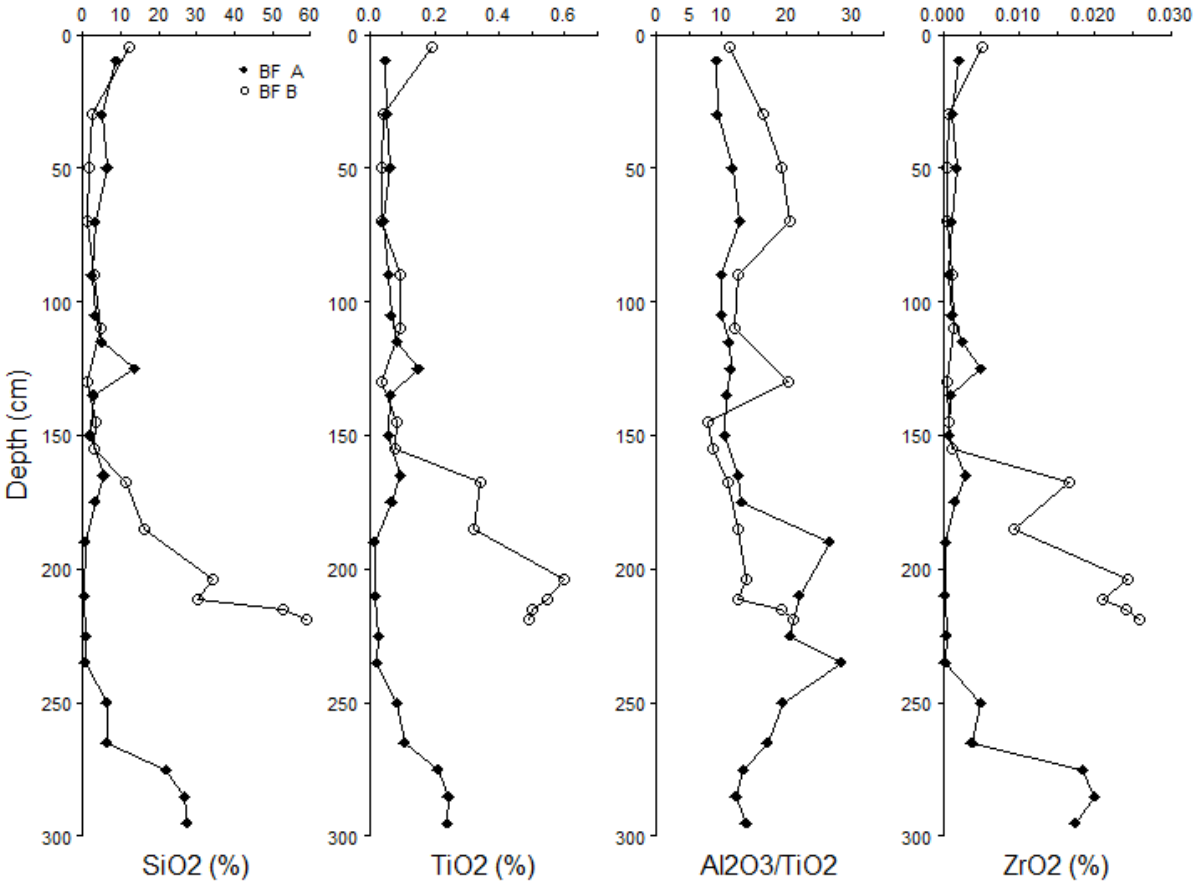

Fig. 3–16: *Silicon–, titanium– and zirconium–oxides (mass–%). Al_2O_3 was normalized to TiO_2 to see the relative accumulation or depletion of aluminium independent from the inorganic matter content..*

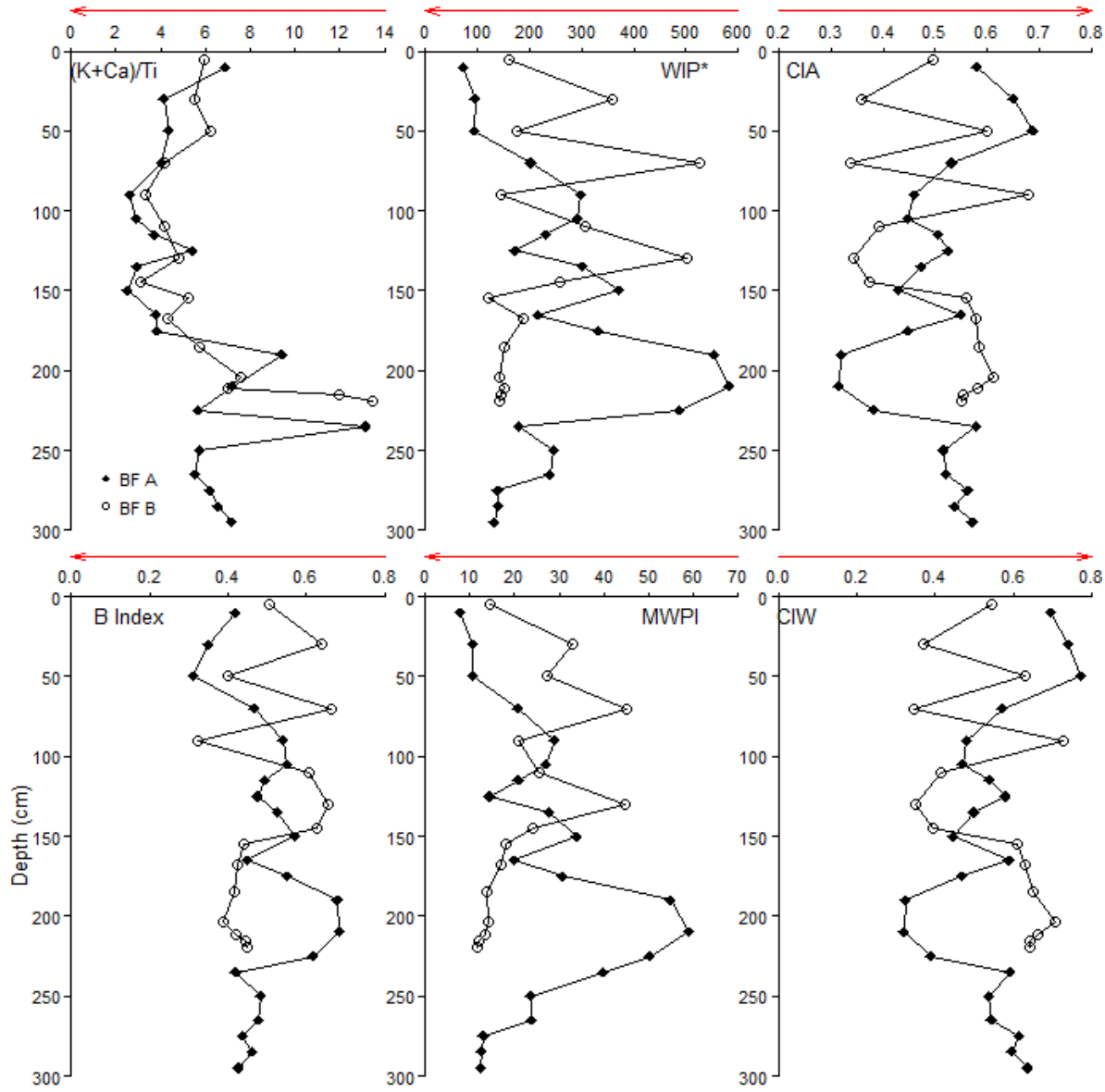

Fig. 3–17: Weathering Indices. *Top row: (K+Ca)/Ti ratio, Weathering Index of Parker, Chemical Index of Alteration. Bottom row: B Index, Modified Weathering Potential Index, Chemical Index of Weathering. The arrows on top of the x–axes indicate towards more weathering. *WIP was corrected for LOI.*

The amount of chemical weathering experienced in the two mires is similar, although they do not correlate well with each other (*fig. 3–17*). There are peaks that do seem to correlate (e.g. the minimum at 200cm in BF A and 130cm in BF B), but radiocarbon dating suggests a temporal shift. It does not, however, exclude the possibility of erosion of peat, skewing the depth profile of BF B.

The (K+Ca)/Ti ratio is rather low down to about 160cm, below which it increases twofold, indicating less weathering.

The most pronounced peak, indicating low chemical weathering at 200cm in core BF A, was not mirrored in the other parameters. There might be some parallels in the nitrogen content (and C/N ratio) or in the Al_2O_3:TiO_2 ratio, though not in the LOI or SiO_2 content. There is a similar peak of lesser chemical weathering in the BF B core at 165cm
The small SiO_2 peak at 125cm in core A was registered as an increase in chemical weathering; the peak at 165cm was as well.

3.3.4. Minerals (DRIFT)

BF A core has a more or less consistent presence of Kaolinite down to 165cm (*tab. 3–IV*) and a possible one from 250–295cm (the base).
Another relatively prominent mineral in this core is muscovite, being most likely present at 30–165cm and not to be excluded entirely at a depth of 175–235cm and 265–285cm. In base sample at 295cm muscovite is most likely present again.
Quartz is similarly often present as muscovite. It is most likely present at 20–235cm (though doubtful at 30cm, 115cm and 210–225cm). It is also present at the bottom of the core, at 265–295cm.
Imogolite seems to have accumulated in the top half of the peat profile (down to 165cm) rather than in the lower section. The certainty of its presence is only sure at 50–90cm and remains doubtful for the top section. The bottom section has either certainly no Imogolite or its presence is doubtful.

BF B core (*tab. 3–V*) doesn't have any obvious trends in its mineral composition. The presence of kaolinite seems to occur throughout the entire core but its likelihood is mostly doubtful. That applies for imogolite as well.
Quartz is present at almost all depths.
Muscovite has a doubtful presence at most depths, but is only certainly present at 50cm, 130cm, 155cm, 211.5cm, and at the basis at 219cm.

Tab. 3–IV: *Brätschenflue A core (split in two). Qualitative evaluation of the likelihood of the presence of a mineral based on the presence of tell–tale absorption peaks in the MIR–spectrum using DRIFT (procedure by Egli et al. 2015). x: presence of mineral very likely, (x): presence of mineral is questionable, no sign: most likely absence of mineral.*

Sample	**122123**	**124125**	**126127**	**128129**	**130131**	**132**	**133**	**134**	**135**	**136137**	**138**
Depth (cm)	20	30	50	70	90	105	115	125	135	150	165
Kaolinite	x	(x)	x	(x)	x	x	(x)	x	(x)	x	(x)
Gibbsite	(x)		(x)	(x)	(x)	(x)		(x)		(x)	
Imogolite	(x)	(x)	x	x	x	(x)		x	(x)	(x)	x
Quartz	x	(x)	x	x	x	x	(x)	x	x	x	x
Muskovite	(x)	x	x	x	x	x	x	x	x	(x)	x

Sample	**139**	**140141**	**142143**	**144**	**145**	**146147**	**148**	**149**	**150**	**151**
Depth (cm)	175	190	210	225	235	250	265	275	285	295
Kaolinite						(x)	(x)	(x)	(x)	(x)
Gibbsite		(x)	(x)	x		(x)			x	x
Imogolite	(x)				(x)		(x)		(x)	(x)
Quartz	x	x	(x)	(x)	x		x	x	x	x
Muskovite	(x)	(x)	(x)	(x)	(x)		(x)	(x)	(x)	x

Tab. 3–V: *Brätschenflue B core (split in two). Qualitative evaluation of the likelihood of the presence of a mineral based on the presence of tell–tale absorption peaks in the MIR–spectrum using DRIFT (procedure by Egli et al. 2015).*

	152	**154155**	**156157**	**158159**	**160161**	**162163**	**164165**	**166**
Depth (cm)	5	30	50	70	90	110	130	145
Kaolinite	x	(x)	(x)	(x)		(x)	(x)	x
Gibbsite		(x)	(x)					
Imogolite	x		(x)	x	(x)	(x)	(x)	x
Quartz	x	x	x		(x)	x	x	
Muskovite	(x)	(x)	x	(x)		(x)	x	(x)

	167	**168**	**169170**	**171**	**172**	**173**	**174**
Depth (cm)	155	166	185	204	211.5	215	219
Kaolinite	(x)	x	(x)	x		(x)	(x)
Gibbsite		(x)		x	x	x	x
Imogolite	x	(x)			(x)	(x)	
Quartz	x	x	x	x	x	(x)	(x)
Muskovite	x	(x)	(x)	(x)	x	(x)	x

3.3.5. Radiocarbon Ages

The 14C ages were calibrated with Oxcal, and are given are given with the 95.4% probability range (*tab. 3–VI,* Oxcal; calibration curves see Appendix XIX).
The peat accumulation seems to have happened rather evenly (*fig. 3–18*). The slope from the uppermost data point to the second is a bit steeper than the slope underneath but all in all it is a fairly linear trend. These difference may suggest that the age trend in the two peat profiles are not just dependent on the general climatic conditions (which influence peat growth), but are more influenced on the (climatic or other) conditions or events on a smaller scale.

Tab. 3–VI: *Radiocarbon results Brätschenflue. Samples159 and 169 belong to core BF B, the others to core BF A.*

Sample ID	**UZH– / ETHZ– Numbers**	**Depth (cm)**	**Material**	**$\delta^{13}C$ (‰)**	**Uncalibrated ^{14}C age (yrs BP)**	**Calibrated age range with 95.4% probability (yrs cal. BP)**
115C15AM**125**	UZ–6330 / ETH–66266	30–40	fiber	–24.2 ± 1.0	427 ± 23	520–463
115C15AM**132**	UZ–6331 / ETH–66267	100–110	fiber	–26.3 ± 1.0	1624 ± 24	1568–1415
115C15AM**137**	UZ–6332 / ETH–66268	150–160	fiber	–26.3 ± 1.0	3071 ± 25	3359–3215
115C15AM**147**	UZ–6333 / ETH–66269	250–260	fiber	–26.6 ± 1.0	6086 ± 28	7149–6859
115C15AM**151**	UZ–6334 / ETH–66270	290–300	fiber	–28.1 ± 1.0	7731 ± 30	8581–8434
115C15AM**159**	UZ–6384 / ETH–69488	70–80	fiber	–24.5 ± 1.0	1910 ± 27	1929–1743
115C15AM**169**	UZ–6385 / ETH–69489	171.5–185	bark	–22.4 ± 1.0	4594 ± 29	5448–5083

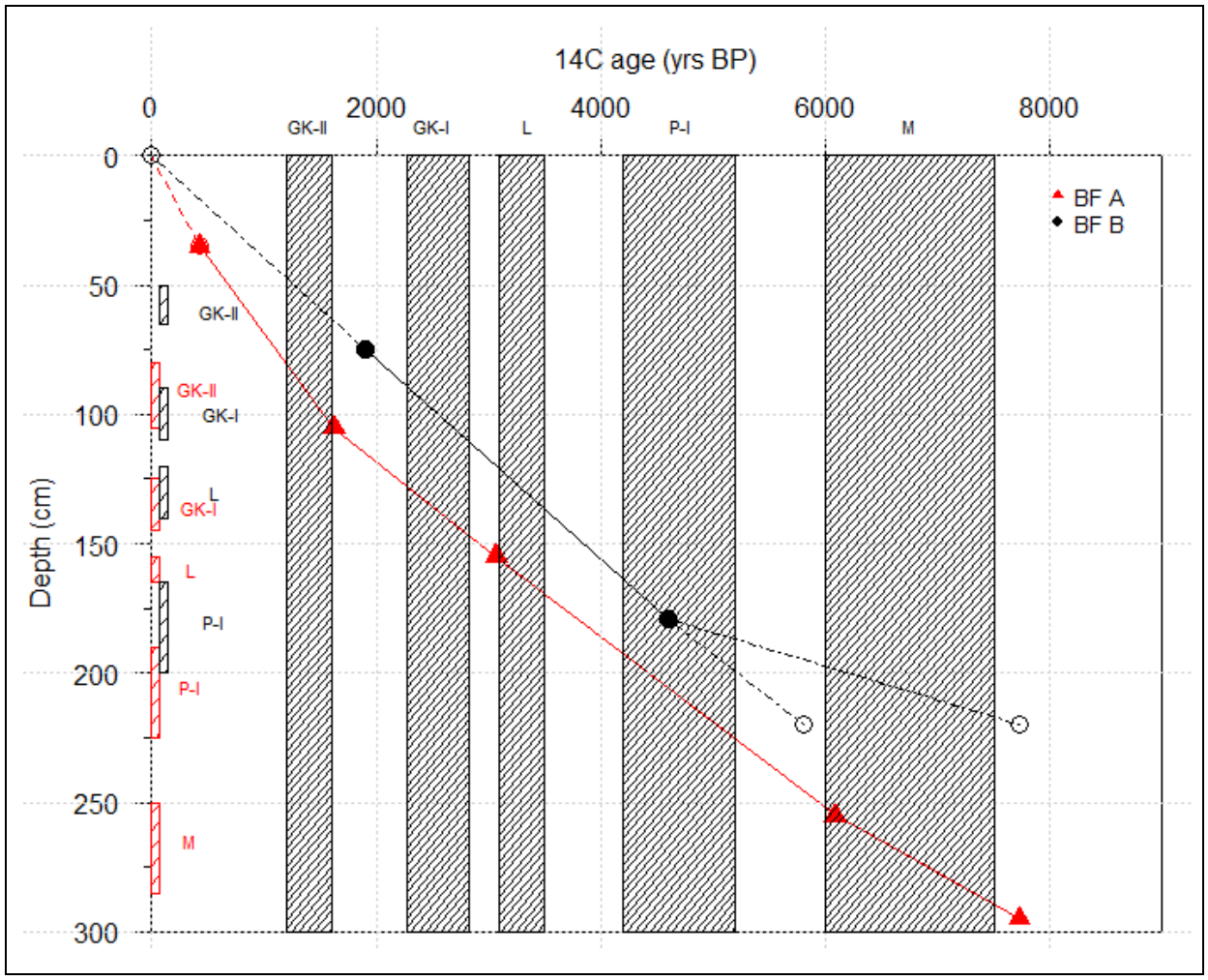

Fig. 3–18: *Radiocarbon ages. Shaded areas: Climatic changes: GKI and II: Göschener Kaltphase I and II (2830–2270 yrs BP, and 1600–1200 yrs BP), L: Löbben Schwankung (3500–3100 yrs BP); P: Piora Kaltphasen (5200–4200 yrs BP); M: Misoxer Schwankung (7500–6000 yrs BP. (Burga and Perret, 1998)). The bars on the left side represent the depth range to which the climatic changes correspond. The dashed lines represent different assumptions: One assumption is that at depth zero, the age is zero as well (i.e. "present", assuming no peat erosion). At the bottom of core BF B ("BF1") the dashed lines represent either the assumption that the peat growth was linear, thus reaching a maximum age of ca. 5800 ^{14}C yrs BP. The other dotted line, assumes that both bogs have the same age at the base, 7700 ^{14}C yrs BP (maximum depth reached in core B was 220cm).*

3.3.6. Pollen

The pollen analysis (*fig. 3–19*) yielded more data from trees and shrubs and little from herbs. The cryptogam group is represented mostly by one species. The tree species that provided the most pollen were *Picea abies*, *Corylus avellana*, Ulnus, *Abies alba*, and to a lesser extent even Quercus and Populus. The herb pollen were mostly made up by Cyperaceae and Poaceae.

The AP:NAP ratio (arboreal pollen to non–arboreal pollen) was at around 80–90% AP with several indentations. Indicating a increasing amount of NAP at 171.5–185cm (ca. 4600 yrs BP), 100–110cm (ca. 2500 yrs BP), 70–80cm (ca 1900 yrs BP) and from 40–50cm on (ca. 1500 yrs BP) to the surface. The variations in the AP:NAP ratio were usually mirrored by *Pinus sylvestris* which increased as the AP did. Betula showed a rapid decrease between the 210–220c sample (219cm depth) and the 160–172.5cm sample, and did not recover.
The core can be subdivided into four zones.

Zone I (220–171.5cm) has a high share of Corylus (20–35%) and is accompanied by Betula (18–28%), Pinus (9–14), Ulmus (8%), Alnus (4–12%), Quercus (3%) and Tilia (2–3%). These species indicate an occurrence of mixed forests at this time period, that were not very dense and had an open structure (Calluna, Poaceae). Salix and *Huperzia selagdo* indicate semi–cold, humid conditions. This period can be linked to the Piora oscillations that occurred around 5200–4200 yrs BP. At the end of Zone I, the assemblage rapidly changes and shifts to Picea, Pinus, Abies and Fagus. There is also a collapse of Betula (3–5%) and an increase of Pinus (around 30%). This rapid change and the shapes of the individual species strongly suggest the presence of a hiatus. This change was probably connected with climate warming, rather than a single disaster.

Zone II (171.5–110cm) was marked by an increase of Pinus (up to 50%), Picea (30%), Alnus (10–25%), Abies (5–7%) and Fagus (3–4%). There is also a constant increase of Cyperacea during this period.

Zone III (110–70cm) begins with as strong decrease of Pinus (from 50% to 20%), accompanied by a decrease of Alnus and Picea. These fluctuations correlate with a an appearance of Populus (2.6%) and an increase of Cyperaceae and Poaceae. The presence of Populus may reflect environmental changes, as it is a plant well adapted to fire.

Zone IV (70–0cm) is dominated by Pinus (30–50%), Piceae (20%) and Alnus (10–15%). Human activity becomes more evident at the surface, with a high share of NAP and the appearance of human activity related species such as Cerealia, Calluna, Rumex, Rannunculaceae, Galium, Plantago, Brassicacea and Cypaeraceae.
(J. Waroszewski, written communication Sept. 2016)

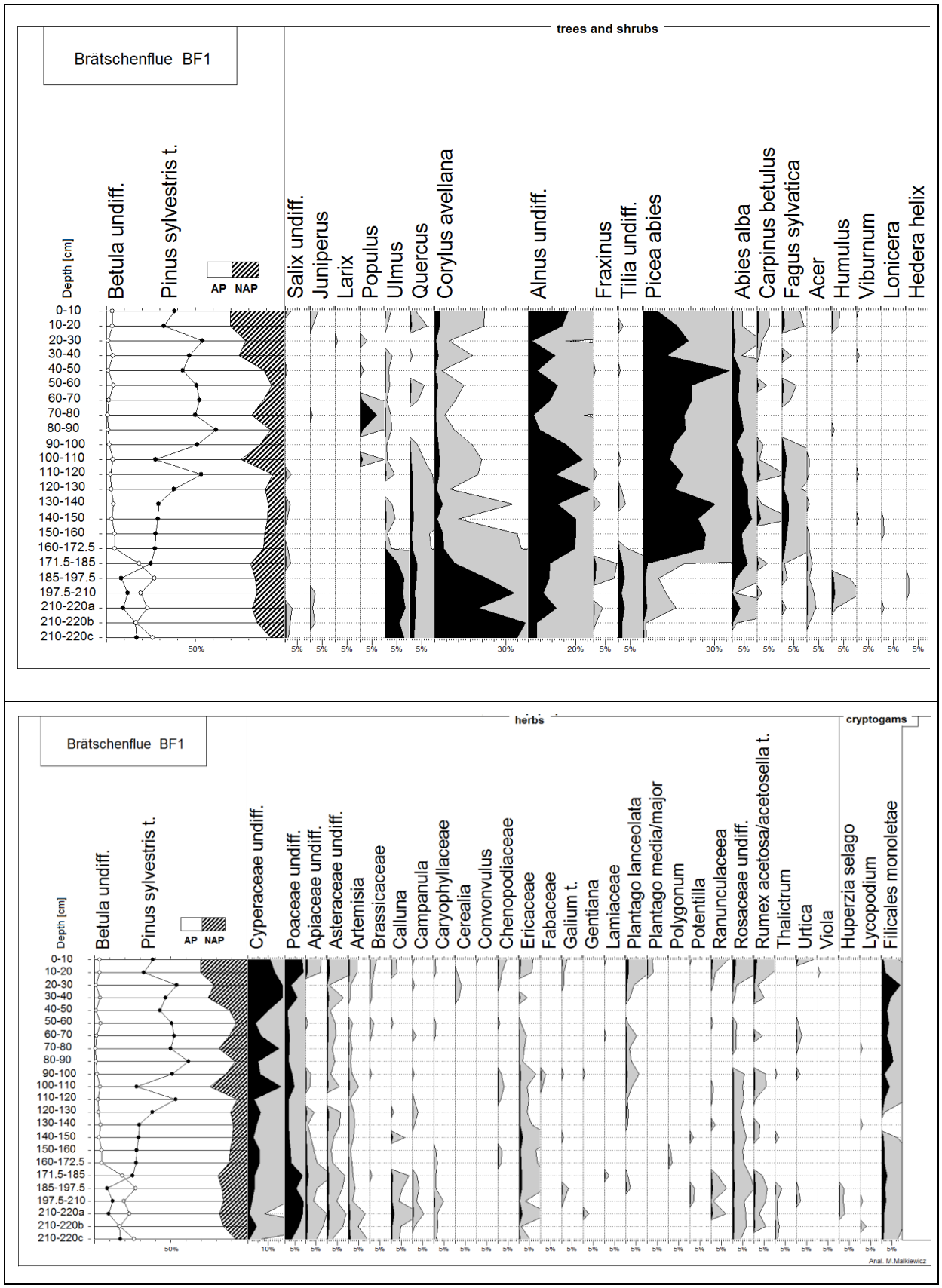

Fig. 3–19: *Pollen diagram for the Brätschenflue site, taken from the BF B core, divided in half with depth and AP/NAP ratio on the left. Top: Trees and shrubs. Bottom: Herbs and cryptogams.(Analysis: M. Malkiewicz)*

3.4. Statistical predictions based on DRIFT data

The aim was to create partial least squares models in order to predict the contents of different elements with DRIFT spectra (which operates with mid-IR).

To produce the model, we used the R package by Mevik et al. (2015) (further adapted and provided by Dr. Samuel Abiven, see Cotrufo et al. 2016). We combined the absorption data at the different wavelengths (ranging from 400–4000) with the XRF–measured data. The elements we tried to predict were the following: Na, Mg, Al, Si, P, K, Ca, Ti, Mn, and Fe.

The highest variance explained was in most cases with 5 components, reaching over 99% (*tab. 3–VII*). Phosphorous was the exception.

The root mean square error of prediction (RMSEP) was calculated for different numbers of components used (*tab. 3–VIII*). 5 components scored the smallest RMSEP for all elements except for phosphorous which had the smallest RMSEP when using only 2 components. *Fig. 3–20* shows the validation models, with the model predictions as a function of the measured data. Silicon, phosphorous and calcium had the poorest fit of these ten elements, explaining 99.1%, 98.98% and 99.02% of the variance. What is also visible in the validation graphs is that many of the values are concentrated in a narrow range, which makes it more difficult for the model to make predictions on (e.g. Ti, K, Mn).

The scores looked satisfactory as well. There were no autocorrelation between the two most explaining components detectable (Appendix XVII).

No validation was performed to test the models as the number of data points was only 70.

Tab. 3–VII: *Variance explained (in %) with increasing number of components.*

	1 Comp	2 Comps	3 Comps	4 Comps	5 Comps
Si	93.84	96.61	97.77	98.56	99.1
Ti	93.83	96.49	97.87	98.77	99.13
Fe	93.86	96.66	97.51	98.51	99.09
P	93.88	96.55	97.52	98.6	98.98
Na	93.89	96.26	97.54	98.52	99.14
Ca	93.89	96.55	97.17	98.41	99.02
Al	93.83	96.55	97.75	98.67	99.14
Mn	93.84	96.67	97.49	98.47	99.02
Mg	93.85	96.61	97.59	98.52	99.12
K	93.84	96.58	97.77	98.55	99.13

Tab. 3–VIII: *Root mean square error of prediction (RMSEP) with number of components.*

	1 Comp	2 Comps	3 Comps	4 Comps	5 Comps
Si	4.489	3.098	2.728	2.181	1.955
Ti	0.07166	0.0456	0.03927	0.03562	0.03554
Fe	0.3896	0.3116	0.3002	0.2857	0.2768
P	0.05639	0.05497	0.05597	0.05586	0.05594
Na	0.4244	0.3793	0.3416	0.2996	0.2943
Ca	0.1906	0.1823	0.1701	0.1642	0.1608
Al	1.26	0.8468	0.7108	0.5809	0.5234
Mn	0.009159	0.007589	0.007395	0.007265	0.007204
Mg	0.1985	0.1492	0.1223	0.09756	0.09227
K	0.4243	0.3076	0.2695	0.2156	0.2016

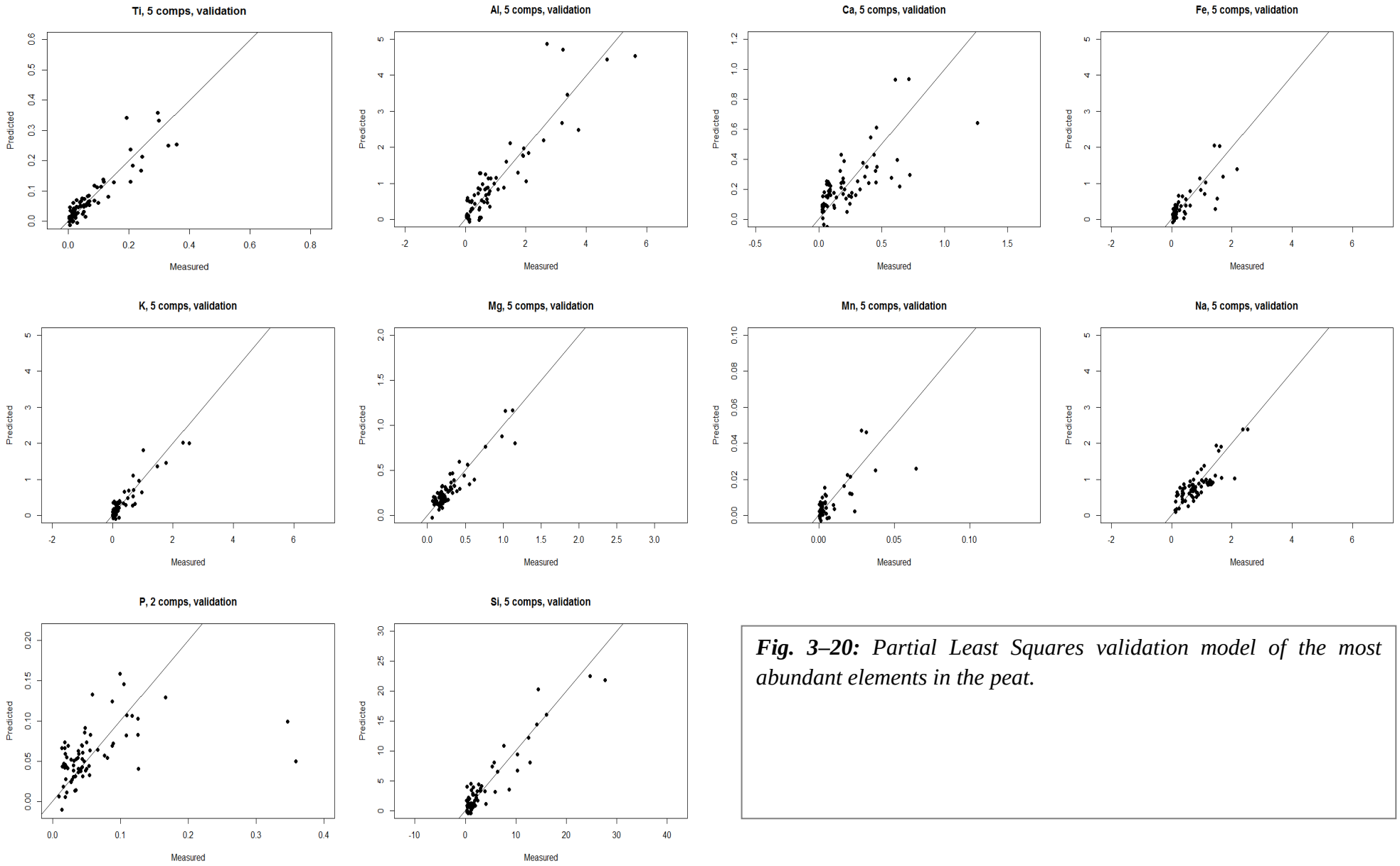

Fig. 3–20: *Partial Least Squares validation model of the most abundant elements in the peat.*

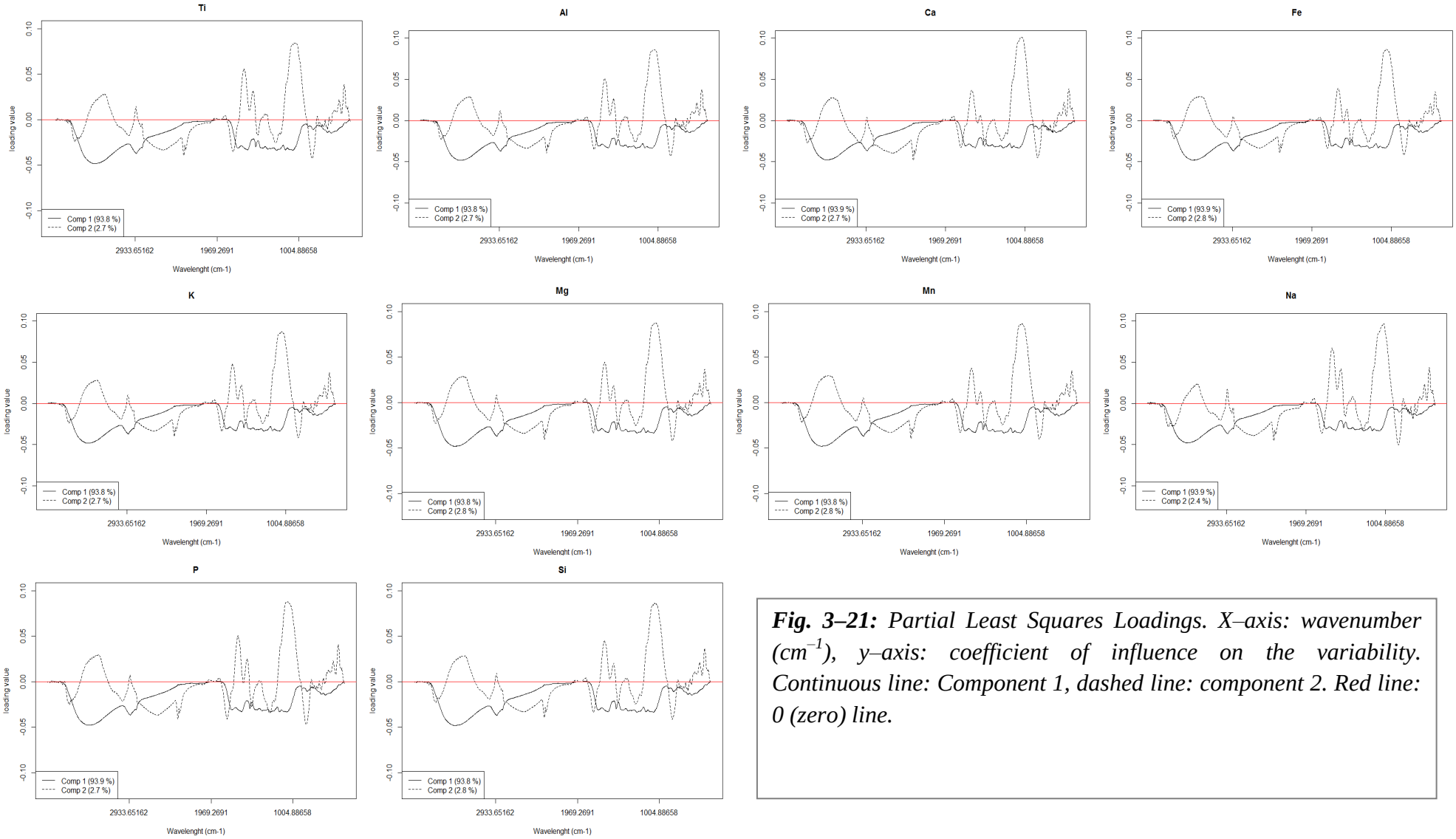

Fig. 3–21: *Partial Least Squares Loadings. X–axis: wavenumber (cm^{-1}), y–axis: coefficient of influence on the variability. Continuous line: Component 1, dashed line: component 2. Red line: 0 (zero) line.*

4. Discussion

4.1. Cross–comparison of Börtli and Brätschenflue

4.1.1. Soil Profiles

The spots of soil profiles 1 and 2 were chosen so as to cover the spatial heterogeneity of the slope. They both show mostly consistent results. We found some indications that some complex erosion processes are going on in this slope, though we could not investigate them very well with the measurements we had conducted.

Both soil profiles fit in well with other podzolic soils in terms of organic matter content or pH (Blume et al., 2010). Profile 1 was located beneath a group of small coniferous trees and had a higher organic matter content than profile 2 (which was located on the open slope). This additional organic matter in profile 1 most likely originated from the trees above. Also, the trees might have provided shelter against wind and rain, and weakened the erosion by run–off.

Texture and physical erosion on the slope

Fig. 4–1 shows a comparison of this study's soil horizons' texture with the classification chart for grain size (FAO).

All in all the soil horizons hover between loam and sandy loam The Bs horizons classify as loam and sandy loam. The BC horizon has the largest sand and lowest clay content and classifies as a sandy loam. The A and the B horizons vary mostly in their clay contents.

There is a succession with increasing exposure to physical and chemical weathering. The soil texture starts out as a sandy loam, decreases its sand fraction and increases in clay, and evolves into loam.

This means for example that the water retention capacity of the soil increases as the particle and pore sizes decrease (enlarging the capillary forces on the water). This partly accounts for the decreasing water content with depth. The texture alone is not solely responsible for the improved adsorption of water and nutrients. The higher organic matter content plays an important role in this as well, as it provides a high surface area and reactive surfaces onto which said water and nutrients can absorb more easily (Saxton and Rawls, 1986, Gupta et al., 1979).

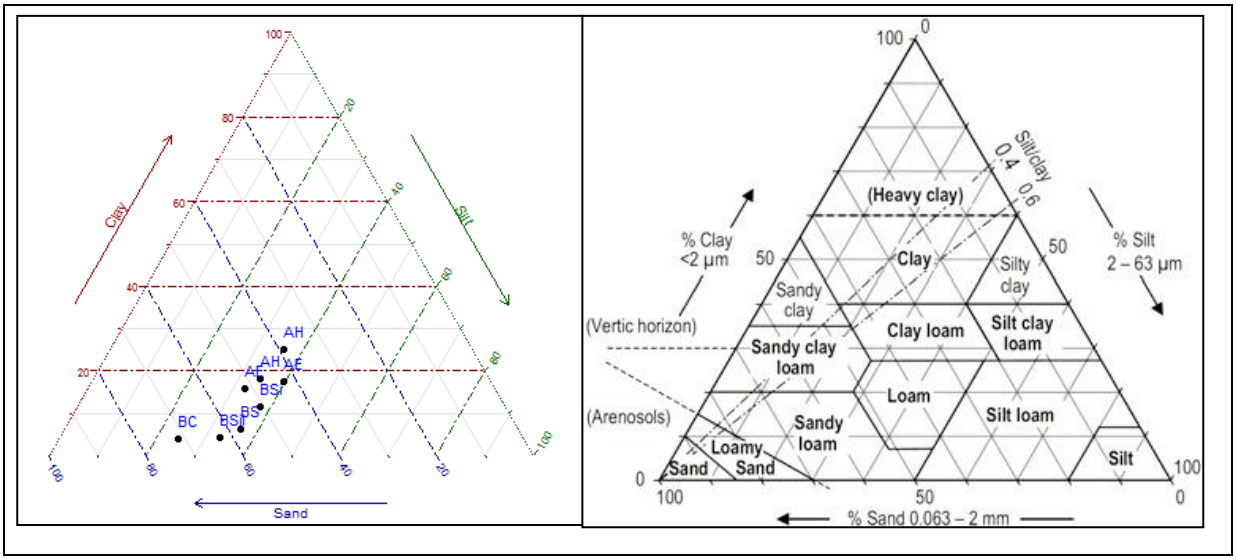

Fig. 4–1: Left: *Horizons of both soil profiles in a ternary diagram with three axes: sand, clay and silt contents (in percent).* ***Right:*** *Grain size classification of soils after the FAO (Blume et al., 2010).*

Though there is a linear trend with prolonged exposure to physical and chemical weathering *(fig.4–1)*, we can expect an upper limit on the fraction of silt– and clay–sized particles. With precipitation comes both a break–down of aggregates and a lateral movement of soil particles as they get dislocated by raindrops and washed out (Gabriels and Moldenhauer, 1978). The steep angle of the slope promotes washing out of soil particles, though there is a stronger cohesion between smaller, clay–sized particles (see Hjulstrom diagram *fig. 4–2*). The grain size distribution profiles strongly suggest the presence of erosive processes on this slope.

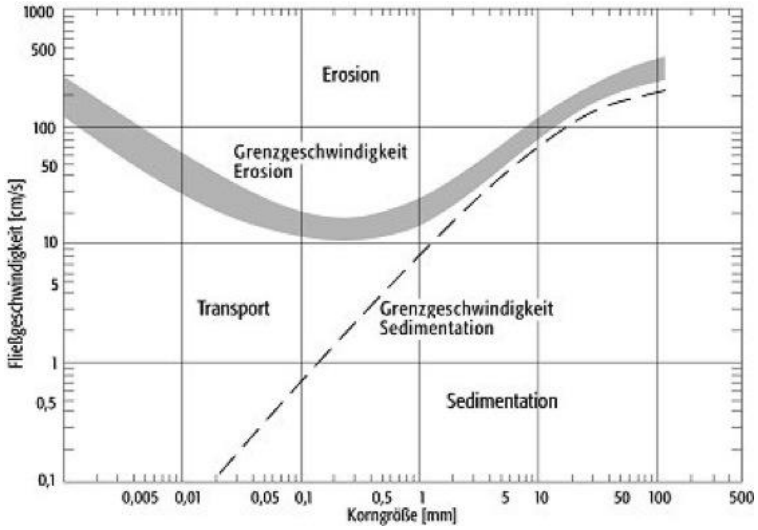

Fig.4–2: *Hjulstrom diagram illustrating the water flow velocity is needed to sediment, transport or erode particles of a given grain size. (Spektrum Verlag, 2000)*

Chemical weathering and leaching

Physical and chemical weathering generally occurs from the surface downwards. Accordingly, weathering is expected to be more advanced at the top and to decrease with depth (Blume et al., 2010). The grain size distribution found agreed with these expectations of top–to–bottom weathering *(fig. 4–1)*. The weathering indices, however, did not. In fact, they show an inversion, in which the upper soil is less weathered than the lower part.

The ratio of mobile to immobile elements can be used to detect leaching of more mobile elements by using ratios. Of the inorganic elements abundant in soils, Ti and Zr are generally considered "immobile" in soils, i.e. forming badly soluble compounds compared to other elements (Kabata–Pendias, 2011). There are, however, conditions under which Ti can be mobile, as shown by Cornu et al (1999), though such conditions do not apply to the Göschenen location. The immobility of Zr is disputable as well (Hodson, 2002, Shahid, 2013). In this study, however, we assumed Ti and Zr mobility to be negligible.

All chemical weathering indices (with exception of the Modified Weathering Potential Index, MWPI) indicate an increase of weathering with larger depth, which raises questions. The key to this could be the steep slope and the constant removal of smaller particles. Physical weathering decreases the particles size, increasing their surface area and making them more vulnerable to chemical weathering (Blume et al., 2010). By preferentially removing these more weathered soil particles from the surface of the soil profile, it could cause this inversion of weathering.

The weathering indices used in this work ((K+Ca)/Ti, B Index, WIP, CIA, CIW indicated more or less consistent trends, except for the MWPI (Modified Weathering Potential Index). It seemed to indicate the opposite of what the others did and is the only index to show results congruent with our expectations on soil weathering.

The reason for this different behavior lies in its formula (Vogel, 1975): the MWPI is the only weathering index that includes MgO in both numerator and denominator (instead of only in the denominator as in other indices):

$$\mathrm{MWPI} = \left[\frac{\mathrm{Na_2O} + \mathrm{K_2O} + \mathrm{CaO} + \mathbf{MgO}}{\mathrm{Na_2O} + \mathrm{K_2O} + \mathrm{CaO} + \mathrm{MgO} + \mathrm{SiO_2} + \mathrm{Al_2O_3} + \mathrm{Fe_2O_3}}\right] * 100$$

If the formula were omit MgO from the numerator, it would result in a decreasing MWPI with depth for profile 1 (indicating more weathering) – in par with the other indices. This illustrates how careful one must chose the indices to be applied, and that the combination of indices produces a more reliable image of reality.

A multi–layered soil?

There still needs to be a satisfying explanation regarding the inversed weathering profile of the slope. There is a possibility that this soil did not form as one layer, but is actually comprised of at least two layers.

A closer look at the grain size distribution shows that the distribution of the profile 2 matches the distribution of profile 1 up to the Bs horizon, but not further up. Profile 2 has much more sand and less clay.

A comparison of the Al_2O_3/TiO_2 and the (K+Ca)/Ti ratios shows two things. First, there is a stark difference between of the two profiles in the top 20cm. Secondly, despite the inter–profile differences, in each profile there is also a discrepancy between the bottom part of the soil and the top 20cm. The (K+Ca)/Ti ratio should sink with increasing age as the base cations are leached with prolonged exposure to weathering,. The bottom two horizons show little change. The top 20cm, however, indicate a sudden and strong shift towards less weathering.

Seeing how the slope is basically a talus slope "overgrown" with soil, a two–layered soil hypothesis could hold out. The bottom layer would have lain in between the rocks and boulders of the talus slope for a long period of time, physically protected from erosion, but the minerals were being weathered and the mobile elements leached. Later, the second layer was accumulated from fresher material.

We cannot make any definite conclusions on the origin of top layer material with the data at hand. Based on the grain size distribution with the large sand content, a predominantly aeolian input seem unlikely. Loess has very well sorted particle sizes, typically smaller than 63µm of which the largest portion of it is silt–sized (63–2µm) (see Gocke et al., 2014). Seeing how the overall chemistry of the soil is not inconsistent, a nearby source bearing a similar chemical signature, such as the rock face above the slope, seems likely.

Seeing these strong erosive processes happening on the slope, it also raises the question on whether this feature between the slope and the mire truly is a moraine or not. Seeing the situation from above (see *fig. 2–1*), it seems that the rocks and boulders have experienced some degree movement towards the mire.

The small "moraine" looks as if it is lying – at least partly – on top of the mire. It impression could also be caused by mass movement after the deposition. Nevertheless it does seems likely that these rocks and boulders originate from the rock face above rather than being deposited by a glacier.

To satisfactorily answer this question, an examination of the rock face above and of the underground of the small "moraine" would be necessary. Surface exposure ages might also shed some light.

Limitations and potential for improvement

One aim of this study was to compare the slope with the bog and to identify regressive pedogenesis phases in which material had been eroded and accumulated in the bog. There was, however, a complication in the terrain: between the slope and the bog lay another small moraine, which we did not sample. It could have acted as a buffer that caught most of the

eroded material from the slope. Accordingly, the material that did reach the mire might actually be moraine material, and not originated from the slope (assuming the small "moraine" truly is a moraine).

The profiles that were taken in this study were situated high enough on the slope to not be sinks of eroded material. One had also been taken in the open and the other one below a group of trees, in order to cover the spectrum of spatial variability.
With more time available in the field and in the lab, the catena effects on the slope could have been examined more closely e.g. by taking cores along the slope using a soil drill (as e.g. done by Jäger et al., 2015). The rocks in the underground would have been an issue, though. In any case, such a sampling approach could have provided more information about the erosion paths through elemental ratios and through grain size distributions along the slope and the small moraine.

4.1.2. Peat: Börtli and Brätschenflue

Physical parameters
At Börtli site, the dry bulk density decreased linearly for the first 50–100cm. This is not what was expected. Genereally, there is an increase of the bulk density expexted. Compaction of peat normally increases with depth and time due to an increasing top load and due to decomposition (Göttlich, 1980; Hansson 2013).
Yet, both Börtli and Brätschenflue sites show very low dry bulk densities, mostly around 0.1–0.2g/cm^3. These values are comparable to what Bindler et al. (2004, Supplement) measured in the ombrotrophic Store Mosse bog, in Sweden. They reported dry densities of 0.02–0.15g/cm^3.
The lack of compaction is easier to explain for Brätschenflue. Both cores originate from small mires which have grown in ponds and were experiencing buoyant force and were thus subjected to less compaction. The mire of BF A still had a rather large area left with water. BF B was taken on more solid ground which shows in the slightly higher bulk densities. Core BF B seems to have also experienced more disturbances during its development than core BF A as its values are less stable.

Acidic conditions with a pH of <3–4, as were found in both Börtli and Brätschenflue, are typical for raised bogs (ger.: Hochmoore). Raised bogs normally feature a low pH and are poor in nutrients because they are not connected to the groundwater. They gain their water from precipitation alone, and rain water is both slightly acidic and does not carry nutrients. The pH of the groundwater also dependent on the parent rock material, which in the present case is granitic. It does not contain carbonates to buffer the pH so that it is already acidic (Blume et al., 2010).
Indeed, neither of the Börtli and the Brätschenflue mires look like typical raised bogs. The Börtli mire does not have a dome–like shape associated with raised bogs and it lies next to a slope, which definitely connects it to the groundwater. The Brätschenflue mires had each developed in a pond that is slowly being filled up with the accumulating peat (sphagnum

mosses) and they looked rather like a fens (ger.: Niedermoore). Although the mires are hydrologically connected to the pond, the ponds themselves did not have an obvious water inlet. It is likely that they gain their water largely from precipitation and are also detached from the ground water of the area, as they seem to be situated in a rock depressions, much like bowls. In addition, we observed through the clear and shallow water that the pond sediment was riddled with desiccation cracks which is proof that the ponds at Brätschenflue occasionally dry out during the summer months. That means that the groundwater level in the peat is subjected to fluctuations as well.

Nutrients

Nutrient ratios like C/N or C/P are indicators for how easily the organic matter in litter or in a soil can be decomposed by microbes. The microbes need a certain ratio of e.g. carbon to nitrogen in their diet and since carbon is much more abundant than nitrogen or phosphorous, they are more likely limited in nitrogen or phosphorous (Wang et al. 2014).

C/N values of <20 are typical for "fresh" organic matter. It provides plenty of nitrogen per carbon and is therefore easily decomposed by microbial biota. Higher C/N values indicate higher degrees of decomposition, because nitrogen had already been preferentially consumed. Raised bogs have C/N ratios typically between 40 and 60 (Blume et al., 2010). C/N values at Brätschenflue are similar to Börtli site.

They are, however, not as expected based from results in literature. Nitrogen has an even stronger control over one C/N value at Brätschenflue than at Börtli. The carbon is in fact quite stable along the profile and only decreases at the bottom due to the increasing content of mineral matter.

The Nitrogen has a much higher variability, causing fluctuations in the C/N ratio (roughly between 20 and 50). Several authors (Malmer and Holm, 1984; Broder et al., 2012, 2012; Kuhry and Vitt, 1996; Hansson et al., 2013) reported high C/N values (C/N>100) at the top of the profile which then decrease to below 20 with increasing depth. These authors attributed this to a preferential loss of carbon due to microbial activity.

Not all studies mentioning this preferential loss of carbon have the same conditions that this present study had encountered, though. Some only looked at less than the first 100cm (Malmer and Holm, 1984; Hansson et al., 2013), some did have bogs similarly deep as in Göschenen, though were situated far away from any human influence and disturbance (Kuhry and Vitt, 1996; Broder et al., 2012). It is possible that the differences between the Göschenen bogs and what is reported literature simply occur because the bogs in this study had been subjected to more human influence than the ones northern Europe Canada or Patagonia (e.g. Hansson et al., 2013; Kuhry and Vitt, 1996; Broder et al., 2012).

What seems puzzling, however, is that it is the carbon that is supposed to be preferentially lost, not the nitrogen. Firstly, in (mineral) soils it is the nitrogen that is decomposed quickly, rather than the carbon, and we expected a similar behavior in peat. Secondly, nitrogen undergoes denitrification and escapes as N_2O under anaerobic conditions (Blume et al., 2010,) Judging from the carbon content in the Brätschenflue cores – which is fairly stable with depth – it doesn't look as if there had occurred any loss of carbon over time. The C/N ratio in this

study is almost entirely controlled by the fluctuations in nitrogen, which contradicts the earlier mentioned explanations about preferential carbon losses.
The elevated nitrogen content in the top 30cm could be attributed to the high modern atmospheric input, which is omnipresent in central Europe, including Switzerland, where bogs in the central alps face atmospheric nitrogen inputs of 10 to 20t N $ha^{-1}a^{-1}$ (Blume et al., 2010; Seitler et al., 2016). On top of any atmospheric input, the Göschenen bogs are far from being undisturbed: a farmer has sheep and goats grazing on the Börtli mire, and he cuts the grass regularly as well. We have also learned from locals that the Brätschenflue bogs have been used for peat cutting and hunting grounds in the past.

A comparison of C/N with C/P and N/P showed that litter decomposition is limited almost all through the peat profiles (at both Börtli and Brätschenflue) in phosphorous, but not necessarily in nitrogen.
Both the C/N and the C/P ratios are higher in the Börtli peat than at Brätschenflue. The N/P ratio is in average even between the two locations, though with a much higher variability in Börtli. If the nutrient stoichiometry of the litter is substantially larger than the one of the microbial biomass then there can be a long–term immobilization of N and P until a critical C/N and C/P ratio in the littler is reached again (Wang et al. 2014).
Typical C/P ratios found in soil humus lie between 100 and 1000 (Blume et al., 2010). The N/P ratio can be used as a tool to assess whether an environment is more depleted in N or P. Koerselman and Meulman (1996) found that for herbaceous freshwater wetlands a N/P ratio of 15 equals to an equilibrium state, whereas a value lower than 14 indicates a limitation in nitrogen, and a value higher than 16 indicates phosphorous–limitation.
The application of this value to the Börtli and Brätschenflue may not be most accurate but it is the closest approximation we could make to gain an idea of the nutrient status and subsequently of the decomposition of the litter. It seems that both mires are indeed more limited in P than in N.

Erosion and chemical weathering
One idea early in this project was to compare the weathering indices of the peat samples with the weathering indices of the soil's BC horizon to use it as a reference. We chose the BC horizon as it was the lowest and in theory least weathered horizon we had. The idea had to be jettisoned due to the inversed weathering profile.

Börtli B core shows several thin layers of sandy detritus which must originate either from the slope, the small moraine, or both. A strong rainfall would have swept the sediment downwards and deposited it in the peat. Naturally, these events appear as peaks in the titanium, aluminium and zirconium profiles, and as depressions in the carbon, LOI and nitrogen profiles.
These sandy deposits were visible in the weathering indices as well. They are evidently more weathered than the surrounding peat (peaks at 125–135cm, 205cm) but less weathered than the top soil horizons (the place of origin).
The base material of the bog exhibits enhanced chemical weathering as well, although it is less weathered than either the top or the bottom of the soil. From the data at our hands we

cannot infer whether these sediments originate from the slope, the moraine, or both; and for how long they have been exposed to weathering. Since the slope soil exhibits a steep inclination and is thus subjected to different weathering and erosion intensities, it would be bold to directly compare the base sediment with it (see Renard et al.,1991).

The top 80cm of the Börtli peat is indicated to exhibit elevated degrees of weathering. This section reaches values comparable to the base sediment in all indices, even though there was no visible detritus input.
There is a rapid increase in mineral matter from 80cm upwards, indicated by e.g. lower LOI. It is accompanied by an increase in zirconium and the presence of kaolonite and gibbsite in this section. It could be interpreted as the result of an eolian input, which in turn could to be connected with human activity or originate from e.g. Saharan dust (Shotyk et al., 1997). Differentiating the origins of mineral input in the mires was not in the scope of this study.

The weathering indices at Brätschenflue are not as consistent and stable as they were at the Börtli site. BF A and BF B were taken from separate mires which each have their own micro–ecosystem, so a higher variability was to be expected.

A major difficulty in interpreting the BF B profile lies in the poor depth resolution. It only has a 20cm resolution in the top 100cm.
It is also in these top 100cm where strong fluctuations in the weathering indices occur. Their onset seems to coincide with the Göschenen Cold Phase. We cannot definitely say what the connection is. We do not have an explanation for why such strong fluctuations appear in BF B but not in BF A. A climate forcing of this signature should have influenced at least both Brätschenflue mires.
The fluctuations are also not accompanied by anomalies in the other parameters. The (K+Ca)/Ti ratio in BF B shows a clearer image than the other indices, with less fluctuation and it stays in the same range as its counterpart in BF A.
An overview of the major element contents shows that the “zigzagging” probably is due to large fluctuations in the Na content (see Appendix XXI). We lack a satisfying explanation for this anomaly and why it is restricted to only one core (see also Appendix XX). There is a possibility of it being an artifact from the XRF measurement. Na is the smallest detectable element and therefore prone to yield poorer results.

Despite the Na fluctuations and the subsequent “zigzagging” of the chemical weathering in BF B core, the data are not entirely inconsistent. Some distinct peaks appear repeatedly throughout the indices (200cm, indicating less weathering; 130cm, less weathering; 50cm, more weathering).
At Börtli, the fluctuations in weathering were normally accompanied by a fluctuation in the mineral input. Increased silicon, titanium and zirconium contents would indicate the presence of mineral dust. It might be the reason why the signals in the two mires are sometimes contradictory: In the depth range in which the Piora oscillations occurred, Börtli had a short but clear signal of enhanced weathering. Brätschenflue indicates enhanced weathering in BF B, combined with an large increase of mineral matter.

BF A indicated strongly decreased weathering, which was not accompanied by any mineral input. This connection suggests an eolian input of weathered material during the Piora cold phases. Nevertheless, it seems hard to believe why so much dust would only be accumulated in one mire but not at all in the other, seeing how close they are situated from each other.

The lack of erosion deposits in the Brätschenflue mires is not surprising. Contrary to Börtli, the Brätschenflue bogs did not have any nearby slopes that could provide input material. The bogs were sitting in rock depressions, carved and smoothed out by the glacier.

Radiocarbon ages

At Börtli, the bottom data point *(fig. 3–12)* shows an age inversion. Possible explanation of this anomaly is that the sampled piece of wood belonged to a root that originated from above but had penetrated all the way to the bottom of the bog, where it was preserved. It does not seem to be a reversal of the stratigraphy, as the two samples above do lie in chronological order. The real age might lie between 8000 and 8500 yrs BP.

Interesting detail is the age of the bottom sample at Brätschenflue *(fig. 3–18)*. At less than 8000 yrs. cal. BP this mire is probably several hundred years younger than the Börtli bog which we estimate to be 8000–8500 years old. The reason for this difference might lie in the fact that the Börtli site was out of the glaciers' influence earlier than Brätschenflue as is situated 2km down the valley and could have started accumulating peat earlier than the Brätschenflue mire.

Limitations and potential for improvement

Although we didn't attampt to quantifiy it, there is little doubt about the large spacial variability concerning the mires.

At Börtli, we sampled the same mire twice in different spots. At Brätschenflue we sampled two different mires approximately 100m apart from each other. They both were situated in rock depressions and were (as far as we could judge) not connected to any slopes or water inlets and had formed in a pond which was filled with peat over time. We do have any data on the hydrological situation in the area. It might have helped understanding some of the variability.

The inter–mire variability stems from the small–scale variations in this highly heterogenous landscape. Be it the depth and shape of the rock depression, exposure wind and rain (influencing plant growth, erosion, weathering), exposure to the sun (evaporation), differences in plant communities and even small–scale differences in the parent rock mineralogy (Egli and Poulenard, 2016). The exact spot in which the mire was sampled also plays an important role. In this study we aimed for the deepest spot for to gain the deepest core and the most information. At Brätschenflue, only two drillings were attempted and performed.

At Börtli, we could see the heterogenity within the same mire. We had sampled in two spots (Börtli A and Börtli B), both times aiming for the deepest spot, but actually drilled seven cores Börtli A core are a combination of three cores each. Börtli A and B were roughly 20m apart from each but did not have the same distance to the slope. In fact, Börtli B was 5–7m

closer to the slope and had indeed several sandy layers which Börtli A did not. It illustratesd impressively how much the information one gathers from such small mires can vary depending on where exactly the sampling is performed. Had we e.g. wanted to calculate deposition rates or fluxes, the data of one single core would not have represented the whole mire well (Bindler et al., 2004).
It would have been a valuable addition to drill a core even closer to the slope simply to find more of these sandy layer which mark the more erosive periods of time in the past.

Due to the little density of the peat, the amount of material gained was often too small to maintain the original 10cm depth resolution. Samples had to be pooled to give a resolution of 20cm in some sections of the cores. In future such undertakings it might be considered to drill several cores very close to each other and pool them in order to retrieve more material per depth. Seeing the spatial heterogenity within a mire, the combination of several cores might also help smooth out variability and give results that are more representative for the sampling area.
With such a sampling approach a higher depth resolution could be ensured and the robustnes of the results improved, which would in turn improve the quality of the interpretations.

4.2. Anchoring in time and linking to Holocene climate

We used the mires as an extension of the moraine timescale. They provided additional information at a higher temporal resolution than moraines.
The information extracted from the peat was linked to a temporal axis by radiocarbon dating. The Börtli mire showed the oldest onset of peat accumulation, around 8500 BP (9400–9500 cal BP), which places it in the Boreal (9000–8000 BP). Yet, we only see the peat that has been preserved until today. We cannot see if peat accumulation at e.g. Brätschenflue truly only started 7700 yrs BP or if there had been peat before and it was eroded or it decomposed due to the dryer conditions during e.g. the Misox or an earlier dry climate phase. The age we obtained for the formation of this mire is therefore merely a youngest age.

The measured parameters and the palynological analysis allowed a link to climatic shifts as well. These shifts were climatic oscillations to colder and wetter climate, which was accompanied by an increase in weathering and erosive processes. The climatic shifts or oscillations were first described by Zoller who had done numerous research in the central and eastern Swiss Alps (e.g. Zoller 1960) doing palynology.
These climatic periods were also picked up by others and their signals tracked to areas further away from the Alps and correlated with other paleoclimatical data to construct a paleoclimatic timeline of the Late glacial and Holocene (e.g. Haas et al., 1998, Magny and Richoz, 1998, Rasmussen et al., 2008, Alley and Agustdottir, 2005).

The **Misox oscillation** (7500–6000 BP) (*Misoxer Schwankung*) could be detected in the Börtli mire, and at Brätschenflue as well, if not very clearly.

The Misox oscillation was an alpine climatic shift which was part of the same cooling event that occurred around 8200 cal BP. A rapid melt water input into the North Atlantic triggered a rapid cooling that led to a colder and dryer climate (and lasted for up to 700 years, Haas et al., 1998). It can be detected through glacial advances, pollen data and speleothem records throughout the northern hemisphere and on oxygen isotopic ratios from Greenland ice cores (a decrease in temperature of most likely around 7°C in less than a decade) (Alley and Agustdottir, 2005).
The Börtli core reached far enough back to detect this cold shift. The pollen profile showed a rapid increase of *Betula* during this time period and was cut off by a hiatus (Waroszewski, written communication). We also found massive wood at 205–235cm, indicating the existence of a carr (ger.: Bruchwald) (results not shown, see *fig. 2–3a.*).
BF A exhibits a higher chemical weathering below 260cm than the peat above, i.e. after the Misox oscillation. It is accompanied by a probable presence of kaolinite which disappears entirely after this period. Nutrient contents abruptly decrease (and C/N and C/P ratios rise) after the this period as well, probably due to enhanced microbial activity in the soil with rising temperature (Korselman and Meuleman, 1996). There is also a remarkably clear transition from stronger humified peat to less humified peat at 260cm in BF A (see fig. 2– c.).

The hiatus of the pollen profile at Börtli (120–150cm) coincided with the **Piora oscillations** (5200–4200 yrs BP) (*Piora Schwankungen*). There was a sandy layer found at this depth which indicates the occurrence of strong erosive processes and recessive pedogenesis on the slope (Waroszewski, written communication; Egli and Poulenard, 2016). Burga and Perret's (1998) report supports our findings. They report sandy layers combined with a decline in arboreal pollen (especially *Pinus*) and an increase in grass species in this period.
Weathering indices at Börtli also showed higher chemical weathering during this period. The DRIFT data does indicate the appearance of kaolinite, gibbsite, imogolite, quartz and probably muskovite at this depth. It is, however, not a singular appearance, as they are present in the peat above and below as well.

Zoller (1960) also reported his findings that the Piora oscillations consisted of two cold phases (5200 BP and 4200 BP). Newer findings (according to Burga and Perret, 1998) could narrow the second Piora cold phase down to 4700–4800 BP for the onset and 4400–4500 BP for the ending. The depth resolution in our profiles was, however, not sufficient to detect more than one period.

A temporally confined but intense fluctuation of the nutrient ratios at Börtli (C/N, C/P and N/P) coincides with decreased weathering at Brätschenflue A (e.g. B Index, WIP and CIA) and an increase of *Pinus* (also at Brätschenflue) (Waroszewski, written communication). It could be interpreted as a result of the **Löbben oscillation** (3500–3100 BP) (*Löbben Schwankung*). This oscillation was primarily detected by an advance of the Frosnitzklees glacier which led to the burial of a mire near Löbben (eastern Alps). There is also evidence of a cooling from pollen profiles in the central and eastern Alps (Burga and Perret, 1998).

The **Göschenen Cold Phases I** (2830–2270 BP) and **II** (1600–1200 yrs BP) (*Göschener Kalptphasen*) are hardly detectable due to the increasing human influence (which in turn is attested by the appearance of numerous grass pollen typically accompanying human presence and by increasing nitrogen and heavy metal contents close to the surface).
The correlation is mostly done by radiocarbon dating. Judging from the age of the peat, Göschenen Coldphases should appear at around 50–100cm at both sites. From 70–60cm on, Börtli pollen show an increase in *Fagus*, *Carpinus* and *Salix* (indicative for warmer and more humid conditions). In the cores, there was an increased amount of either roots or twigs in the peat (results not shown).
There is also a tendency towards increased chemical weathering. This depth probably marks the onset of the Subatlantic (2.5ka to present), during which the Göschenen Coldphases had occurred. The Little Ice Age (approx. 1300–1870 AD) could not be detected, as the human influence on plant communities are very similar to a cold shift. (Waroszewski, written communication, Burga and Perret, 1998).

4.4. Predicting elemental contents using DRIFT spectra

We wanted to test whether it was possible to replace the slower and costlier XRF measurement with the quick and cheap Infrared measurement by using a statistical prediction model.
To determine elemental contents we used X–ray fluorescence (XRF). Approximately 5g of milled sample are needed for measurement. The measurement of one sample takes 35mins and yields the contents of about half of the elements in the periodic table, with Na as the lightest detectable element.
To analyze the organic matter, one uses mid–Infrared spectroscopy with DRIFT. The sample sizes required are less than 500mg of milled material and the measurement of one sample takes less than 2mins.
The idea to replace a costly and time consuming analysis with spectroscopy using PLS is not a new one and occupies researchers from different field. The interest seems to come from ecology (e.g. Stuth et al., 2003), agriculture and in general soil science, where it has been successfully applied on agricultural soils (Janik et al., 1995; 1998; Pirie et al., 2005), to determine pyrogenic carbon contents (Cotrufo et al., 2016) or heavy metal contamination (Niazi et al., 2005).
We created models for the ten most abundant elements in soils, which are: Na, Mg, Al, Si, P, K, Ca, Ti, Mn, and Fe. The models worked quite well, explaining around 99% of the variance. The most difficult element to predict was phosphorous (variance explained: 98.98%). Reason for this might lie in the broader distribution of values. Other elements, Ti for example were limited to a very small range, making the values easier to predict. The prediction of these most abundant elements worked very well. It is probably less due to the individual influence of each element but because they are all strongly correlated with mineral matter in general, which in turn is easily detectable (S. Abiven, personal communication). Therefore, if there is more mineral matter, there will also be larger quantities of elements such as e.g. Al or Si The same holds true when predicting organic matter or organic carbon contents.

Limitations and potential for improvement
This present test results for predicting different elements are, though quite promising, limited in their applicability for other studies. The number of data points was only 70, which is why we refrained from doing a leave–out cross validation. Also, we only used peat samples. Most studies using infrared spectroscopy to predict soil properties focus on soils for application in agricultural sciences. There has been little interest in using this substitution on mires so far. It’s is good starting point and it could be easily applied to already existing, larger databases.

This prediction method has a lot of potential to help extending the possibilities and insights of soil science research while keeping the costs and the amount of work in limits.
The accuracy may be smaller than from extensive chemical analysis but there are enough areas of applications where speed and low costs are more important than accuracy (or quantitative results as such) (Janik and Skiemstad, 1995). The costs of mid–IR spectroscopy are also affordable even for modestly equipped laboratories and the models can be calculated using an R package which is freely available (Janik et al., 1998, Mevik et al., 2015).

5. Conclusion

We successfully managed to expand the previous knowledge about the Göschenen valley environment during the Holocene. We used mires as environmental archives, did a broad pedological examination and managed to gain insight on the dynamics of the erosive processes on the slope at Börtli, which also influenced the Börtli mire.

In the very beginning, we formulated four research questions that guided us through our undertaking:

1. **Can phases favoring or inhibiting soil formation be recognized in the mires?**
2. **Is there a (geochemical) connection between the mires and soils on the nearby slopes?**
3. **Can regressive soil formation phases be connected to climatic cold shifts?**
4. **Can we predict elemental contents based on infrared spectroscopy (DRIFT) by making a statistical model?**

To answer the first three questions we combined a broad pedological analysis with palynology and radiocarbon dating. We managed to detect some of the climatic shifts clearly in our data, but not all of them. The combined data was not always consistent or showed distinct trends. There are, after all, many factors contributing to the build–up of these environmental archives and they are not necessarily all climate-forced or directly correlated to it.

We have managed to detect erosion processes on the Börtli slope and we found proof of past soil erosion events in the mire which are likely to be connected to phases of regressive soil formation. The progressive soil formation phases in the other hand could not be detected. They have to be assumed to have occurred during more climatically stable phases.

We expected a stronger geochemical connection between the slope and the mire. We also detected mineral input most likely being of eolian origin.
Comparing the elemental contents to e.g. an Upper Continental Crust standard was of little help, as the high organic matter input in the mires overshadowed all the smaller variations. The inclusion of rare earth element fractionation might have brought better results on the erosion dynamics, but we were only able to measure less than half of these elements.

More information on erosion paths might be gained by extending the sampling scheme of the slope with a line of soil cores along the gradient of the slope. It would allow a quantitative analysis of the erosion and accumulation processes that are going on at Börtli.

We also learned how heterogeneous a mire can be and how much the location of the core can influence the findings. The closer a core is drilled to the slope, the larger the probability to find deposits from soil erosion. Drilling an additional core closer to the slope could have added further information on the frequency of deposits, and would have strengthened the argument about the connection between the deposits and regressive soil formation.

The fourth research question on the predictability of elemental contents with DRIFT spectra could be answered satisfactorily. We could predict the contents of the ten most abundant elements based on the mid–IR spectra we had obtained with DRIFT. While researchers had tried before to predict different properties of mineral soils before, it had not been tried on peat.

We had concerns that the very high organic matter content might pose difficulties but the models performed well.

One drawback, however, was the low number of data points we could use for the models. The results should therefore only be regarded with caution. One would have to extend the database to allow for example a proper validation of the models.

References

ALLEY, R., AUGUSTDOTTIR, A. M., 2005. The 8k event: Cause and consequences of a major Holocene abrupt climate change. Quaternary Science Reviews. 24. 1123–1149.

AMERICAN CHEMICAL SOCIETY. National Historic Chemical Landmarks. Discovery of Radiocarbon Dating. http://www.acs.org/content/acs/en/education/whatischemistry/landmarks/radiocarbon-dating.html (accessed Oct 15th, 2016).

BINDLER, R.; KLARQVIST, M.; KLAMINDER, J.; FÖRSTER, J., 2004. Does within-bog spatial variability of mercury and lead constrain reconstructions of absolute deposition rates from single peat records? Global Biogeochemical Cycles. 18. n/a-n/a.

BLACKFORD, J., 2000. Palaeoclimatic records from peat bogs. Trends in Ecology & Evolution. 15. 193–198.

BLUME, H.-P.; BRÜMMER, G. W.; HORN, R.; KANDELER, E.; KÖGEL-KNABNER, I.; KRETZSCHMAR, R.; STAHR, K.; WILKE, B.-M., 2010. Scheffer/Schachtschabel: Lehrbuch der Bodenkunde. Spektrum, Heidelberg, 16. Ed.

BÖHLERT, R.; MIRABELLA, A.; PLÖTZE, M.; EGLI, M., 2011. Landscape evolution in Val Mulix, eastern Swiss Alps – soil chemical and mineralogical analyses as age proxies. Catena. 87. 313–325.

BRODER, T.; BLODAU, C.; BIESTER, H.; KNORR, K. H., 2012. Peat decomposition records in three pristine ombrotrophic bogs in southern Patagonia. Biogeosciences. 9. 1479–1491.

BROEKER, W., 1991. The Great Ocean Conveyor. Oceanography. 4. 79–89.

BUIJSMAN, E.; MAAS, H. F.; ASMAN, W. A., 1987. Anthropogenic NH3 emissions in europe. Atmospheric Environment. 21. 1009–1022.

BURGA, C., 1979. Postglaziale Klimaschwankungen in Pollendiagrammen der Schweiz. Vierteljahrsschrift der Naturforschenden Gesellschaft in Zürich. 124. 265–283.

BURGA, C., 1989. Gletscher- und Vegetationsgeschichte der Südrätischen Alpen seit der Späteiszeit : (Puschlav, Livigno, Bormiese), Zürich.

BURGA, C. Pollen analytical evidence of Holocene climate fluctuations in the European central alps. In: Burkhard Frenzel; Eronen, Matti; Vorren, Karl-Dag, Gläser, Birgit. Oscillations of the alpine and polar tree limits in the Holocene, 1993. Fischer. Stuttgart.

BURGA, C.; PERRET, R., 1998. Vegetation und Klima der Schweiz seit dem jüngeren Eiszeitalter. Ott, Thun, Switzerland.

CERLING, T.; CRAIG, H., 1994. Geomorphology and In-Situ Cosmogenic Isotopes. Annual Review of Earth and Planetary Sciences. 22. 273–317.

CHAMBERS, F. M.; CHARMAN, D. J., 2004. Holocene environmental change: contributions from the peatland archive. The Holocene. 14. 1–6.

CHOLEWA, G.; DRIZA, M.; EINHORN, S.; FELLING, J., 2010. Vom Leben. Ed. Hölzel, Wien.

CLARK, P. U.; SHAKUN, J. D.; BAKER, P. A.; BARTLEIN, P. J.; BREWER, S.; BROOK, E.; CARLSON, A. E.; CHENG, H.; KAUFMAN, D. S.; LIU, Z.; MARCHITTO, T. M.; MIX, A. C.; MORRILL, C.; OTTO-BLIESNER, B. L.; PAHNKE, K.; RUSSELL, J. M.; WHITLOCK, C.; ADKINS, J. F.; BLOIS, J. L.; CLARK, J.; COLMAN, S. M.; CURRY, W. B.; FLOWER, B. P.; HE, F.; JOHNSON, T. C.; LYNCH-STIEGLITZ, J.; MARKGRAF, V.; MCMANUS, J.; MITROVICA, J. X.; MORENO, P. I.; WILLIAMS, J. W., 2012. Global climate evolution during the last deglaciation. Proceedings of the National Academy of Sciences of the United States of America. 109. E1134-42.

CORNU, S.; LUCAS, Y.; LEBON, E.; AMBROSI, J.; LUIZÃO, F.; ROUILLER, J.; BONNAY, M.; NEAL, C., 1999. Evidence of titanium mobility in soil profiles, Manaus, central Amazonia. Geoderma. 91. 281–295.

COTRUFO, M. F.; BOOT, C.; ABIVEN, S.; FOSTER, E. J.; HADDIX, M.; REISSER, M.; WURSTER, C. M.; BIRD, M. I.; SCHMIDT, M. W., 2016. Quantification of pyrogenic carbon in the environment. Organic Geochemistry. 100. 42–50.

DENTON, G.; ANDERSON, R. F.; TOGGWEILER, J. R.; EDWARDS, R. L.; SCHAEFER, J. M.; PUTNAM, A. E., 2010. The last glacial termination. Science. 328. 1652–1656.

DOKUCHAEV, V. V. Russian chernozem. 1883. In: Kaner, N. Selected Work of V.V. Dokuchaev, 1967. Int. Program Sci. Transl. Jerusalem. 1–149.

EGLI, M.; BRANDOVA, D.; RÖTHLISBERGER, S.; WOODHATCH, I.; ZOLLINGER, B., 2015. Geochronology laboratory methods. University of Zurich.

EGLI, M.; FITZE, P.; MIRABELLA, A., 2001. Weathering and evolution of soils formed on Weathering and evolution of soils formed on granitic, glacial deposits: results from chronosequences of Swiss alpine environments. Catena. 45. 19–47.

EGLI, M.; POULENARD, J. Soils of mointainous landscapes. In: Richardson, D.; Castree, N.; Goodchild, M. M.; Kobayashi, A.; Liu, W.; Marston, R.; Richardson, Douglas; Castree, Noel; Goodchild, Michael F.; Kobayashi, Audrey; Liu, Weidong; Marston, Richard A. The International Encyclopedia of Geography // International Encyclopedia of Geography: People, the Earth, Environment and Technology, 2016. John Wiley & Sons, Ltd. Oxford, UK.

EHU. http://www.ehu.eus/biomoleculas/isotopos/jpg/?C=M;O=A. Accessed: 19.09.2016.

FEDO, C. M.; WAYNE NESBITT, H.; YOUNG, G. M., 1995. Unraveling the effects of potassium metasomatism in sedimentary rocks and paleosols, with implications for paleoweathering conditions and provenance. Geology. 23. 921.

FOOD AND AGRICULTURE ORGANISATION (FAO) , 2015. World reference base for soil resources 2014.

GABRIELS, D.; MOLDENHAUER, W. C., 1978. Size distribution of eroded material from simulated rainfall: Effect over a range of texture. Soil Science Society of America Journal. 42. 954–958.

GOCKE, M.; HAMBACH, U.; ECKMEIER, E.; SCHWARK, L.; ZÖLLER, L.; FUCHS, M.; LÖSCHER, M.; WIESENBERG, G., 2014. Introducing an improved multi-proxy approach for

paleoenvironmental reconstruction of loess–paleosol archives applied on the Late Pleistocene Nussloch sequence (SW Germany). Palaeogeography, Palaeoclimatology, Palaeoecology. 410. 300–315.

GÖTTLICH, K., 1980. Moor- und Torfkunde. Schweizerbart'sche Verlagsbuchhandlung, Stuttgart, 2. Ed.

GUPTA, S. C.; LARSON, W. E., 1979. Estimating soil water retention characteristics from particle size distribution, organic matter percent, and bulk density. Water Resources Research. 15. 1633–1635.

HAAS, J. N.; RICHOZ, I.; TINNER, W.; WICK, L., 1998. Synchronous Holocene climatic oscillations recorded on the Swiss Plateau and at timberline in the Alps. The Holocene. 8. 301–309.

HANSSON, S. V.; RYDBERG, J.; KYLANDER, M.; GALLAGHER, K.; BINDLER, R., 2013. Evaluating paleoproxies for peat decomposition and their relationship to peat geochemistry. The Holocene. 23. 1666–1671.

HARNOIS, L., 1988. The CIW index: A new chemical index of weathering. Sedimentary Geology. 55. 319–322.

HARRINGTON, C. D.; WHITNEY, J. W., 1987. Scanning electron microscope method for rock-varnish dating. Geology. 15. 967.

HAUG, G. H.; TIEDEMANN, R.; ZAHN, R.; RAVELO, A. C., 2001. Role of Panama uplift on oceanic freshwater balance. Geology. 29. 207–210.

HEIRI, O.; LOTTER, A. F.; LEMCKE, G., 2001. Loss on ignition as a method for estimating organic and carbonate content in sediments: reproducibility and comparability of results. Journal of Paleolimnology. 101–110.

HODSON, M. E., 2002. Experimental evidence for mobility of Zr and other trace elements in soils. Geochimica et Cosmochimica Acta. 66. 819–828.

IVY-OCHS, S., 1996. The dating of rock surfaces using in situ produced 10Be, 26Al and 36Cl, with examples from Antarctica and the Swiss Alps, Zürich (Switzerland).

JÄGER, H.; ACHERMANN, M.; WAROSZEWSKI, J.; KABAŁA, C.; MALKIEWICZ, M.; GÄRTNER, H.; DAHMS, D.; KREBS, R.; EGLI, M., 2015. Pre-alpine mire sediments as a mirror of erosion, soil formation and landscape evolution during the last 45ka. Catena. 63–79.

JANIK, L. J.; MERRY, R. H.; SKJEMSTAD, J. O., 1998. Can mid infrared diffuse reflectance analysis replace soil extractions? Australian Journal of Soil Research. 38. 681–696.

JANIK, L. J.; SKJEMSTAD, J. O., 1995. Characterization and analysis of soils using mid-infrared partial least-squares .2. Correlations with some laboratory data. Australian Journal of Soil Research. 33. 637.

JANIK, L. J.; SKJEMSTAD, J. O.; SHEPHERD, K. D.; SPOUNCER, L. R., 2007. The prediction of soil carbon fractions using mid-infrared-partial least square analysis. Australian Journal of Soil Research. 45. 73.

JENNY, H., 1941. Factors of Soil Formation: a system of quanntitative pedology. Mc Graw-Hill Book Company, New York.

JOHNSON, D. L.; WATSON-STEGNER, D., 1987. Evolution model of pedogenesis. Soil Science. 143.

KABATA-PENDIAS, A., 2011. Trace elements in soils and plants. CRC Press, Boca Raton.

KAUFMANN, G., 1998. HInteralp und Gwüest: Siedlungsgeschichte der Göscheneralp. Gisler, Altdorf.

KERSCHNER, H. Gletscher und Klima im Alpinen Spätglazial und frühen Holozän. In: Schmidt, Roland; Matulla, Christoph; Psenner, Roland. Klimawandel in Österreich, 2009. Innsbruck University Press. Innsbruck. 5–26.

KOERSELMAN, W.; MEULEMAN, A. F., 1996. The Vegetation N:P Ratio: a New Tool to Detect the Nature of Nutrient Limitation. Journal of Applied Ecology. 33. 1441–1450.

Kraftwerk Göschenen AG. http://www.kw-goeschenen.ch/Geschichte.18.0.html. Accessed: 20.10.2016.

KRONBERG, B.I., NESBITT, H.W., 1981. Quantification of weathering, soil geochemistry and soil fertility. Journal of Soil Science. 32. 459.

KUHRY, P.; VITT, D. H., 1996. Fossil Carbon/Nitrogen Ratios as a Measure of Peat Decomposition. Ecology. 77. 271–275.

LISIECKI, L. E.; RAYMO, M. E., 2005. A Pliocene-Pleistocene stack of 57 globally distributed benthic δ 18 O records. Paleoceanography. 20. n/a-n/a.

MADSEN, P. P., 1981. Peat bog records of atmospheric mercury deposition. Nature. 293. 127–130.

MAGNY, M.; RICHOZ, I., 1998. Holocene lake-level fluctuations in Lake Seedorf, southern Swiss Plateau. Eclogae Geologicae Helvetiae. 91.

MAISCH, M., 1982. Zur Gletscher- und Klimageschichte des alpinen Spätglazials. Geographica Helvetica. 37. 93–104.

MALKIEWICZ, M.; WAROSZEWSKI, J.; BOJKO, O.; EGLI, M.; KABAŁA, C., 2016. Holocene vegetation history and soil development reflected in the lake sediments of the Karkonosze Mountains (Poland). The Holocene. 26. 890–905.

MALMER, N.; HOLM, E., 1984. Variation in the C/N-Quotient of Peat in Relation to Decomposition Rate and Age Determination with ^{210} Pb. Oikos. 43. 171.182.

MEEHL, G.; ZWIERS, F.; EVANS, J.; KNUTSON, T.; MEARNS, L.; WHETTON, P., 2000. Trends in Extreme Weather and Climate Events: Issues Related to Modeling Extremes in Projections of Future Climate Change. Bulletin of the Americal Meteorological Society. 81. 427.

MEVIK, B. H.; WEHRENS, R.; LILAND, K. H., 2015. Partial Least Squares and Principal Component Regression, R package.

MOORE, P. D.; WEBB, J. A.; COLLINSON, M. E., 1991. Pollen Analysis. Blackwell Scientific Publications, Oxford.

NALEPKA, D.; WALANUS, A., 2003. Data processing in pollen analysis. Acta Palaeobotanica. 43. 125–134.

NESBITT, H. W.; YOUNG, G. M., 1984. Prediction of some weathering trends of plutonic and volcanic rocks based on thermodynamic and kinetic considerations. Geochimica et Cosmochimica Acta. 48. 1523–1534.

NIAZI, N. K.; SINGH, B.; MINASNY, B., 2015. Mid-infrared spectroscopy and partial least-squares regression to estimate soil arsenic at a highly variable arsenic-contaminated site. International Journal of Environmental Science and Technology. 12. 1965–1974.

OxCal 4.2. https://c14.arch.ox.ac.uk/oxcal/OxCal.html. Accessed: April and August 2016.

PARKER, A., 1970. An index of weathering for silicate rocks. Geology Magazine. 501–504.

PIRIE, A.; SINGH, B.; ISLAM, K., 2005. Ultra-violet, visible, near-infrared, and mid-infrared diffuse reflectance spectroscopic techniques to predict several soil properties. Australian Journal of Soil Research. 43. 713.

PRESSLINGER, H.; EIBNER, C., 2003. Industrieregion der Bronzezeit: die Alpen. Ruperto Carola.

PRICE, J. R.; VELBEL, M. A., 2003. Chemical weathering indices applied to weathering profiles developed on heterogeneous felsic metamorphic parent rocks. Chemical Geology. 202. 397–416.

RASMUSSEN, P.; HEDE, M. U.; NOE-NYGAARD, N.; CLARKE, A. L.; VINEBROOKE, R. D., 2008. Geological Survey of Denmark and Greenland Bulletin. Geological Survey of Denmark and Greenland Bulletin. 15. 57–60.

REICHE, P., 1943. Graphic Representation of Chemical Weathering. Journal of Sedimentary Petrology. 13. 58–68.

REIMER, P. J.; BARD, E.; BAYLISS, A.; WARREN BECK, J.; BLACKWELL, P. G.; RAMSEY, C. B.; BUCK, C. E.; CHENG, H.; EDWARDS, R. L.; FRIEDRICH, M.; GROOTES, P. M.; GUILDERSON, T.; HAFLIDASON, H.; HAJDAS, I.; HATTÉ, C.; HEATON, T. J.; HOFFMAN, D. L.; HOGG, A. G.; HUGHEN, K. A.; KAISER, K. F.; KROMER, B.; MANNING STURT W; NIU, M.; REIMER, R. W.; RICHARDS, D. A.; SCOTT, E. M.; SOUTHON, J. R.; STAFF, R. A.; TURNEY, C. S. M.; VAN DER PLICHT, J., 2013. IntCal13 and Marine13 Radiocarbon Age Calibration Curves 0–50,000 Years cal BP. Radiocarbon. 55. 1869–1887.

RENARD, K. G.; FOSTER, G. R.; WEESIES, G. A.; PORTER, J. P., 1991. RUSE Revised universal soil loss equation. Journal of Soil and Water Conservation. 46.

RONOV, A. B.; YAROSHEVSKY, A. A. Chemical composition of the Earth's crust. In: Hart, P. J. The earth's crust and upper mantle, geophysical monograph, 1969. Americal Geophysical Union. Washington DC. 37–57.

RÖTHLISBERGER, S.; SCHINDLER, C.; ZOLLER, H., 1966. Postglaziale Gletscherstände und Klimaschwankungen im Gotthardmassiv und Vorderrheingebiet. Verhandlungen der Naturforschenden Gesellschaft in Basel. 77. 97–164.

SAVI, S.; NORTON, K.; PICOTTI, V.; AKCAR, N.; DELUNEL, R.; BRARDINONI, F.; KUBIK, P.; SCHLUNEGGER, F., 2014. Quantifying sediment supply at the end of the last gaciation: Dynamic reconstruction of an alpine debri-flow fan. GSA Bulletin. 126. 773–790.

SAXTON, K. E.; RAWLS, W. J., 1986. Soil Water Characteristic Estimates by Texture and Organic Matter for Hydrologic Solutions. Soil Science Society of America Journal. 70. 1569–1578.

SCHALTEGGER, U., 1998. Geochemische und isotopengeochemische Untersuchungen am Zentralen Aaregranit und seinen assoziierten Gesteinen zwischen Aare und Reuss (Aarmassiv, Schweiz), Bern.

SEITLER, E.; THÖNI, L.; MEIER, M., 2016. Atmosphärische Stickstoff-Deposition in der Schweiz. 2000-2014. Forschungsstelle für Umweltbeobachtung.

SHAHID, M.; FERRAND, E.; SCHRECK, E.; DUMAT, C., 2013. Behavior and impact of zirconium in the soil-plant system: plant uptake and phytotoxicity. Reviews of environmental contamination and toxicology. 221. 107–127.

SHAKUN, J. D.; CLARK, P. U.; HE, F.; MARCOTT, S. A.; MIX, A. C.; LIU, Z.; OTTO-BLIESNER, B.; SCHMITTNER, A.; BARD, E., 2012. Global warming preceded by increasing carbon dioxide concentrations during the last deglaciation. Nature. 484. 49–54.

SHOTYK, W., 1997. Atmospheric deposition and mass balance of major and trace elements in two oceanic peat bog profiles, northern Scotland and the Shetland Islands. Chemical Geology. 138. 55–72.

SHOTYK, W.; WEISS, D.; APPLEBY, P. G.; CHEBURKIN, A. K.; FREI, R.; GLOOR, M.; KRAMERS, J. D.; REESE, S.; VAN DER KNAAP, W. O., 1998. History of atmospheric lead deposition since 12,370 14C BP from a peat bog, Jura Mountains, Switzerland. Science. 281. 1635–1640.

Spektrum Verlag. Hjulstrom Diagramm. http://www.spektrum.de/lexikon/geowissenschaften/hjulstroem-diagramm/6931. Accessed: 20.11.2016.

STUTH, J.; JAMA, A.; TOLLESON, D., 2003. Direct and indirect means of predicting forage quality through near infrared reflectance spectroscopy. Field Crops Research. 84. 45–56.

SUCCOW, M., 2001. Landschaftsökologische Moorkunde. Schweizerbart, Stuttgart, 2. Ed.

TAYLOR, S. R.; MCLENNAN, S. M., 1995. The geochemical evolution of the continental crust. Reviews of Geophysics. 33. 241–265.

TINNER, W.; CONEDERA, M.; AMMAN, B.; LOTTER, A. F., 2005. Fire ecology north and south of the Alps since the last ice age. The Holocene. 15. 1214–1226.

VOGEL, D. E., 1975. Precambrian Weathering in Acid Metavolcanic Rocks from the Superior Province, Villebon Township, South-Central Québec. Canadian Journal Earth Science. 2080–2085.

WALSER, G. Die militärische Bedeutung der Alpen in der Antike. In: Schweizerischen Vereinigung für Militärgeschichte und Militärwissenschaft. Krieg und Gebirge : der Einfluss der Alpen und des Juras auf die Strategie im Laufe der Jahrhunderte, 1998. Attinger. Hauterive.

WANG, M.; MOORE, T. R.; TALBOT, J.; RICHARD, P. J. H., 2014. The cascade of C:N:P stoichiometry in an ombrotrophic peatland: from plants to peat. Environmental Research Letters. 9. 1–7.

YANAGI, T., 2011. Arc Volcano of Japan: generation of continental crust from the mantle. Springer, Heidelberg.

ZACHOS, J.; PAGANI, M.; SLOAN, L.; THOMAS, E.; BILLUPS, K., 2001. Trends, rhythms, and aberrations in global climate 65 Ma to present. Science. 292. 686–693.

ZOLLER, H., 1960. Pollenanlytische Untersuchungen zur Vegetationsgeschichte der insubrischen Schweiz. Denkschriften der Schweizerischen Naturforschenden Gesellschaft. 83. 45–156.

Appendix

Sample	Depth (cm)	C (%)	N (%)	Na (%)	Mg (%)	Al (%)	S (%)	Si (%)	P (%)	K (%)	Ca (%)	Ti (%)	Mn (%)	Fe (%)	LOI (%)	(K+Ca)/Ti	B Index	WIP	MWPI	CIA	CIW	Bulk dens. (g/cm3)	Water cont. (%)	pH
1	Ah	20.04	1.16	1.926	0.986	5.376	0.146	21.043	0.110	1.851	0.873	0.450	0.149	3.166	31.1	7.36	0.47	135.41	12.72	0.53	0.61	0.52	39.5	4.54
2	AE	10.80	0.65	2.212	0.941	6.698	0.090	26.600	0.071	2.281	0.661	0.496	0.090	3.346	16.1	7.23	0.43	129.10	10.74	0.57	0.66	0.81	14.5	3.80
3	Bs	3.99	0.25	2.172	1.242	7.950	0.067	27.789	0.099	2.573	0.684	0.629	0.153	4.485	8.4	6.31	0.40	125.32	11.19	0.60	0.70	0.88	19.8	4.16
4	BC	3.12	0.16	2.089	1.928	9.025	0.065	26.802	0.074	2.584	0.643	0.593	0.075	5.263	6.6	6.63	0.36	124.16	12.95	0.64	0.73	1.23	15.1	4.50
13	Ah	16.97	1.17	2.399	0.701	5.892	0.138	26.154	0.102	2.530	0.671	0.309	0.100	2.023	20.4	12.62	0.48	147.00	10.94	0.52	0.61	0.70	34.3	3.95
14	AE	7.92	0.58	2.433	0.605	6.435	0.083	29.774	0.070	2.757	0.597	0.328	0.062	2.026	11.8	12.47	0.46	138.07	9.65	0.54	0.64	0.86	25.8	3.68
15	BsI	2.90	0.18	2.592	0.709	7.272	0.042	31.248	0.065	2.941	0.686	0.459	0.040	2.570	5.5	9.64	0.45	137.86	9.94	0.55	0.65	0.88	21.1	3.90
16	BsII	2.16	0.12	2.443	1.488	8.273	0.044	28.704	0.059	2.868	0.648	0.518	0.086	4.531	5.1	8.27	0.41	135.50	12.09	0.59	0.69	1.28	18.1	4.13

Appendix I. Soils. Most important elemental contents and weathering indices.

Sample	Zr (%)	Pb (%)	Th (%)	U (%)	Sr (%)	V (%)	La (%)	Ce (%)	Pr (%)	Nd (%)	Sm (%)	Hf (%)
1	0.02161	0.00427	0.00102	0.00035	0.01648	0.01037	0.004	0.0063	0.00391	0.00561	< 0.00081	0.00062
2	0.02467	0.00383	0.00134	0.00038	0.01772	0.0102	0.00614	0.01004	0.00565	0.0085	< 0.00081	0.0006
3	0.02314	0.00386	0.00146	0.00049	0.01936	0.01304	0.00511	0.00894	0.00447	0.00727	< 0.00081	0.00072
4	0.01791	0.0042	0.00145	0.00034	0.02005	0.0158	0.00485	0.00861	0.00511	0.00772	< 0.00081	0.00044
13	0.022	0.0035	0.00138	0.00046	0.01289	0.0033	0.00515	0.00848	0.00647	0.00785	< 0.00081	0.00061
14	0.02593	0.00275	0.00146	0.00059	0.01392	0.00343	0.00648	0.01003	0.00824	0.01067	< 0.00081	0.0006
15	0.02733	0.00246	0.00181	0.00059	0.01674	0.00652	0.00783	0.01287	0.00764	0.01114	< 0.00081	0.0006
16	0.02426	0.00305	0.00201	0.00051	0.01763	0.0097	0.00679	0.01183	0.00676	0.01046	< 0.00081	0.00078

Appendix II. Soils. Trace elements and rare earth elements.

Soil

Normalized with Upper Continental Crust (LOI corrected)										
	Na2O	MgO	Al2O3	SiO2	P2O5	K2O	CaO	TiO2	MnO	Fe2O3
1	0.97	1.08	0.97	0.99	1.82	0.95	0.42	2.18	2.79	3.13
2	0.91	0.85	0.99	1.03	0.97	0.96	0.26	1.97	1.38	2.72
3	0.82	1.02	1.08	0.98	1.24	1.00	0.25	2.29	2.16	3.33
4	0.77	1.56	1.20	0.93	0.91	0.98	0.23	2.12	1.04	3.84
13	1.04	0.66	0.92	1.07	1.47	1.13	0.28	1.30	1.62	1.73
14	0.95	0.52	0.91	1.09	0.91	1.11	0.23	1.24	0.91	1.56
15	0.95	0.57	0.96	1.07	0.78	1.10	0.24	1.62	0.55	1.85
16	0.89	1.18	1.08	0.98	0.71	1.07	0.23	1.82	1.17	3.25
Normalized with Central Aaregranite (LOI corrected)										
	Na2O	MgO	Al2O3	SiO2	P2O5	K2O	CaO	TiO2	MnO	Fe2O3
1	0.92	4.74	1.10	0.90	5.20	0.74	1.99	4.19	3.99	3.13
2	0.87	3.72	1.13	0.93	2.77	0.75	1.24	3.79	1.97	2.72
3	0.78	4.50	1.22	0.89	3.55	0.78	1.17	4.41	3.09	3.33
4	0.74	6.85	1.36	0.85	2.60	0.76	1.08	4.08	1.49	3.84
13	0.99	2.92	1.04	0.97	4.20	0.88	1.32	2.49	2.32	1.73
14	0.91	2.28	1.03	1.00	2.61	0.86	1.06	2.39	1.29	1.56
15	0.90	2.49	1.08	0.97	2.23	0.86	1.14	3.11	0.79	1.85
16	0.85	5.20	1.23	0.89	2.04	0.84	1.07	3.51	1.67	3.25

Börtli A

Normalized with Upper Continental Crust (LOI corrected)										
	Na2O	MgO	Al2O3	SiO2	P2O5	K2O	CaO	TiO2	MnO	Fe2O3
24	1.42	0.97	0.71	0.93	13.57	0.78	0.71	1.46	1.02	3.25
26	4.10	2.38	0.85	0.53	10.54	0.58	2.52	1.56	1.30	4.36
28	4.37	2.38	0.89	0.69	8.43	0.73	1.28	2.23	0.60	1.14
30	6.57	3.86	0.81	0.46	14.05	0.51	1.76	2.41	0.73	1.31
32	7.72	5.03	0.57	0.32	10.43	0.37	2.90	1.90	1.00	1.72
34	6.03	4.01	0.88	0.42	11.36	0.42	2.44	1.91	0.81	1.92
3674	3.65	2.30	0.34	0.90	7.17	0.25	1.40	1.14	0.54	1.08
7677	3.22	2.47	0.26	0.92	5.80	0.23	1.78	0.79	0.63	1.16
5178	3.18	2.12	0.28	0.96	4.93	0.24	1.42	0.82	0.62	1.19
5380	6.49	4.17	0.63	0.39	10.61	0.52	2.37	1.71	1.08	2.41
5582	4.62	3.05	0.26	0.76	4.87	0.18	1.99	0.67	0.85	2.11
8485	3.22	2.30	0.78	0.80	7.24	0.64	1.04	1.32	0.47	1.28
8687	3.31	2.38	0.20	0.96	5.06	0.25	1.11	0.85	0.45	1.16
8889	3.17	1.93	0.33	0.98	5.27	0.28	0.81	0.87	0.35	1.01
9091	1.99	1.30	0.46	1.06	3.34	0.32	0.48	1.02	0.24	0.84
Normalized with Central Aaregranite (LOI corrected)										
	Na2O	MgO	Al2O3	SiO2	P2O5	K2O	CaO	TiO2	MnO	Fe2O3
24	1.35	4.26	0.81	0.84	38.77	0.61	3.33	2.81	1.46	3.25
26	3.91	10.49	0.97	0.49	30.11	0.45	11.89	3.00	1.85	4.36
28	4.17	10.48	1.01	0.62	24.08	0.57	6.03	4.29	0.86	1.14
30	6.27	17.00	0.92	0.42	40.16	0.40	8.33	4.63	1.04	1.31
32	7.36	22.12	0.64	0.29	29.79	0.29	13.67	3.65	1.43	1.72
34	5.75	17.63	0.99	0.38	32.46	0.33	11.50	3.66	1.16	1.92
3674	3.48	10.12	0.38	0.82	20.49	0.20	6.61	2.18	0.77	1.08
7677	3.07	10.86	0.30	0.84	16.56	0.18	8.41	1.52	0.90	1.16
5178	3.03	9.35	0.32	0.87	14.08	0.19	6.71	1.57	0.89	1.19
5380	6.19	18.33	0.71	0.36	30.31	0.40	11.19	3.28	1.54	2.41
5582	4.40	13.41	0.30	0.69	13.90	0.14	9.41	1.28	1.21	2.11
8485	3.07	10.14	0.88	0.72	20.68	0.50	4.92	2.54	0.68	1.28
8687	3.16	10.47	0.23	0.87	14.46	0.19	5.22	1.64	0.65	1.16
8889	3.02	8.49	0.38	0.89	15.07	0.22	3.81	1.68	0.50	1.01
9091	1.90	5.70	0.53	0.96	9.56	0.25	2.29	1.95	0.34	0.84

Appendix III. Soil and Börtli A. UCC and Central Aaregranite normalizations (using LOI corrected data)

Sample	Depth (cm)	C (%)	N (%)	Na (%)	Mg (%)	Al (%)	S (%)	Si (%)	P (%)	K (%)	Ca (%)	Ti (%)	Mn (%)	Fe (%)	LOI (%)	(K+Ca)/Ti	B Index	WIP	MWPI	CIA	CIW	Bulk dens. (g/cm3)	Water cont. (%)	pH
24	5	34.40	2.90	1.245	0.389	1.737	0.534	8.659	0.359	0.672	0.643	0.133	0.024	1.447	69.7	11.98	0.62	160.80	16.08	0.38	0.43	0.17	77.6	3.90
26	25	48.60	1.90	1.138	0.303	0.658	0.221	1.579	0.088	0.158	0.725	0.045	0.010	0.614	90.4	23.60	0.79	370.23	43.67	0.21	0.22	0.15	78.2	3.70
28	45	48.40	1.91	1.315	0.329	0.744	0.242	2.202	0.076	0.214	0.399	0.069	0.005	0.175	89.6	10.63	0.75	384.45	36.89	0.25	0.26	0.13	86.1	3.55
30	65	50.48	1.76	0.855	0.231	0.294	0.125	0.644	0.055	0.065	0.238	0.032	0.003	0.087	95.5	11.20	0.82	544.21	54.45	0.18	0.18	0.10	88.6	3.60
32	85	54.08	1.42	0.670	0.200	0.137	0.106	0.298	0.027	0.032	0.261	0.017	0.002	0.076	97.0	20.54	0.89	638.50	68.28	0.11	0.11	0.09	90.0	3.45
34	105	51.64	1.61	0.785	0.239	0.317	0.141	0.579	0.045	0.053	0.329	0.026	0.003	0.127	95.5	17.82	0.82	508.25	56.45	0.18	0.19	0.09	88.7	3.50
3674	125	52.70	1.75	0.355	0.103	0.091	0.071	0.932	0.021	0.024	0.142	0.011	0.001	0.054	96.6	17.32	0.87	305.77	30.88	0.13	0.13	0.06	87.2	3.50
7677	150	52.54	1.56	0.355	0.125	0.080	0.076	1.083	0.019	0.024	0.204	0.009	0.002	0.065	96.2	30.16	0.90	278.42	31.00	0.10	0.10	0.08	89.0	3.60
5178	165	52.44	1.35	0.387	0.119	0.096	0.075	1.246	0.018	0.028	0.180	0.010	0.002	0.074	95.8	24.18	0.88	270.35	27.91	0.12	0.12	0.08	92.3	3.60
5380	185	51.95	1.51	0.770	0.227	0.208	0.166	0.497	0.038	0.060	0.292	0.021	0.003	0.145	95.9	20.13	0.87	547.52	59.90	0.13	0.14	0.09	92.1	3.70
5582	205	50.70	0.97	0.443	0.134	0.071	0.085	0.776	0.014	0.017	0.198	0.007	0.002	0.103	96.7	38.96	0.92	382.51	40.49	0.08	0.08	0.15	82.8	3.75
8485	230	51.55	1.53	0.710	0.233	0.477	0.200	1.873	0.048	0.139	0.238	0.030	0.003	0.143	92.4	15.08	0.72	294.09	29.90	0.28	0.29	0.08	88.4	3.80
8687	250	52.55	1.46	0.356	0.117	0.061	0.091	1.098	0.016	0.026	0.123	0.009	0.001	0.063	96.3	18.87	0.91	278.77	28.15	0.09	0.09	0.08	89.1	3.75
8889	270	53.31	1.46	0.455	0.127	0.132	0.112	1.502	0.023	0.039	0.120	0.013	0.001	0.074	95.0	14.71	0.85	264.04	24.76	0.15	0.16	0.08	88.4	3.90
9091	290	50.60	1.77	0.352	0.105	0.228	0.159	1.987	0.018	0.055	0.089	0.019	0.001	0.076	93.9	9.32	0.71	174.86	16.44	0.29	0.30	0.11	87.1	3.80

Appendix IV. Börtli A. Most important elemental contents and weathering indices

Sample	Zr (%)	Pb (%)	Th (%)	U (%)	Sr (%)	V (%)	La (%)	Ce (%)	Pr (%)	Nd (%)	Sm (%)	Hf (%)
30	0.00135	0.00032	0.00005	< 0.00004	0.00131	0.0006	0.00371	0.00365	0.00771	0.00721	< 0.00081	< 0.00020
3675	0.00083	0.00029	0.00001	< 0.00004	0.0015	0.00044	0.00466	0.00446	0.00979	0.01	< 0.00081	< 0.00020
5178	0.0011	0.00035	0.00002	< 0.00004	0.00167	0.00039	0.00278	0.00387	0.00596	0.00562	< 0.00081	< 0.00020
5380	0.00092	0.0003	0.00002	0.00001	0.00158	0.0004	0.00218	0.00247	0.00431	0.0037	< 0.00081	< 0.00020
5582	0.00049	0.00017	< 0.00004	< 0.00004	0.00189	0.00032	0.00339	0.0046	0.00753	0.00749	< 0.00081	< 0.00020
7677	0.00068	0.00035	0.00001	< 0.00004	0.00155	0.00042	0.00314	0.00418	0.00651	0.00673	< 0.00081	< 0.00020
8485	0.00267	0.00033	0.00004	< 0.00004	0.00132	0.00063	0.00263	0.0036	0.00556	0.00508	< 0.00081	< 0.00020
8687	0.00057	0.0003	0.00001	< 0.00004	0.00122	0.00083	0.00181	0.00257	0.00435	0.00333	< 0.00081	< 0.00020
8889	0.00128	0.00038	0.00004	< 0.00004	0.00115	0.00063	0.0026	0.00335	0.00514	0.00463	< 0.00081	< 0.00020
9091	0.00253	0.00062	0.00008	0.00004	0.00127	0.00057	0.00382	0.00491	0.00763	0.00747	< 0.00081	< 0.00020
24	0.00632	0.00565	0.00038	0.00008	0.00509	0.01804	0.0028	0.0042	0.00372	0.00435	< 0.00081	0.00046
26	0.002	0.0008	0.00005	0.00001	0.00264	0.00067	0.00271	0.00341	0.00511	0.0044	< 0.00081	< 0.00020
28	0.00277	0.00075	0.00008	0.00004	0.0017	0.00076	0.00256	0.00358	0.00483	0.00462	< 0.00081	< 0.00020
30	0.00076	0.00035	0.00005	< 0.00004	0.00113	0.00179	0.00081	0.00137	0.00188	0.00142	< 0.00081	< 0.00020
32	0.00026	0.00016	< 0.00004	< 0.00004	0.00131	0.00262	0.0005	0.00065	0.00141	0.00073	< 0.00081	0.00007
34	0.00067	0.00033	0.00002	< 0.00004	0.00152	0.00083	0.00233	0.00294	0.0046	0.00395	< 0.00081	< 0.00020
5380	0.0006	0.00028	0.00003	< 0.00001	0.00151	0.00201	< 0.00026	0.00092	0.00116	0.00099	< 0.00081	0.00008

Appendix V. Börtli A. Trace elements and rare earth elements

Sample	Depth (cm)	C (%)	N (%)	Na (%)	Mg (%)	Al (%)	S (%)	Si (%)	P (%)	K (%)	Ca (%)	Ti (%)	Mn (%)	Fe (%)	LOI (%)	(K+Ca)/Ti	B Index	WIP	MWPI	CIA	CIW	Bulk dens. (g/cm3)	Water cont. (%)	pH
37	5	36.71	3.17	1.268	0.346	1.905	0.478	10.287	0.347	0.681	0.579	0.117	0.021	1.517	66.1	13.05	0.59	144.79	13.53	0.41	0.46	0.21	74.6	3.90
39	25	50.02	1.72	0.991	0.252	0.431	0.181	1.239	0.056	0.102	0.455	0.039	0.004	0.191	93.1	17.30	0.81	427.40	45.30	0.19	0.20	0.13	85.0	3.50
41	45	51.81	1.41	0.830	0.239	0.164	0.109	0.398	0.033	0.036	0.264	0.015	0.002	0.093	96.4	23.82	0.89	650.26	65.93	0.11	0.11	0.11	89.7	3.35
98	65	53.35	1.19	0.742	0.218	0.206	0.080	0.480	0.022	0.058	0.157	0.021	0.002	0.101	96.5	12.08	0.84	605.52	57.72	0.16	0.16	0.12	82.4	3.30
43	65	52.17	1.41	0.981	0.272	0.451	0.177	1.035	0.034	0.090	0.310	0.030	0.002	0.171	93.8	16.25	0.78	460.89	46.97	0.22	0.22	0.11	87.1	3.35
45	80	53.88	1.18	0.346	0.088	0.073	0.056	0.503	0.009	0.013	0.095	0.005	0.000	0.037	97.8	23.73	0.88	436.55	41.11	0.12	0.12	0.09	86.2	3.35
100	85	51.46	1.60	0.404	0.102	0.141	0.084	0.878	0.016	0.019	0.120	0.009	0.001	0.061	96.6	17.66	0.82	333.05	32.01	0.18	0.18	0.06	88.8	3.40
46	90	53.19	1.27	0.696	0.183	0.232	0.132	0.318	0.019	0.032	0.192	0.014	0.001	0.095	96.8	18.53	0.83	608.03	62.82	0.17	0.18	0.17	77.3	3.35
112117	105	53.61	1.51	0.588	0.162	0.192	0.129	0.906	0.028	0.036	0.178	0.012	0.001	0.095	95.8	21.21	0.83	398.55	39.93	0.17	0.17	0.10	85.3	3.45
119	125	44.89	1.02	2.092	0.555	2.006	0.321	5.881	0.049	0.748	0.624	0.099	0.004	0.477	76.3	16.77	0.66	304.72	27.15	0.34	0.38	0.17	80.6	3.50
114	125	50.45	1.79	0.708	0.231	0.715	0.232	0.853	0.063	0.073	0.324	0.033	0.002	0.186	93.9	14.66	0.65	349.46	42.83	0.35	0.36	0.06	89.2	3.50
120	135	51.46	1.44	1.374	0.357	0.948	0.263	3.186	0.067	0.364	0.351	0.042	0.003	0.237	86.8	20.79	0.71	337.04	30.35	0.29	0.31	0.12	82.5	3.65
121	145	55.05	1.72	0.381	0.087	0.041	0.063	0.546	0.020	0.009	0.079	0.003	0.000	0.048	97.7	31.97	0.93	448.43	40.29	0.07	0.07	0.10	86.2	3.80
116	145	51.61	1.40	0.863	0.255	0.568	0.277	1.655	0.047	0.142	0.333	0.045	0.002	0.199	92.0	12.68	0.73	333.91	35.60	0.27	0.28	0.11	84.7	3.70
103	165	55.80	1.69	0.273	0.067	0.051	0.049	0.986	0.014	0.010	0.062	0.003	0.000	0.038	97.0	26.46	0.89	250.45	22.16	0.11	0.11	0.10	85.9	3.60
105	185	54.60	1.56	0.251	0.063	0.028	0.059	0.550	0.014	0.008	0.069	0.003	0.000	0.029	98.0	31.81	0.93	345.38	32.65	0.07	0.07	0.09	87.0	3.70
107	205	48.42	1.17	1.651	0.425	1.270	0.285	3.891	0.054	0.437	0.461	0.052	0.003	0.306	83.8	20.99	0.69	330.85	29.96	0.31	0.33	0.12	83.2	3.55
109	225	56.34	1.63	0.373	0.087	0.044	0.063	0.651	0.021	0.009	0.081	0.003	0.000	0.049	97.5	31.62	0.93	401.33	36.17	0.07	0.07	0.07	86.0	3.60
111	245	53.50	1.68	0.380	0.084	0.053	0.078	0.690	0.018	0.014	0.077	0.005	0.000	0.051	97.3	23.62	0.91	388.71	34.65	0.09	0.09	0.06	86.2	3.80
47	255	49.97	1.60	1.064	0.315	0.693	0.233	1.544	0.054	0.145	0.365	0.040	0.002	0.259	91.6	15.22	0.73	382.69	40.16	0.27	0.28	0.12	86.7	3.45
48	265	50.70	1.39	0.624	0.153	0.209	0.098	1.692	0.019	0.041	0.195	0.015	0.001	0.135	94.1	19.16	0.83	298.67	27.88	0.17	0.17	0.15	84.7	3.50
49	277.5	29.24	0.84	1.647	0.983	3.222	0.425	14.469	0.059	1.008	1.263	0.205	0.065	2.172	51.4	13.38	0.57	145.20	16.88	0.43	0.47	0.28	75.7	3.85

Appendix VI. Börtli B. Most important elemental contents and weathering indices

Sample	Zr (%)	Pb (%)	Th (%)	U (%)	Sr (%)	V (%)	La (%)	Ce (%)	Pr (%)	Nd (%)	Sm (%)	Hf (%)
45	0.00014	0.00019	< 0.00004	< 0.00004	0.00123	0.00047	0.00223	0.00311	0.00486	0.00453	< 0.00081	< 0.00020
48	0.00128	0.00041	0.00002	< 0.00004	0.00186	0.00051	0.0045	0.00564	0.0088	0.00917	< 0.00081	< 0.00020
98	0.00045	0.00022	0.00006	< 0.00004	0.00115	0.00122	0.00048	0.00079	0.00075	0.00096	< 0.00081	< 0.00020
100	0.00032	0.00036	< 0.00004	< 0.00004	0.00165	0.00179	0.00128	0.00152	0.00185	0.00146	< 0.00081	< 0.00020
103	0.00069	0.00032	< 0.00004	< 0.00004	0.00134	0.00031	0.00391	0.00503	0.00822	0.00777	< 0.00081	< 0.00020
105	0.00007	0.00039	< 0.00004	< 0.00004	0.00113	0.00105	0.001	0.00104	0.00146	0.00075	< 0.00081	0.00009
107	0.0037	0.00032	0.00013	0.00004	0.00201	0.00033	0.00372	0.00492	0.0074	0.00755	< 0.00081	< 0.00020
109	0.00048	0.00037	< 0.00004	< 0.00004	0.00135	0.00028	0.00453	0.00594	0.00948	0.00988	< 0.00081	< 0.00020
111	0.00047	0.00069	0.00003	< 0.00004	0.00129	0.00038	0.00413	0.00432	0.00919	0.00932	< 0.00081	< 0.00020
111	0.00047	0.00071	0.00003	< 0.00004	0.00131	0.00075	0.00295	0.00359	0.00623	0.00595	< 0.00081	< 0.00020
114	0.00055	0.00059	0.00009	0.00003	0.00248	0.00144	0.00063	0.00098	0.00065	0.00072	< 0.00081	0.00016
116	0.00128	0.00043	0.0001	0.00004	0.00255	0.00409	0.00053	< 0.00037	< 0.00061	< 0.00075	0.0011	0.00028
119	0.00513	0.00037	0.00025	0.00006	0.00225	0.0003	0.0021	0.00348	0.00485	0.00541	< 0.00081	< 0.00020
121	0.00028	0.00034	< 0.00001	< 0.00004	0.00128	0.00029	0.00363	0.00459	0.00721	0.0071	< 0.00081	< 0.00020
112117	0.00047	0.00036	0.00001	< 0.00004	0.00154	0.00069	< 0.00025	0.0025	0.00434	0.00394	< 0.00081	< 0.00020
120	0.00255	0.00036	0.00024	0.00004	0.00178	0.00045	0.0031	0.00466	0.00512	0.0055	< 0.00081	< 0.00020
37	0.00617	0.00775	0.0003	0.00006	0.00536	0.01038	0.00301	0.0043	0.0046	0.00516	< 0.00081	0.00036
39	0.00154	0.00033	0.00003	0.00001	0.00205	0.00059	0.00226	0.00284	0.00449	0.00423	< 0.00081	< 0.00020
41	0.0003	0.0007	< 0.00004	< 0.00004	0.00148	0.00143	0.00069	< 0.00035	0.00093	< 0.00070	< 0.00081	< 0.00020
43	0.00079	0.00038	0.00004	< 0.00004	0.00184	0.00062	0.00186	< 0.00034	0.00358	0.00315	< 0.00081	< 0.00020
46	0.00036	0.00027	0.00001	< 0.00004	0.00146	0.00062	0.00065	0.00116	0.00159	0.00099	< 0.00081	0.00011
47	0.002	0.00052	0.00005	0.00003	0.00193	0.00064	0.00256	0.00371	0.00566	0.00549	< 0.00081	< 0.00020
49	0.0081	0.00181	0.00028	0.00017	0.01051	0.01286	0.00262	0.00395	0.00344	0.00417	0.00079	0.00059

Appendix VII. Börtli B. Trace elements and rare earth elements

Sample	Depth (cm)	C (%)	N (%)	Na (%)	Mg (%)	Al (%)	S (%)	Si (%)	P (%)	K (%)	Ca (%)	Ti (%)	Mn (%)	Fe (%)	LOI (%)	(K+Ca)/Ti	B Index	WIP	MWPI	CIA	CIW	Bulk dens. (g/cm3)	Water cont. (%)	pH
122123	10	44.14	2.09	0.119	0.155	0.525	0.170	4.127	0.032	0.218	0.067	0.050	0.002	0.136	88.6	6.89	0.42	73.44	7.84	0.58	0.70	0.02	90.4	3.40
124125	30	47.35	2.23	0.137	0.148	0.564	0.151	2.399	0.044	0.154	0.028	0.053	0.002	0.097	92.4	4.16	0.35	97.05	10.81	0.65	0.74	0.04	91.3	3.40
126127	50	45.67	2.23	0.174	0.192	0.837	0.153	3.042	0.044	0.193	0.033	0.063	0.002	0.119	90.3	4.35	0.31	95.73	10.69	0.69	0.77	0.05	92.1	3.40
128129	70	47.86	2.32	0.363	0.176	0.617	0.147	1.510	0.050	0.113	0.029	0.043	0.001	0.070	94.0	4.06	0.47	203.78	20.81	0.53	0.57	0.05	90.5	3.45
130131	90	51.43	2.47	0.586	0.180	0.684	0.204	1.156	0.042	0.092	0.039	0.060	0.001	0.076	94.2	2.63	0.54	298.41	29.02	0.46	0.48	0.07	90.2	3.50
132	105	50.06	2.62	0.684	0.200	0.766	0.201	1.526	0.037	0.118	0.043	0.067	0.001	0.092	93.0	2.91	0.55	292.65	27.03	0.45	0.47	0.07	90.9	3.45
133	115	49.08	2.46	0.708	0.212	1.081	0.221	2.409	0.043	0.191	0.072	0.086	0.002	0.125	90.2	3.74	0.49	231.67	20.95	0.51	0.54	0.09	90.6	3.50
134	125	42.32	2.26	1.003	0.314	1.936	0.285	6.411	0.047	0.502	0.171	0.151	0.004	0.234	78.5	5.44	0.48	173.30	14.57	0.52	0.58	0.10	89.8	3.50
135	135	51.44	2.52	0.653	0.185	0.808	0.193	1.332	0.038	0.127	0.033	0.066	0.001	0.089	93.4	2.96	0.53	301.32	27.72	0.47	0.50	0.08	91.0	3.60
136137	150	51.59	2.19	0.713	0.166	0.707	0.194	0.935	0.039	0.093	0.030	0.059	0.001	0.079	94.5	2.53	0.57	371.84	34.03	0.43	0.45	0.09	91.0	3.60
138	165	49.23	2.87	0.732	0.232	1.351	0.299	2.629	0.050	0.234	0.064	0.095	0.002	0.172	88.8	3.81	0.45	216.85	20.00	0.55	0.59	0.08	91.0	3.65
139	175	47.73	1.96	0.899	0.242	1.019	0.197	1.523	0.035	0.142	0.076	0.069	0.002	0.167	92.0	3.84	0.55	332.80	30.82	0.45	0.47	0.09	91.5	3.50
140141	190	48.38	0.99	0.719	0.193	0.467	0.086	0.323	0.019	0.027	0.096	0.016	0.002	0.162	96.5	9.41	0.68	553.67	54.90	0.32	0.32	0.06	90.2	3.50
142143	210	49.06	1.48	0.691	0.176	0.431	0.106	0.221	0.027	0.024	0.080	0.017	0.002	0.145	96.8	7.20	0.68	582.51	58.90	0.32	0.32	0.06	93.7	3.50
144	225	50.10	1.72	0.768	0.209	0.650	0.137	0.400	0.031	0.041	0.091	0.028	0.002	0.172	95.7	5.66	0.62	487.52	50.23	0.38	0.39	0.07	92.8	3.60
145	235	47.53	0.84	0.187	0.208	0.735	0.123	0.296	0.022	0.036	0.215	0.023	0.006	0.408	96.1	13.15	0.42	179.78	39.89	0.58	0.59	0.06	94.3	3.55
146147	250	44.11	2.38	1.169	0.290	1.898	0.370	2.973	0.081	0.218	0.192	0.086	0.005	0.423	85.6	5.74	0.48	246.62	23.68	0.52	0.54	0.08	92.3	4.00
148	265	44.16	2.28	1.205	0.275	2.086	0.506	3.015	0.127	0.246	0.249	0.108	0.007	0.449	84.5	5.55	0.48	239.58	23.80	0.52	0.54	0.07	92.9	3.95
149	275	34.65	2.54	1.265	0.481	3.191	0.496	10.341	0.117	0.701	0.382	0.212	0.017	0.967	64.7	6.21	0.44	139.78	13.11	0.56	0.61	0.08	89.7	4.10
150	285	31.30	2.30	1.451	0.528	3.375	0.438	12.565	0.109	0.877	0.439	0.244	0.021	1.130	58.9	6.56	0.46	140.91	12.67	0.54	0.60	0.09	89.2	4.15
151	295	29.87	2.23	1.303	0.618	3.739	0.494	12.851	0.126	0.961	0.452	0.240	0.022	1.099	57.4	7.16	0.43	132.45	12.59	0.57	0.64	0.13	87.7	4.20

Appendix VIII. Brätschenflue A. Most important elemental contents and weathering indices.

Sample	Zr (%)	Pb (%)	Th (%)	U (%)	Sr (%)	V (%)	La (%)	Ce (%)	Pr (%)	Nd (%)	Sm (%)	Hf (%)
133	0.00187	0.0017	0.00036	0.00022	0.00102	0.00145	0.00182	0.00241	0.00274	0.00316	< 0.00081	0.00015
135	0.00072	0.00093	0.0004	0.00017	0.00071	0.00501	0.00073	0.00083	0.00074	< 0.00074	0.00118	0.00019
136137	0.00058	0.0008	0.00041	0.00021	0.00051	0.00423	0.00049	0.00104	0.00069	< 0.00073	0.00098	0.00015
138	0.0022	0.00104	0.0004	0.00023	0.00105	0.00116	0.00294	0.00407	0.00561	0.00627	< 0.00081	0.00014
144	0.0003	0.00057	0.00019	0.00011	0.00081	0.00295	0.00065	0.00101	0.00121	0.00136	0.00102	0.00018
145	0.00022	0.00076	0.00006	< 0.00004	0.00189	0.00592	< 0.00028	0.00066	< 0.00063	< 0.00078	0.00254	0.00009
148	0.00283	0.00187	0.00062	0.00052	0.00237	0.00174	0.00252	0.00356	0.00319	0.00368	< 0.00081	0.00026
149	0.01363	0.0021	0.00075	0.00052	0.00532	0.00253	0.00402	0.00648	0.00662	0.00797	< 0.00081	0.00035
150	0.01477	0.002	0.0007	0.0005	0.0056	0.00237	0.00354	0.0063	0.0062	0.00808	< 0.00081	0.00036
122123	0.00155	0.00385	0.00024	< 0.00004	0.00142	0.00631	0.00041	0.00067	< 0.00061	< 0.00076	0.00159	0.00019
124125	0.00089	0.00237	0.00025	< 0.00002	0.00091	0.0069	0.0005	< 0.00038	< 0.00063	< 0.00077	0.0019	0.00013
126127	0.0013	0.00194	0.00026	< 0.00004	0.00104	0.00587	0.00057	0.00077	< 0.00061	< 0.00075	0.00148	0.00016
128129	0.00082	0.00081	0.00018	0.00004	0.00063	0.0043	0.00052	0.00077	< 0.00061	< 0.00075	0.00115	0.00015
130131	0.00056	0.0017	0.00034	0.00021	0.00049	0.00308	0.00078	0.00109	0.00161	0.00073	< 0.00081	0.00017
146147	0.00367	0.0013	0.00038	0.00032	0.00227	0.00114	0.00265	0.00392	0.00519	0.00517	< 0.00081	0.00018
132	0.00087	0.00145	0.00035	0.00016	0.00073	0.00406	0.00055	0.00101	0.00114	< 0.00074	0.00084	0.00016
134	0.0037	0.00121	0.00064	0.00036	0.00236	0.00246	0.00069	0.00101	0.00086	0.00074	< 0.00081	0.00028
139	0.00117	0.00108	0.00028	0.00015	0.0008	0.00248	0.00157	0.00228	0.0025	0.0023	< 0.00081	0.00013
140141	0.00027	0.00035	0.00004	< 0.00004	0.00071	0.00137	< 0.00026	< 0.00035	0.00161	0.00118	< 0.00081	< 0.00020
142143	0.0002	0.0004	0.00009	0.00003	0.00063	0.00161	0.00144	0.00205	0.00236	0.00221	< 0.00081	< 0.00020
151	0.01289	0.00331	0.00146	0.00106	0.00822	0.00517	0.00369	0.00572	0.00466	0.00599	< 0.00081	0.00084

Appendix IX. Brätschenflue A. Trace elements and rare earth elements.

Sample	Depth (cm)	C (%)	N (%)	Na (%)	Mg (%)	Al (%)	S (%)	Si (%)	P (%)	K (%)	Ca (%)	Ti (%)	Mn (%)	Fe (%)	LOI (%)	(K+Ca)/Ti	B Index	WIP	MWPI	CIA	CIW	Bulk dens. (g/cm3)	Water cont. (%)	pH
152	5	41.51	2.52	0.852	0.301	1.473	0.272	5.682	0.109	0.387	0.178	0.115	0.004	0.610	80.7	5.97	0.51	161.25	14.64	0.49	0.54	0.16	81.6	3.60
154155	30	46.84	1.50	0.653	0.192	0.499	0.095	1.102	0.038	0.063	0.060	0.027	0.001	0.120	94.8	5.49	0.64	357.90	32.99	0.36	0.37	0.10	90.8	3.30
156157	50	47.56	1.22	0.172	0.196	0.469	0.086	0.778	0.031	0.057	0.054	0.022	0.001	0.088	96.3	6.24	0.40	176.46	27.18	0.60	0.63	0.10	91.3	3.25
158159	70	48.09	1.33	0.832	0.182	0.532	0.079	0.632	0.034	0.051	0.028	0.023	0.001	0.073	95.7	4.14	0.66	526.66	44.92	0.34	0.34	0.08	90.9	3.30
160161	90	47.60	1.87	0.211	0.252	0.808	0.132	1.395	0.042	0.113	0.043	0.058	0.001	0.119	93.9	3.29	0.32	145.17	21.01	0.68	0.73	0.11	90.0	3.30
162163	110	49.11	2.40	0.894	0.231	0.780	0.136	2.205	0.047	0.160	0.036	0.058	0.001	0.092	91.3	4.16	0.61	306.72	25.39	0.39	0.42	0.17	89.9	3.45
164165	130	48.09	1.34	0.731	0.184	0.492	0.081	0.595	0.031	0.045	0.041	0.022	0.001	0.061	96	4.84	0.66	501.77	44.85	0.34	0.35	0.15	92.0	3.30
166	145	49.79	2.53	0.553	0.185	0.455	0.185	1.682	0.045	0.091	0.039	0.051	0.001	0.051	93.6	3.12	0.63	259.31	24.06	0.37	0.39	0.19	90.3	3.50
167	155	49.36	1.87	0.138	0.154	0.475	0.169	1.435	0.044	0.101	0.107	0.048	0.002	0.080	94.6	5.27	0.44	122.13	18.00	0.56	0.61	0.06	91.3	3.30
168	167.5	44.27	1.77	1.074	0.330	2.582	0.303	5.283	0.126	0.534	0.200	0.206	0.005	0.357	79	4.34	0.42	189.67	16.93	0.58	0.63	0.11	89.0	3.65
169170	185	39.54	3.11	0.985	0.417	2.702	0.464	7.598	0.089	0.688	0.223	0.193	0.011	0.476	73.1	5.75	0.42	153.38	14.01	0.58	0.65	0.10	88.8	3.80
171	203.75	24.50	1.74	1.479	1.159	5.611	0.560	16.049	0.167	1.773	0.460	0.358	0.038	1.708	43.5	7.59	0.39	141.54	14.17	0.61	0.70	0.19	81.6	4.15
172	211.5	28.24	1.97	1.553	0.766	4.679	0.535	14.203	0.088	1.475	0.412	0.329	0.019	0.941	51.6	6.98	0.42	152.38	13.58	0.58	0.66	0.15	85.6	3.90
173	215	13.97	0.89	2.353	1.029	6.456	0.272	24.704	0.099	2.332	0.609	0.299	0.028	1.412	22.95	11.97	0.45	146.77	12.04	0.55	0.64	0.42	67.7	4.05
174	219	10.13	0.61	2.521	1.121	6.956	0.194	27.673	0.105	2.540	0.717	0.295	0.032	1.592	14.8	13.45	0.45	143.56	11.82	0.55	0.64	0.44	54.2	4.15

Appendix X. Brätschenflue B. Most important elemental contents and weathering indices.

Sample	Zr (%)	Pb (%)	Th (%)	U (%)	Sr (%)	V (%)	La (%)	Ce (%)	Pr (%)	Nd (%)	Sm (%)	Hf (%)
166	0.00061	0.0006	0.00023	0.00012	0.00061	0.00403	0.00063	0.0008	0.00096	< 0.00074	0.00097	0.0002
167	0.00085	0.0015	0.00016	< 0.00002	0.00108	0.00596	0.00057	0.00051	0.00058	< 0.00078	0.00173	0.00013
173	0.01786	0.00329	0.00139	0.00077	0.01322	0.00504	0.00585	0.01015	0.00809	0.01044	< 0.00081	0.00055
156157	0.00042	0.00092	0.00002	< 0.00004	0.00079	0.00413	< 0.00028	< 0.00038	0.00061	< 0.00076	0.00139	0.00007
158159	0.00037	0.00179	0.00012	< 0.00004	0.00061	0.00329	0.00044	< 0.00037	< 0.00061	< 0.00075	0.00109	0.00011
160161	0.00085	0.0016	0.00017	0.00003	0.00086	0.005	0.00065	0.00086	< 0.00062	< 0.00076	0.00141	< 0.00005
169170	0.00684	0.00271	0.00093	0.00074	0.00396	0.00412	0.00225	0.00373	0.00198	0.00328	0.00098	0.00054
152	0.00393	0.00348	0.00028	0.00008	0.00192	0.00157	0.00174	0.00285	0.00258	0.0032	< 0.00081	0.00018
154155	0.00037	0.00098	0.00012	0.00002	0.00064	0.00288	0.00058	0.00057	< 0.00061	< 0.00075	0.00082	0.00008
162163	0.00101	0.00059	0.00016	0.00007	0.0007	0.00318	0.00092	0.00118	0.00109	0.00072	0.00077	0.00014
164165	0.00035	0.00063	0.00008	0.00002	0.00043	0.00171	0.00072	0.00096	0.0011	< 0.00070	< 0.00081	0.00008
168	0.00961	0.00123	0.00047	0.00033	0.00269	0.00196	0.00357	0.00509	0.00674	0.00684	< 0.00081	0.00026
171	0.0176	0.00594	0.00154	0.00137	0.00929	0.00686	0.00368	0.00642	0.00334	0.00498	0.00077	0.00082
172	0.01532	0.00525	0.00147	0.00128	0.00814	0.00601	0.0039	0.00662	0.00498	0.0065	< 0.00081	0.00072
174	0.02163	0.00275	0.00138	0.00069	0.0155	0.00516	0.00952	0.015	0.01381	0.01741	< 0.00081	0.00051

Appendix XI. Brätschenflue B. Trace elements and rare earth elements

Sample	2000–1000µm	1000–500µm	500–250µm	250–125µm	125–63µm	63–45µm	45–32µm	32–2µm	<2µm	Sum
1	7.1	7.7	7.9	8.4	7.9	3.7	3.7	28.6	25.0	100.0
2	8.7	9.0	8.5	8.5	8.2	3.7	3.0	33.0	17.6	100.0
3	9.8	12.4	10.1	11.9	13.1	9.1	7.3	20.1	6.2	100.0
4	14.8	16.4	14.1	13.4	12.6	5.3	3.8	15.5	4.1	100.0
13	9.0	8.6	9.6	10.1	10.0	5.0	4.0	25.4	18.3	100.0
14	8.7	10.8	10.5	11.4	10.2	4.9	3.5	24.0	15.9	100.0
15	6.0	10.0	10.1	11.8	12.7	5.6	5.5	26.6	11.7	100.0
16	9.4	13.5	9.5	12.7	17.6	7.6	6.3	19.3	4.2	100.0

Appendix XI. Soils. Grain size fractions.

Wavelength	(cm^{-1})	**1**	**2**	**3**	**4**	**13**	**14**	**15**	**16**
Kaolinite	3694		x	x		x	x	x	
	3652		(x)			x	(x)	x	
	3620	(x)	(x)	x	x	(x)	x	x	x
	474	x	x	x		x	x	x	x
	348		(x)	x	x	x			(x)
Gibbsite	3620	(x)	(x)	x	x	(x)	x	x	x
	3526			x	(x)	(x)	(x)		
	3469		x				(x)	x	(x)
	1017	x	x	x	x	x	x	x	x
	366			x	x	x	(x)	(x)	
Chlorite	3676								
	3575		(x)	(x)	(x)	(x)		(x)	
	3428		(x)		(x)	x	(x)	(x)	
	750	x	x	x	x		(x)	x	x
Imogolite	375	x		x	x		(x)	(x)	(x)
	348	x	(x)	x	x	x			(x)
Kaolinite, Qz or Illite	474	x	x	x		x	x	x	x
Illit, Muskovite	531/474	x/x	/x	x/x	x/	x/x	x/x	x/x	x/x
	831/752	x/	x/x	x/x	x/x	x/(x)	x/(x)	x/x	x/x
oct. Mg/Fe	650	x		x	x	x	x	x	x
dioct. Smectite	690	x	x	x	x	(x)	(x)	(x)	(x)
Quartz	692	x	x	x	x	x	x	(x)	(x)
Muskovite and Chlorite	750	x	x	x	x		(x)	x	x
Qz-Doublet	780/800		(x)/x	(x)/x	/x	/(x)	x/x	x/x	(x)/x
AlMgOH	830	x	x	x	x	(x)	(x)	x	x
Kaolinite	915	x	x	x	x	x	x	x	x
Enstatite (Pyr)	1064		x		x		(x)	x	x
	952					(x)		(x)	(x)
	645	x	x	x	x	x	x	x	x
	513		x		(x)	(x)	x	(x)	(x)
Forsterite (Pyr)	885		(x)	(x)	(x)				
	490		x	x	x	x			x
	315		x	x	x	x	(x)	(x)	(x)
Amphibole	3674		(x)				x	(x)	(x)
	3618	x	(x)	x	x	x	x	x	x

Appendix XII. Soils. DRIFT peak identification list.

Wavelength	(cm^{-1})	24	26	28	30	32	34	3674	7677	5178	5380	5582	8485	8687	8889	9091
Kaolinite	3694	x	x	x	x	x		(x)		(x)	(x)		(x)			
	3652		x			(x)		(x)			(x)		(x)			
	3620	x	x	(x)	(x)	x	x	(x)		x	x	x				
	474	x	x	x	(x)		(x)	x	x							
	348		(x)	(x)	x	(x)		(x)	x		x	x	x	x	(x)	
Gibbsite	3620	x	x	x	(x)	x	x	(x)		x	x	x				
	3526	(x)	x		x	(x)	x	(x)	(x)		(x)	(x)			(x)	
	3469	(x)	(x)	x		(x)	x	(x)	(x)	(x)	(x)					(x)
	1017	x										(x)	(x)			
	366	(x)	x	x		x		(x)	x	x	x	(x)	(x)	(x)	x	x
Chlorite	3676	(x)	x			(x)	(x)									
	3575															
	3428	x		x		x	(x)	x	(x)	x	(x)					x
	750	(x)		(x)	(x)		x	x	(x)			x	(x)			x
Imogolite	375			(x)	x	(x)		(x)	x	x	x	x	x	x	x	(x)
	348		(x)	(x)	x	(x)		(x)	x		x	(x)	(x)	x	(x)	
Kaolinite, Qz or Illite	474	x	x	x	(x)		(x)	x	x	(x)						
Illit, Muskovite	531/474	x/x	(x)/x	/x	(x)/(x)	(x)/(x)	(x)/(x)			/(x)			/(x)	x/	(x)/	x/
	831/752	(x)/(x)	(x)/	x/(x)	x/(x)	x/(x)	(x)/x	x/x	x/x	x/(x)	x/	x/	x/	x/	x/	/(x)
oct. Mg/Fe	650	(x)	(x)	x		x		(x)	x						(x)	(x)
dioct. Smectite	690	x		(x)			x	x	x							
Quartz	692				(x)	x	x	x	x					(x)	x	
Muskovite and Chlorite	750	(x)		(x)	(x)		x	x	(x)		(x)	x	(x)			x
Qz-Doublet	780/800	x/x	(x)/	/(x)	(x)/	x/	x/x	(x)/(x)	(x)/	(x)/x	(x)/(x)	x/	x/		(x)/	x/
AlMgOH	830	x	(x)	x	x	x	x	x	x	x	x	(x)	(x)	x	x	x
Kaolinite	915	x	x	(x)	(x)			(x)	(x)		x		(x)			
Enstatite (Pyr)	1064	x	x	x	x	x	(x)	x	x	x	(x)	x	x	x	x	x
	952	(x)		(x)	(x)		(x)	?	?			(x)	(x)			(x)
	645	x	(x)	(x)				x	(x)	(x)	(x)			(x)	(x)	x
	513	x	(x)	x	(x)	(x)			(x)	x		x	x		(x)	x
Forsterite (Pyr)	885		(x)	(x)	(x)		x	(x)	(x)							
	490		x	x	(x)	x	x	x		x	x	x	(x)			x
	315	x	x	x	x	x	x	x		x	x			x	x	x
Amphibole	3674	(x)	(x)			(x)	x		(x)		(x)					
	3618	x	(x)	x	(x)	x	x	(x)		x	x					

Appendix XIII. Börtli A. DRIFT peak identification list.

Wavelength	(cm^{-1})	37		39	41	43	45	100	46	112117	119	120	121	103	105	107	109	47	48	49
Kaolinite	3694	x	x	x		x	x	x	(x)	x		x		(x)	(x)	x	x	x	x	(x)
	3652	x				x	(x)	(x)				(x)			(x)	(x)		(x)	(x)	
	3620	x	(x)	x		x	x	x		x	x	x	x	x	x	x	x	x	x	x
	474	(x)	x	x		(x)	(x)		x		(x)	x		x	x	x		x		x
	348	x		(x)		x	x	x	x	(x)	x	x	x	x	x	x	x	x	x	x
Gibbsite	3620	x	(x)	x		x	x	x		x	x	x	x	x	x	x	x	x	x	x
	3526	x	(x)	x			x		x		x	(x)	x	x	x				x	(x)
	3469	x	x	x		x	x	x	x	x	(x)	(x)	x		x	x	x	(x)	x	(x)
	1017						x				(x)	(x)					x			x
	366	x	(x)	x		x	x	x	(x)	x	(x)	x	x		x	x	x	x	x	
Chlorite	3676	x				(x)									(x)	(x)	(x)	(x)	(x)	x
	3575		(x)								(x)	(x)				x				(x)
	3428	(x)				x	(x)	(x)		x		(x)	x	(x)		x	x	x	x	
	750	x	x	(x)		x	x		x	x	x		x	(x)	x	x	x	x	x	x
Imogolite	375						(x)		x	(x)	x	x		x	x	x	x			x
	348	x		(x)		x	x	x	x	(x)	x	x	x	x	x	x	x	x	x	x
Kaolinite, Qz or Illite	474	(x)	x	x		(x)	(x)		x		(x)	x		x	x	x		x		x
Illit, Muskovite	531/474	x/(x)	(x)/x	x/x		x/(x)	x/x	x/	(x)/x	x/	x/(x)	x/x	x/(x)	x/x		x/x	x/(x)	x/x	x/	x/x
	831/752	/x	x/	x/		x/	x/x	x/	x/(x)	x/(x)	x/x	x/	x/x	x/x	x/	x/	x/	x/(x)	x/(x)	x/x
oct. Mg/Fe	650	x	(x)				(x)	x	(x)	x	x	(x)	x	x	(x)	x	x	x	x	x
dioct. Smectite	690		x	x			x		(x)	(x)		x	(x)	x	x	x	x	x	x	x
Quartz	692	(x)	x	x		x	x		(x)	x	(x)	x	(x)	x	x	x	x	x	x	x
Muskovite and Chlorite	750	x	x	(x)		x	x		x	x	x		x	(x)	x	x	x	x	x	x
Qz-Doublet	780/800	x/x	(x)/(x)	(x)/?		x/	x/x	(x)/(x)	(x)/x	x/x	x/(x)	(x)/(x)	(x)/(x)	(x)/(x)	(x)/(x)	x/(x)	x/(x)	x/(x)	x/(x)	x/x
AlMgOH	830	x	x	x		x	x	x	(x)	x	(x)	x	x	x	x	x	x	x	x	x
Kaolinite	915	x	x					(x)			(x)	(x)	(x)	(x)		(x)		x	(x)	x
Enstatite (Pyr)	1064	x	(x)	x		(x)	x	x	(x)	x	x	x		x	x	(x)	x	x	x	x
	952	(x)	(x)	(x)						(x)		(x)	(x)	(x)		(x)			(x)	
	645		x	(x)		x	(x)	x	x		x	(x)	(x)		(x)	(x)	x	x	x	x
	513	x	(x)	x		x	(x)	x	x	x	x	(x)	(x)	(x)			x	(x)	(x)	(x)
Forsterite (Pyr)	885		(x)	(x)		(x)	x		x		(x)			(x)		(x)	(x)	x	(x)	(x)
	490		x	x		x	x			x		(x)	x		(x)	x	(x)	(x)	x	(x)
	315	x	x			x	x			(x)	(x)	x	(x)		(x)	(x)	(x)	(x)	(x)	
Amphibole	3674					(x)	(x)								(x)	(x)	(x)			x
	3618						(x)				x	(x)	(x)	(x)	(x)					x

Appendix XIV. Börtli B. DRIFT peak identification list.

Wavelength	(cm^{-1})	122123	124125	126127	128129	130131	132	133	134	135	136137	138	139	140141	142143	144	145	146147	148	149	150	151
Kaolinite	3694	x	x	x	x	x	x	x	x	x	x	x	(x)	(x)	(x)	(x)	(x)			x	(x)	(x)
	3652	(x)				(x)						(x)		(x)	(x)	(x)	(x)	x	x		x	x
	3620	x		x		x	x	(x)	x	(x)	x	(x)	(x)	x	x	x		x	x		x	x
	474	(x)	x	x	x	x	x	x	x	x	x	x	x	x	x	x	(x)	x	x	x	(x)	x
	348	(x)		x	x	x	x		x	(x)		x	x				x	(x)	(x)		x	
Gibbsite	3620	x		x		x	x	(x)	x	(x)	x	(x)	(x)	x	x	x		x	x		x	x
	3526				x	(x)	x	(x)	(x)	(x)	(x)	(x)	(x)		x	x	(x)	x	(x)		x	x
	3469	x	(x)		x				(x)		(x)	(x)	x	(x)	(x)	x	(x)	x	(x)		x	x
	1017		(x)									(x)	(x)							?	?	(x)
	366	x	x	x	x	x	x	(x)			x	(x)	x	x	(x)	(x)	x		x	(x)	x	x
Chlorite	3676	(x)				(x)		x		(x)	x		(x)	(x)	x		(x)	x	x			
	3575										(x)		(x)		x		(x)	(x)	(x)	x		(x)
	3428	(x)				(x)			(x)			x		(x)	(x)	(x)	x	x	(x)	x	(x)	(x)
	750	(x)	x	x	x	x	x	x	x	x	(x)	x	(x)	(x)	(x)	(x)	(x)		x	x	x	x
Imogolite	375	(x)	x	x	x	x		(x)	x	x	x	x	(x)						x	(x)		x
	348	(x)		x	x	x	x		x	(x)		x	x				x	(x)	(x)		x	
Kaolinite, Qz or Illite	474	(x)	x	x	x	x	x	x	x	x	x	x	x	x	x	x	(x)	x	x	x	(x)	x
Illit, Muskovite	531/474	x/(x)	x/(x)	x/x	x/x	(x)/x	x/x	x/x	x/x	x/x	x/x	x/x	x/x	x/x	x/x	x/x	/(x)	x/x	x/(x)	(x)/x	x/(x)	x/x
	831/752	/(x)	x/x	x/(x)	x/x	x/x	x/x	x/(x)	x/x	x/(x)	x/(x)	x/(x)	x/(x)	x/(x)	x/(x)	x/(x)	(x)/x	(x)/	(x)/x	(x)/x	/x	(x)/x
oct. Mg/Fe	650	(x)	(x)			(x)		x	x	x	x	x	(x)	(x)	(x)	(x)	x	x	x	x	x	x
dioct. Smectite	690		x	x	x	(x)	(x)	(x)	x	x	x	x	(x)	x	x	x	x	x	x	x	x	x
Quartz	692		x	x	x	x	x	x	x	x	x	x	x	(x)		(x)	x	x	x	x	x	x
Muskovite and Chlorite	750	(x)	x	x	x	x	x	x	x	x	(x)	x	(x)	(x)	(x)	(x)	(x)		x	x	x	x
Qz-Doublet	780/800	x/x	(x)/	x/x	x/x	(x)/x	x/x	(x)/(x)	x/(x)	x/x	x/x	x/x	x/x	x/(x)		x/(x)	x/(x)	/(x)	(x)/x	x/(x)	(x)/x	x/x
AlMgOH	830	x	x	x	x	x	x	x	x	x	x	x	x	x	x	x	(x)	(x)	(x)	(x)		x
Kaolinite	915	(x)	(x)	x	x	(x)	x	x	x	(x)	(x)	x	x	(x)	(x)	(x)	(x)	(x)		(x)	(x)	(x)
Enstatite (Pyr)	1064	(x)	x	x	x	x	x	x	x	x	x	x	x	x	x	x	x	x	x	x	x	(x)
	952		(x)	(x)				(x)	(x)	(x)				x	x	x	x	x	x	(x)		x
	645	(x)	(x)	(x)	x		x		x	(x)	x	x	x	x	x	x	x	(x)	x	x	x	x
	513		x	x	x	x	x	(x)		(x)	x	x	(x)	x	x	x	x	(x)	(x)	x	x	
Forsterite (Pyr)	885	(x)		(x)	(x)	(x)	x	(x)	(x)	(x)	(x)	(x)	(x)	x	x	(x)	(x)	x	x	(x)	(x)	(x)
	490	x	x	(x)	x	x		x	(x)	x		x	(x)	x	x		x	x			x	x
	315	x	x				x	x	(x)	x		(x)	(x)	(x)	(x)	x	(x)	x	x		(x)	(x)
Amphibole	3674							(x)					(x)		(x)			(x)	(x)			
	3618	x		x		x	x	(x)		(x)	x	(x)	(x)	(x)		x		x	x	x		x

Appendix XV. Brätschenflue A. DRIFT peat identification list.

Wavelength	(cm^{-1})	152	154155	156157	158159	160161	162163	164165	166	167	168	169170	171	172	173	174
Kaolinite	3694	x	x	x	x	(x)	x	x	x	x	x	x	x	(x)	x	x
	3652	x									(x)		x			?
	3620	x	(x)	(x)			(x)		(x)		x	(x)	x	x	x	x
	474	x	(x)	x	x	(x)	x	x	x	x	x	x	x	x	x	x
	348	x	x		x	(x)	(x)	x	x	x	(x)		(x)			
Gibbsite	3620		(x)	(x)			(x)		(x)		x	(x)	x	x	x	x
	3526				x	x	x		(x)	x	(x)					(x)
	3469		(x)	x			(x)	(x)	(x)	x	x	x			(x)	(x)
	1017	(x)	(x)	(x)	x		(x)	(x)	(x)	(x)	(x)		x	x	x	x
	366	x	x	x	(x)	(x)	(x)	(x)	x	x	(x)	(x)	(x)	(x)		
Chlorite	3676												(x)		x	
	3575	(x)											(x)	(x)	x	x
	3428	(x)		(x)	x	(x)	(x)			(x)	(x)	x	(x)		x	
	750	(x)	(x)	x	(x)	(x)	(x)	x	(x)	x	(x)	(x)	(x)	x	(x)	x
Imogolite	375	x		x	x	x	x	(x)	x	x	x	(x)	(x)	x	x	(x)
	348	x	x		x	(x)	(x)	x	x	x	(x)		(x)			
Kaolinite, Qz or Illite	474	x	(x)	x	x	(x)	x	x	x	x	x	x	x	x	x	x
Illit, Muskovite	531/474	x/x	x/(x)	x/x	x/x	x/(x)	x/x	x/x	x/x	x/x	x/x	x/x	x/x	x/x	x/x	x/x
	831/752	(x)/(x)	(x)/(x)	(x)/(x)	(x)/x	x/(x)	x/	x/x	x/(x)	x/x	x/(x)	(x)/	x/x	x/x	x/(x)	x/x
oct. Mg/Fe	650	(x)		x	x	(x)	x	(x)	(x)	(x)	x	x	x	x	x	x
dioct. Smectite	690	x	x	(x)	x	x	(x)	x		(x)	x	(x)	x	(x)	x	x
Quartz	692	x	x	(x)	x	(x)	(x)	x	(x)	x	x	x	x	x	x	x
Muskovite and Chlorite	750	(x)	(x)	x	(x)	(x)	(x)	x	(x)	x	(x)	(x)	(x)	x	(x)	x
Qz-Doublet	780/800	x/x	x/x	x/x	/?	x/(x)	x/x	x/x	(x)/(x)	x/x	x/x	x/x	x/x	x/x	x/(x)	(x)/(x)
AlMgOH	830	x	(x)	(x)	(x)	x	x	x	x	x	x	(x)	x	x	x	x
Kaolinite	915	x		(x)		(x)	(x)		(x)	(x)	x	x	x	x	x	x
Enstatite (Pyr)	1064	x	x	x	x	x	x	x	x	x	x	x	(x)	x	x	(x)
	952		x	x	x	x	(x)	x		(x)	(x)		(x)		(x)	(x)
	645	x	(x)	x	(x)	x	(x)	(x)	x	x	x	x	x	x	x	x
	513	x	(x)	x	x	(x)	x	x	(x)		(x)	(x)	x	x	x	x
Forsterite (Pyr)	885	(x)	(x)	(x)	(x)	(x)	(x)	(x)	(x)		(x)	(x)	(x)	(x)	(x)	(x)
	490	(x)		x	(x)	x	x	(x)	(x)	x	(x)	(x)			(x)	(x)
	315	x	x	x	(x)	x	x		x			x		(x)	x	
Amphibole	3674														x	
	3618	x							(x)		x	(x)	(x)	x	x	x

Appendix XVI. Brätschenflue B. DRIFT peat identification list.

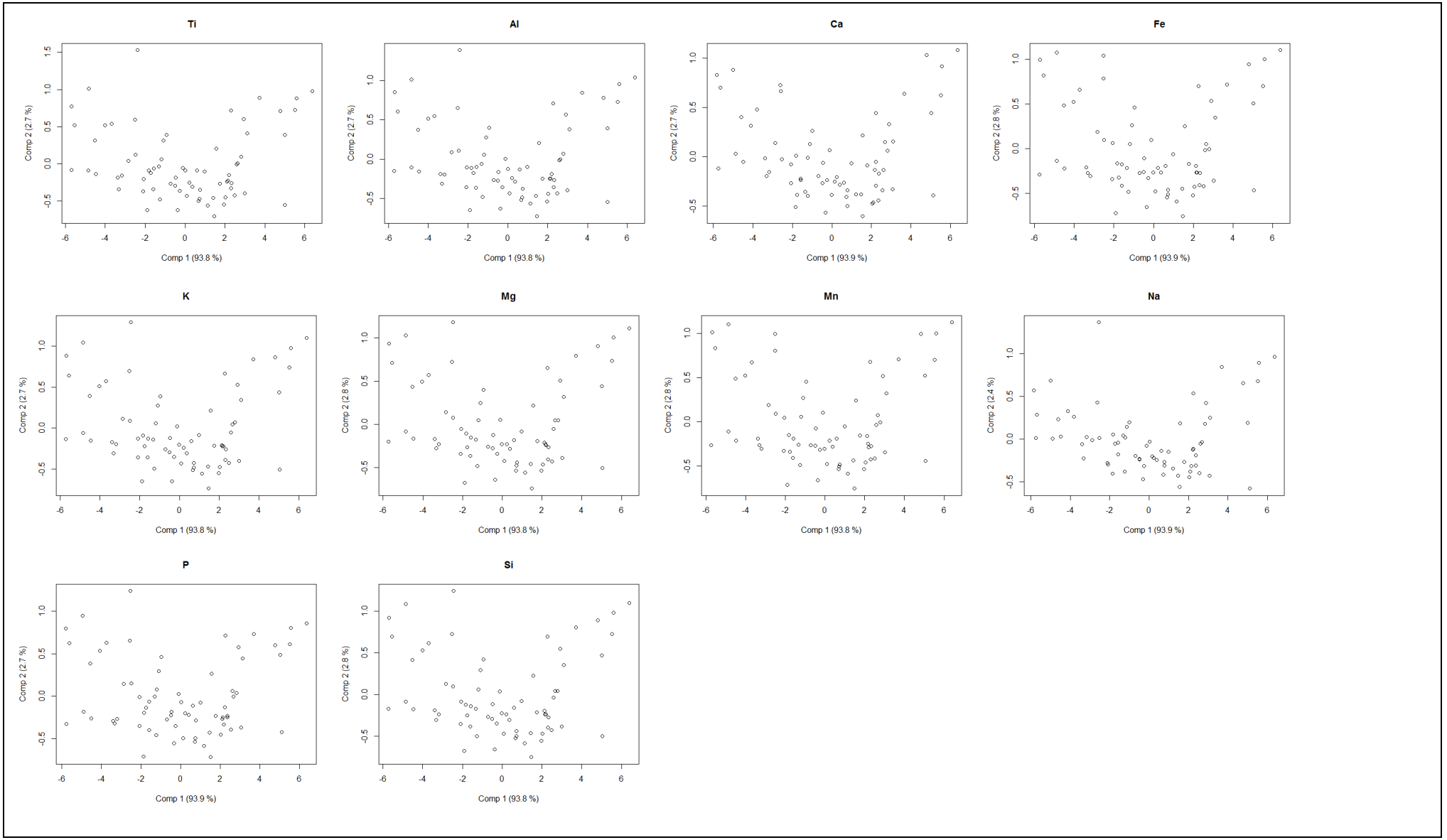

Appendix XVII. PLS scores. Correlation between the two components explaining the most variability.

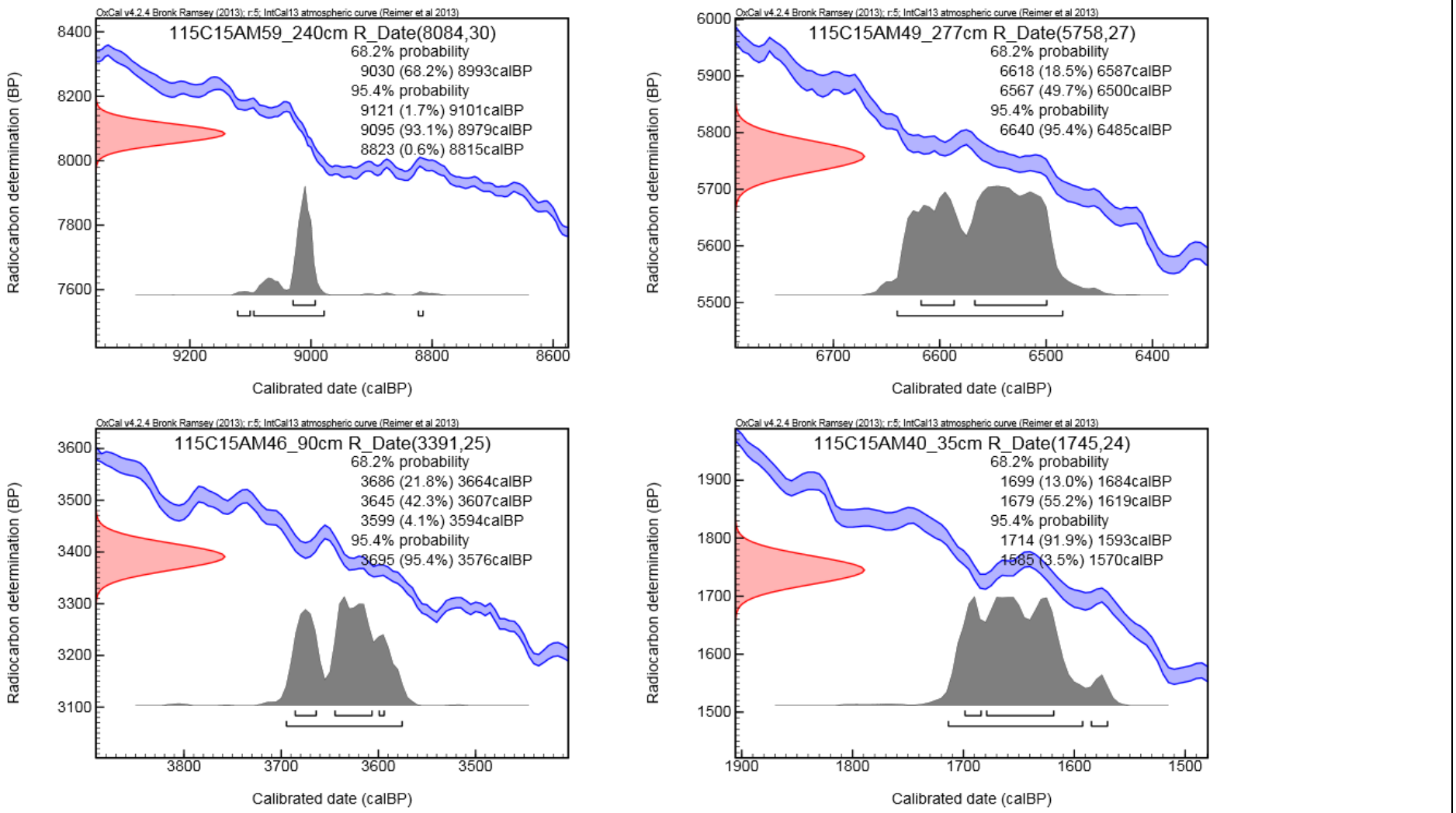

Appendix XIXa. 14C. Oxcal calibrations.

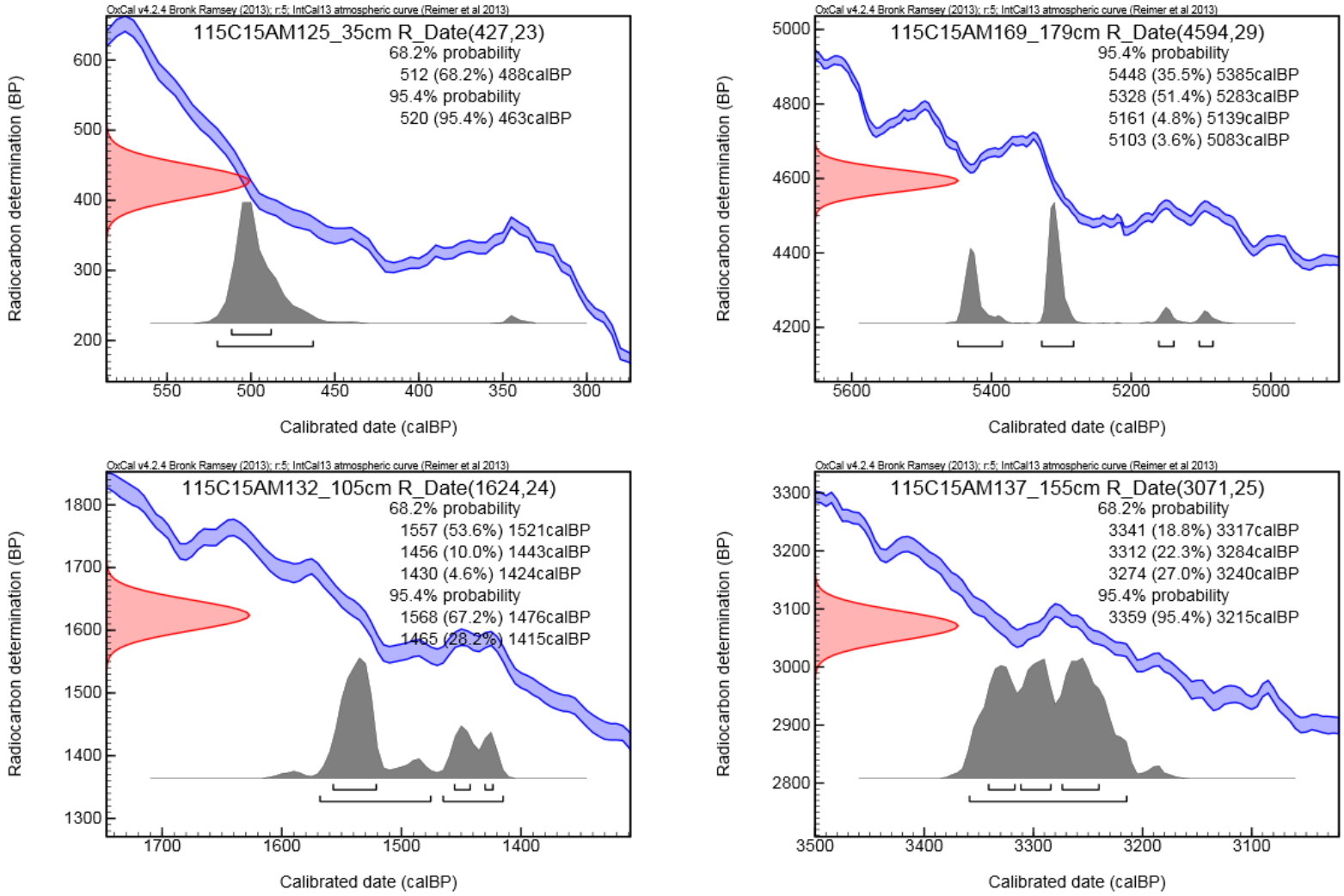

Appendix XIXb. 14C. Oxcal calibrations

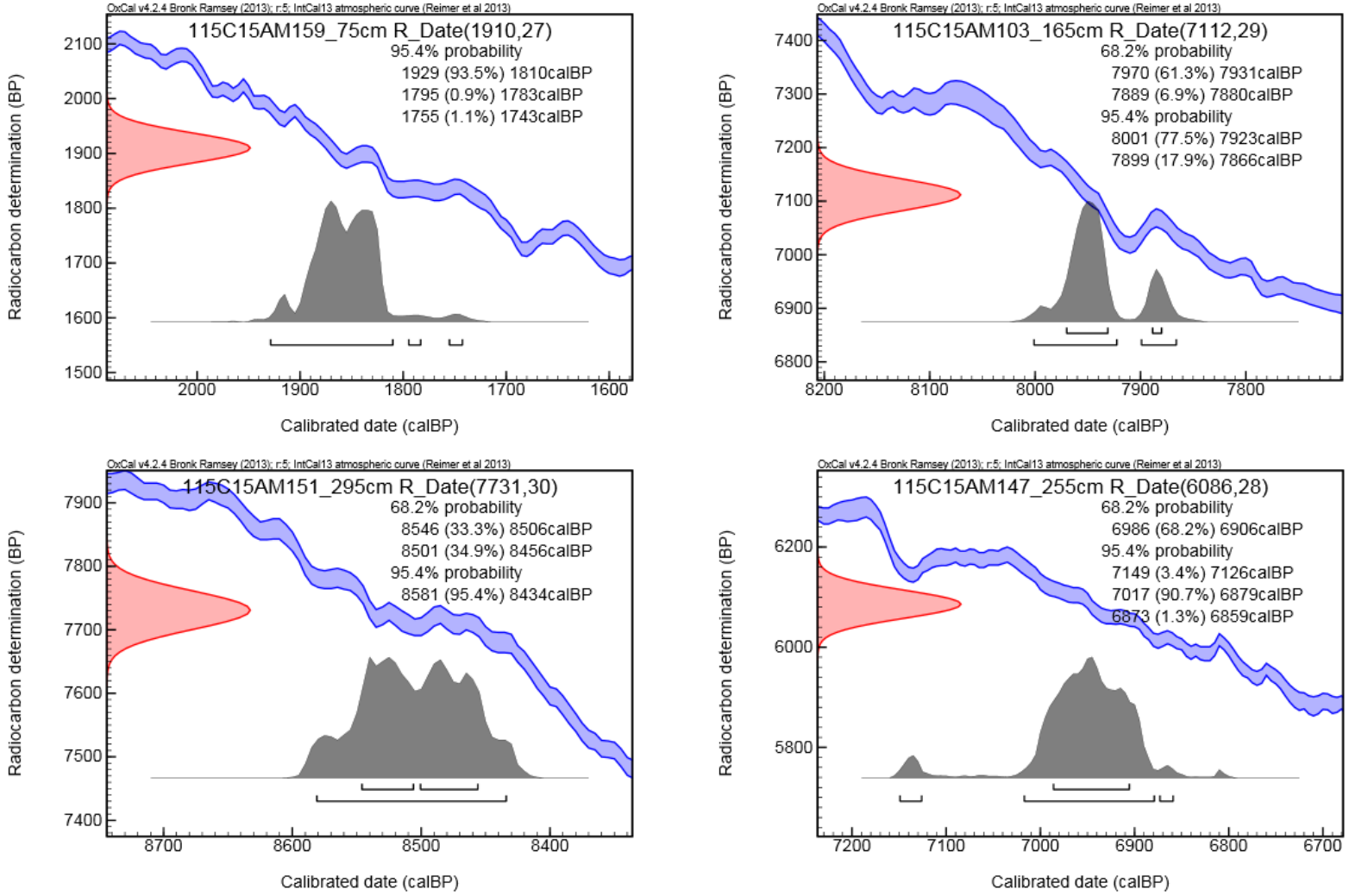

Appendix XIXc. 14C. Oxcal calibrations

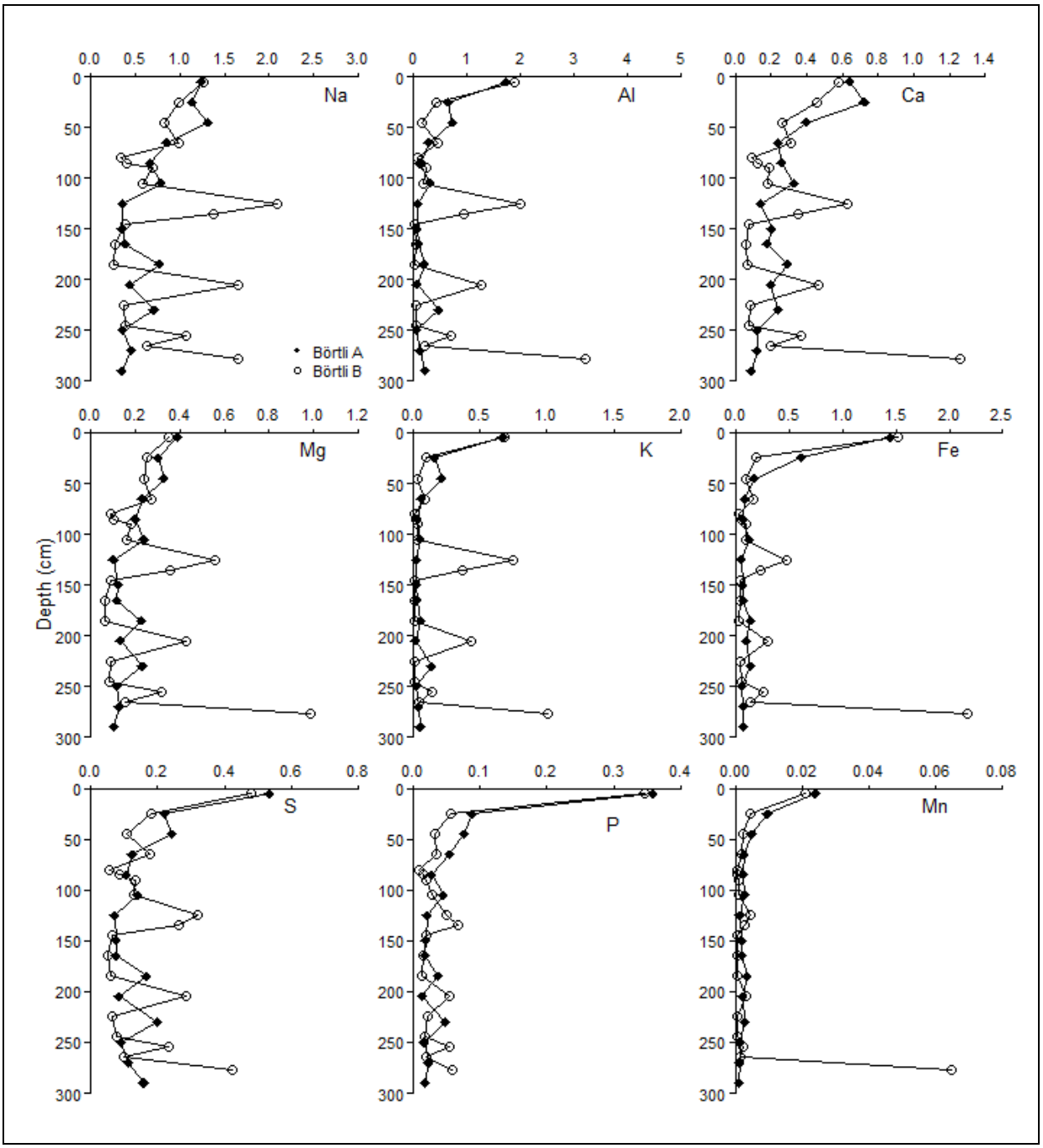

Appendix XX. Börtli Element contents.

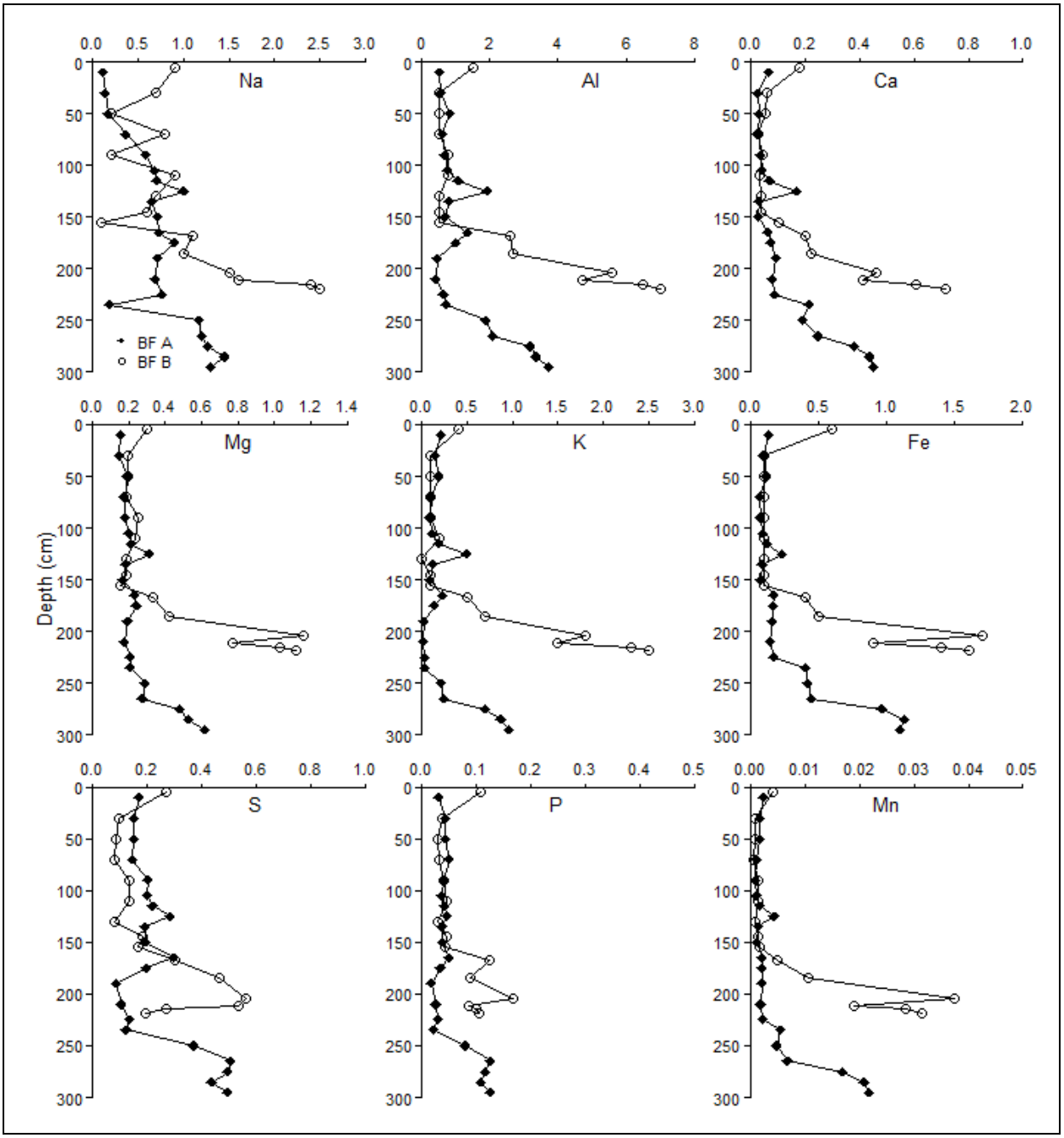

Appendix XXI. Brätschenflue. Element contents.

Personal Declaration

I hereby declare that the submitted thesis is the result of my own, independent work. All external sources are explicitly acknowledged in the thesis.

_____

The author

Acknowledgements

I owe thanks to many people but first and foremost to my supervisor Markus Egli, for I could always rely on his help and his kind words whenever I had stared into the data for too long and the data was staring into me.

My friend Ivan Woodhatch, for his calm and steadfast moral support in times of crisis and for teaching me the secrets of radiocarbon dating.

Jaroslaw Waroszewski and Malgorzata Malkiewicz at the Wroclaw University. While the latter did all kinds of nasty things to my samples, for the good of palynology and the glory of science, the first one kindly offered me his expertise for the interpretations of the pollen profiles.

Samuel Abiven, for guiding me safely through the jungle of statistics, generously offering me his code, and for the interesting discussions that followed.

Guido Wiesenberg, for the critical questions in the lab which reminded me to chose the best path not with my eyes but with my brain.

The expedition team members (Markus Egli, Dennis Dahms, Max Maisch, Max Boxleitner and Ksenia) that accompanied me into the field and weren't shy about getting their feet wet and their hands (or everything, really) dirty.
The group of us also indebted to the farmer of Börtli, Christian Näf, for his permission to drill and his help with transporting our heavy equipment. Also, thanks to Stefan Gamma and his dog Aragorn, who accompanied us to Brätschenflue.

Sandy Röthlisberger, for her help with lab procedures and her patient explanations of the equipment.

My fellow master's student Annina Ruppli and my parents, for their proof–reading, constructive criticism and generally helping me not lose sight of the forest among the many trees.

Finally, all those left unmentioned who listened patiently, offered their insights, encouraged me or simply made my day a little brighter.